Surface Radiation Datasets from Geostationary Satellites
Subcontract AXL-3-23362-01

Christine Molling[1], Andrew Heidinger[2]
1. UW SSEC CIMSS, 2. NOAA NESDIS STAR

Final Report
Date: June 2014

Abstract

The version of Pathfinder Atmospheres – Extended (PATMOS-x) processing system that had been earlier used to process GOES Imager data from 2005 through 2011 was used to produce surface irradiance and cloud products from GOES-WEST and -EAST Imager data for 2012. Statistics of global horizontal irradiance, diffuse horizontal irradiance and direct normal irradiance were computed and compared with statistics from earlier years. Results show accuracy with respect to surface observations is similar from 2005 through 2012. A version of PATMOS-x was also used to compute real-time products, which are hosted on a CIMSS website and ftp site. The Bird and Hulstrom algorithm for clear sky irradiance was used to compute an alternative global horizontal irradiance (GHI) for clear sky conditions. The comparison compared to the standard PATMOS-x GHI, the Bird and Hulstrom GHI shows a slight improvement in terms of RMSE and R^2. The least squares fit statistics between observed GHI and calculated at the seven SURFRAD sites were similar at most locations, except at Desert Rock, where Bird and Hulstrom outperformed PATMOS-x significantly.

Contents

1. Introduction

In September, 2010, a subcontract agreement was made between the National Renewable Energy Laboratory and the University of Wisconsin – Madison in order to compute cloud and surface products from Geostationary Operational Environmental Satellite (GOES) Imager data for the years 2005 through 2009. This data set was computed by inserting the Global Solar Insolation Project (GSIP) algorithm Satellite Algorithm for Shortwave RAdiation Budget (SASRAB) into the Pathfinder Atmospheres – Extended (PATMOS-x) processing system in order to compute the desired surface products of global horizontal irradiance (GHI) and direct normal irradiance (DNI) and cloud products at a higher resolution than was available from GSIP. The data set consisted of 2.4 Tb of files, each containing about 60 different data variables at the resolution of the GOES Imager thermal data (4km at the equator). This data set was delivered in 2011 (Heidinger and Molling, 2011, included as Appendix A).

A subsequent modification to the subcontact was signed in 2012 to support the production of another 2 years of analysis (2010-2011) plus a reanalysis of 2005-2009 (Molling et al., 2013, included as Appendix B). This data set was approximately 16.2 Tb and delivery was completed in Dec 2013. A second subcontract was signed in June of 2013 to compute products for 2012 and to create a real-time products stream from GOES Imager. This report covers these activities under this second subcontract.

Funds under this subcontract were used for labor (salary, fringe benefits and indirect costs), data acquisition and supplies.

2. Algorithm

The version of PATMOS-x used to create the data set is the development branch version tagged "nrel_2010-11_and_2005-9_reanalysis" and dated March 23, 2013. This is the same version as used to process the 2005-2011 data. The only changes between the 2005-2011 and the 2012 data set processes were calibrations for GOES-13 and -15. Effects of the calibration change should be minor.

3. 2012 Results

Level2 files (data products at the thermal pixel resolution) were computed for 2012, for which the total size was about 2.4 Tb. There are two gaps in the 2012 output due to satellite failures. There is a gap in GOES-15 (WEST) data beginning on day 81, and resolving part way through day 83. There are no files at all on day 82. The cause according to NOAA status reports: "GOES-15 went into sun acquisition mode (due to momentum dump) and unable to do any imaging." Gaps exist for GOES-13 (EAST) starting on day 267 and resolving on day 293. This is a result of GOES-13 being placed into standby mode in response to a scan motor overload, according to NOAA status reports. GOES-14 (an on-orbit spare in a central location) was activated on day 269 and continued to serve in place of GOES-13 (on the -EAST

schedule) through day 292. GOES-14 drifted eastward from day 275 through day 293. GOES-13 was reactivated on day 292.

3.1. Files

The level2 file format is HDF4 and is the same as the previous analysis. Each level2 file contains approximately 60 observed and computed products. See the previous report (NRELmodificationreport_Oct2013final.docx) for a header list that contains product names and other metadata. There is one level2 file every 30 minutes when available, with WEST having files 00 and 30 minutes after the hour and EAST 15 and 45 minutes after the hour. Files are Northern Hemisphere (WEST) or Northern Hemisphere Extended (EAST) for most times, and Full Disk, when a Full Disk image is available (every 3 hours beginning 0000 UTC for WEST and 0245 for EAST). Below are plots showing data availability for the year 2012. A **black** square indicates that no file is present for that satellite at that time. A **green** square indicates that a file is present and more than 99% of the earth pixels have a valid insolation calculation. A **yellow** square indicates that at least 95%, but less than 99% of the pixels have a valid insolation calculation. **Red** indicates that less than 95% of the pixels have a valid insolation calculation. A common pattern emerges from studying these quicklooks. Besides the semi-random nature of lower quality images due to solar activity, transmission errors, satellite/instrument ageing, and malfunction, the main patterns are the red and yellow "wings" due to the very few pixels which are candidates for the insolation calculation at certain hours and times of the year. GOES-13 and -15 have greater battery storage than previous editions of GOES, so that the data loss during the spring and fall eclipse periods is very small for GOES-15 (black squares 830-930 UTC) and non-existent for GOES-13. GOES-15 imaging is also cancelled periodically at 2000 UTC for calibration. GOES-15 is missing the entire day 82. GOES-13 was placed into abbreviated full disk mode on the hh15 images that day. Unfortunately, that caused the dark sky compositing code to fail on those images as the images were not the correct size. GOES-13 had an extended period of failure days 268-292. GOES-15, which was switched to full-disk mode for additional images, should be used for day 268 (dark sky compositing failed on some images there as well), while GOES-14, which was brought out of storage mode, should be used for days 269-292.

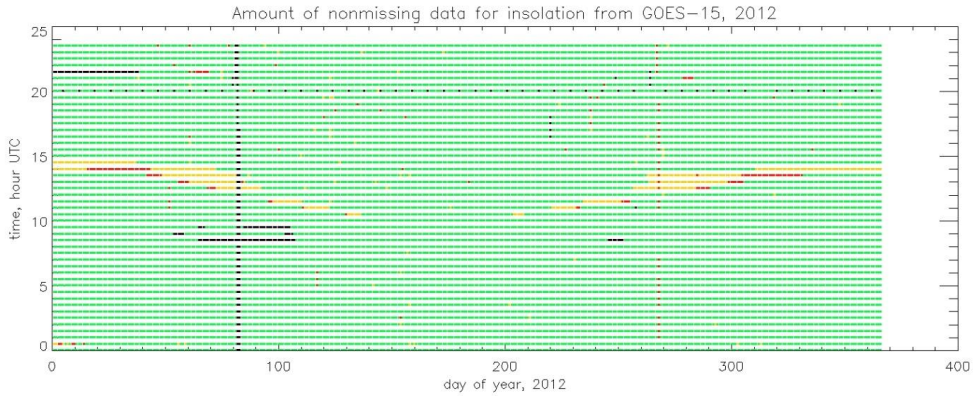

Figure 1 Amount of non-missing insolation data for GOES-15 (WEST) processed during 2012.

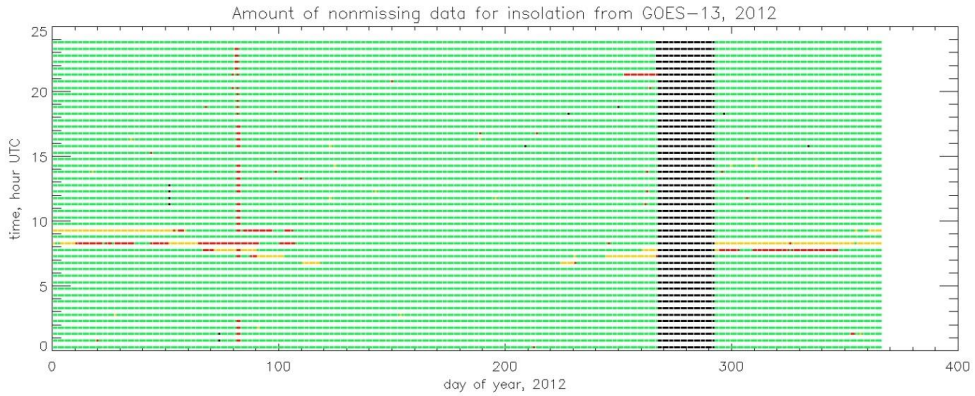

Figure 2 As above, but for GOES-13 (EAST), 2012.

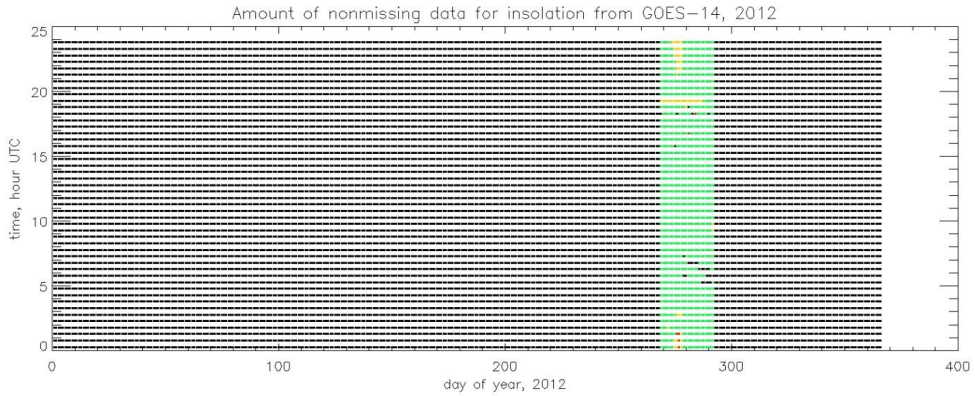

Figure 3 As above, but for GOES-14 (EAST fill-in), 2012.

3.2. Statistics

The statistics for a linear least squares fit and the root mean squared error (RMSE) were computed between the PATMOS-x (SASRAB algorithm) and SURFRAD quantities of global horizontal irradiance (GHI, known as insolation in the level2 files), direct normal irradiance (DNI, computed from insolation, diffuse, and solar zenith angle in the level2 files) and diffuse irradiance. GOES-WEST data are compared to SURFRAD observations at sites Fort Peck, MT (fpk), Boulder, CO (tbl), and Desert Rock, NV (dra). GOES-EAST data are compared to sites Bondville, IL (bon), Goodwin Creek, MS (gwn), Penn State, PA (psu), and Sioux Falls, SD (sxf). SURFRAD observations used were a mean of all data within 5 minutes of the satellite pixel acquisition time at the site. Skies are considered clear if the average cloud fraction in PATMOS-x within 10km of the SURFRAD sites is less than 0.1, cloudy if the cloud fraction is greater than 0.9, and partly cloudy otherwise. Table 1 contains the all-site average statistics of slope and RMSE for years 2009 through 2012. The values in the table are single statistics for all data during the entire year, averaged over the seven sites. Performance of PATMOS-x is similar in 2012 to the previous three years.

Comment [CCM1]: Unless specified as Bird (see section 4), all discussions are using the SASRAB algorithm embedded within PATMOS-x.

Comment [CCM2]: 1 minute data were averaged over +/- 5 minutes of satellite acquisition time.

Comment [CCM3]: 2009 had transcription errors. Fixed. Also added discussion about why the slopes for all sky in some case are larger than each of the separate sky conditions.

Table 1 Statistics for seven SURFRAD sites for entire year under different sky conditions. Slope is the least squares fit slope between the PATMOS-x computed quantity and that observed at each SURFRAD site, subsequently averaged over all sites. RMSE is the root mean squared error (Wm^{-2}) between the PATMOS-x computed quantity and that observed at the SURFRAD site, subsequently averaged over all seven sites.

		All Conditions		Clear		Partly Cloudy		Cloudy	
Quantity	Year	Slope	RMSE	Slope	RMSE	Slope	RMSE	Slope	RMSE
GHI	2009	0.83	105	0.88	73	0.73	130	0.81	109
GHI	2010	0.82	106	0.87	71	0.71	134	0.79	112
GHI	2011	0.82	103	0.88	75	0.73	126	0.78	110
GHI	2012	0.82	102	0.87	72	0.72	129	0.80	107
DNI	2009	0.67	243	0.61	221	0.34	282	0.50	227

DNI	2010	0.66	244	0.50	222	0.30	289	0.51	225
DNI	2011	0.67	246	0.53	240	0.36	277	0.53	219
DNI	2012	0.68	240	0.51	222	0.35	278	0.49	223
Diffuse	2009	0.90	85	1.00	65	0.97	92	0.96	86
Diffuse	2010	0.85	88	0.94	69	0.92	95	0.89	90
Diffuse	2011	0.85	85	0.96	68	0.90	89	0.89	87
Diffuse	2012	0.91	83	1.07	67	0.98	89	0.96	84

Note that in the table above there are some seemingly strange results in which the slope of the fit for all conditions is closer to 1.0 than is the slope of the fit for each of the individual sky conditions. This can be explained by the fact that for the individual sky conditions, the clusters of points have a more horizontal shape, while taking all the points together, the entire cluster has a shape more along the 1:1 line. Figure 4 through Figure 6 show the fit of all sky condition data for the 2012, with clear, partly cloudy, and cloudy symbols. The shape of the clusters can be seen in these plots. Take particular note of the station dra for DNI, where one can see that the individual sky state clusters are of a different orientation than all of the points together. Table 2 contains the statistics of average error (PATMOS-x minus SURFRAD) and the average percent error. Here one can also see that in some cases, the mean error is of opposite sign as the percent error, which also is indicative somewhat of the shape of the cloud of points.

Comment [CM4]: Since I was a little uncertain of the definition of mean bias error based on internet definitions, I gave you both mean error and mean percentage error. Probably you consider one or the other to be mean bias error, so you can choose the one you prefer. I find it interesting how common these two statistics have opposite signs!

Table 2 Additional statistics for seven SURFRAD sites for entire year under different sky conditions. Mean Error (Wm^{-2}) is the mean error between the PATMOS-x computed quantity and that observed at each SURFRAD site, subsequently averaged over the seven SURFRAD sites. Mean % Error is similar, but is the percentage error that is averaged at each site and subsequently over the seven sites.

		All Conditions		Clear		Partly Cloudy		Cloudy	
Quantity	Year	Mean Error	Mean % Error	Mean Error	Mean % Error	Mean Error	Mean % Error	Mean Error	Mean % Error
GHI	2009	-26	9	-38	-4	-33	8	-9	-19
GHI	2010	-26	10	-38	-4	-34	7	-7	25
GHI	2011	-25	12	-42	-5	-30	8	-4	28
GHI	2012	-24	12	-40	-4	-29	7	-2	28
DNI	2009	-114	181	-141	4	-124	257	-57	357
DNI	2010	-105	232	-128	26	-114	374	-48	481
DNI	2011	-107	204	-138	22	-98	296	-51	435
DNI	2012	-109	167	-128	0	-106	253	-63	385
Diffuse	2009	29	34	42	50	44	33	10	15
Diffuse	2010	29	39	41	55	40	31	10	20
Diffuse	2011	31	41	40	53	34	30	15	24
Diffuse	2012	36	42	42	51	40	30	21	27

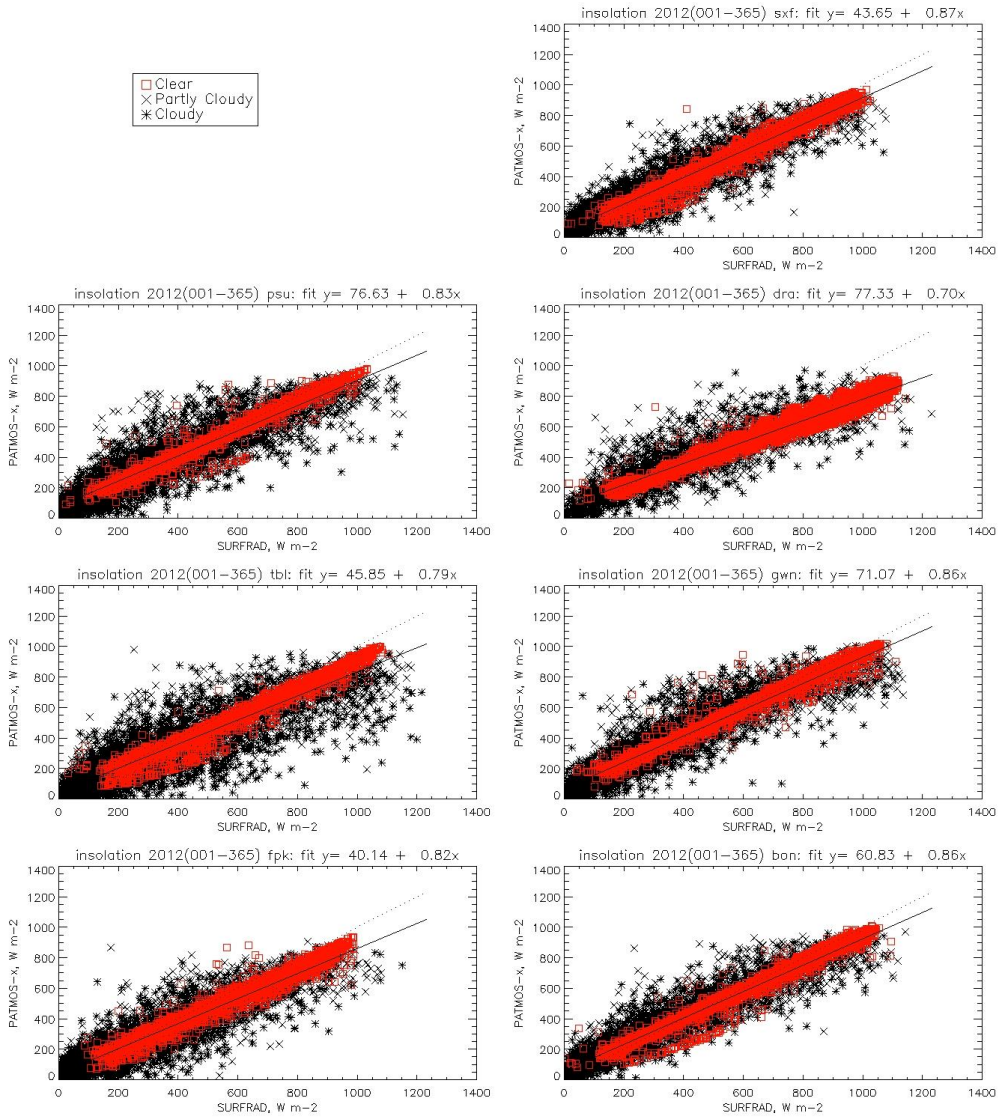

Figure 4 Relationship between PATMOS-x calculated GHI and SURFRAD observed by site for 2012. Solid line is the line of least squares fit (see fit terms atop frames). Dotted line is the 1:1 line.

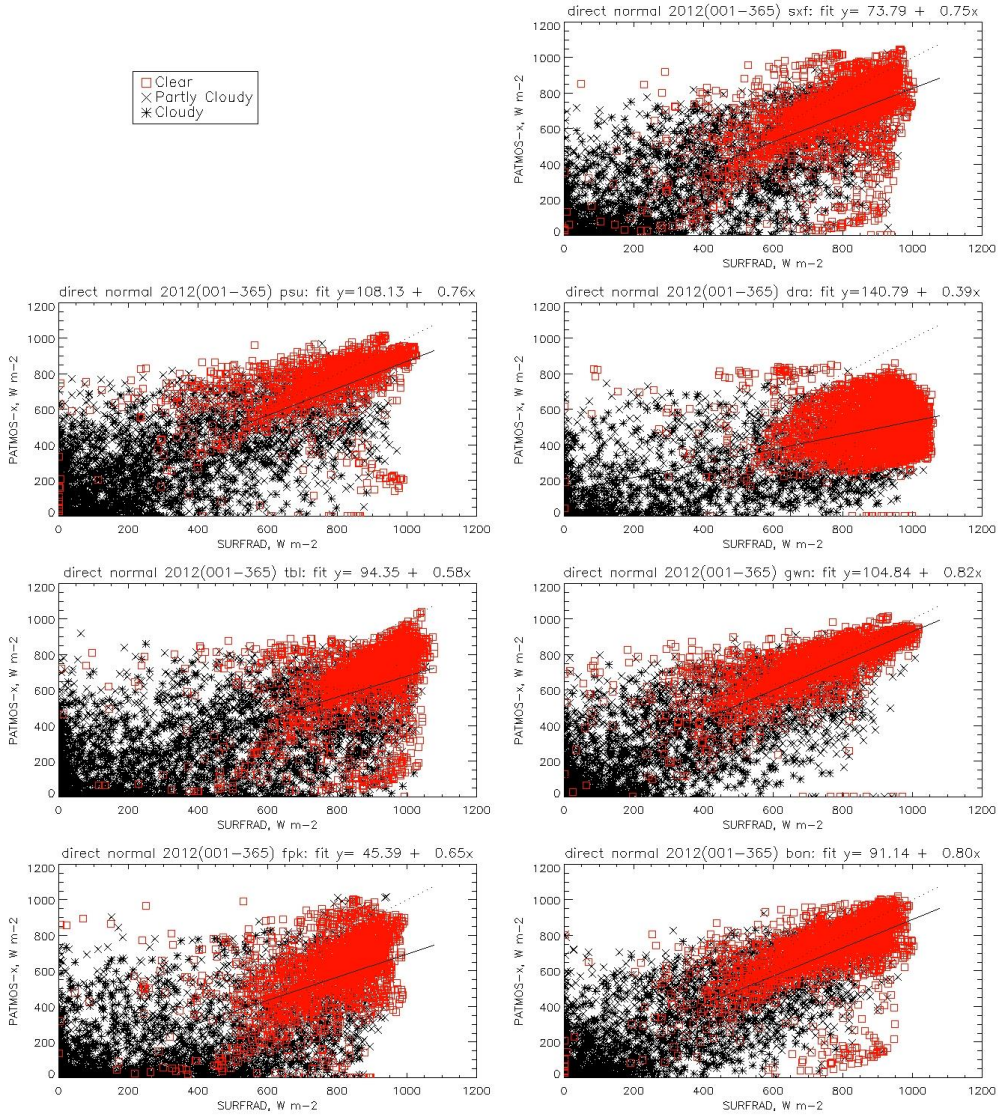

Figure 5 As above, but for direct normal irradiance.

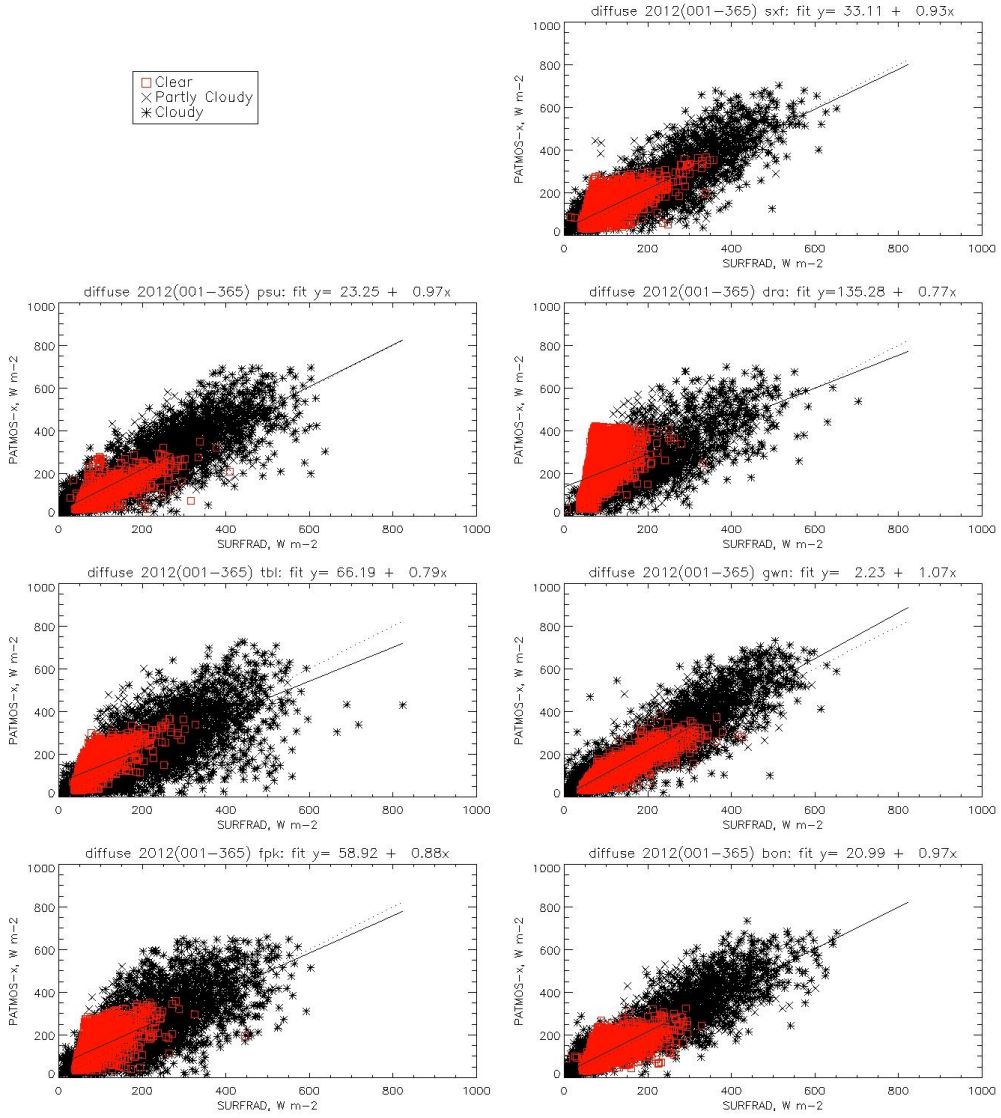

Figure 6 As above, but for diffuse irradiance.

4. Real Time Analysis

During the period of this contract, a real-time analysis of GOES-WEST and -EAST was run on a continuous basis. The real-time processing differs from the processing of data in the past in several ways. Firstly,

the latest version of the algorithm is used. This is referred to as CLAVR-x (as opposed to when the algorithm is used in the past and is referred to as PATMOS-x). At this time, CLAVR-x, the real-time algorithm does not differ significantly from the version of PATMOS-x used for the 2012 analysis for the purposes of GHI, DHI, and DNI. Slight differences may exists in whether a pixel is classified as probably or confidently clear/cloudy, as there are small differences in thresholds in the latest version. More significant differences are due to the differing NWP data source. PATMOS-x uses CFSR, while the real-time CLAVR-x uses GFS. GFS is used for real-time because it is quickly available. It takes some time for the CFSR NWP files to be produced – not soon enough to be used in a real-time processing stream. When GFS NWP fields are used, the grids are interpolated between the two closest 12 hour forecasts – that analysis is not used (due to it being too old by the time the fields are available). When CFSR fields are used in PATMOS-x, the data are interpolated from the 6 hour forecasts produced 4 times daily. As they are 6 hours forecasts forward from delayed analyses (more opportunity for quality control on observations), the fields are believed to better represent actual conditions.

Real-time level 2 files are available from http://cimss.ssec.wisc.edu/clavr/google_earth_main.html, either in level2 format (all variables), or in graphical form (html or Google Earth, selected variables).

5. Alternative Clear Sky Algorithm

In an effort to improve the irradiance products computed from satellite, an alternative model for clear sky irradiance was used to compute GHI under clear skies at the seven SURFRAD sites. This computation of GHI primarily used data taken at the SURFRAD sites at the same time as the PATMOS-x level2 products. The algorithm used was Bird and Hulstrom (1981), henceforth referred to as Bird. Bird requires the following variables to compute GHI: solar constant, aerosol absorptance, forward scattering coefficient, surface albedo, precipitable water depth, aerosol optical depths (AOD) at 380 and 500 nm, ozone depth, and solar zenith angle. Constants provided by P. Gotseff (personal communication, 2013) were used for solar constant, aerosol absorptance, forward scattering coefficient. All other inputs for Bird were taken from available SURFRAD measurements, except for solar zenith angle and (for one of the Bird computations) precipitable water. These were taken from the PATMOS-x level2 files. The PATMOS-x precipitable water comes from the CFSR numerical weather prediction (NWP) grids. Aerosol optical depths at 380 and 500 nm were derived from the aerosol optical depths nearest to 500 and 868 nm according to Appendix A of Sengupta and Gotseff (2013). [Note: this analysis was originally to have been computed using aerosol climatology grids computed by C. Gueymard and provided by P. Gotseff. However, P. Gotseff communicated that the alpha component that is used to compute AOD at other wavelengths was poorly behaved. Therefore, observed AOD values were used for this analysis and not the Gueymard values.] Daily average values were used for aerosol optical depths and ozone. Clear skies were identified by SURFRAD clear fraction from the "SWF" files in the "clearid_old" folder at the SURFRAD data download site, which use Long and Ackerman (2000).

Two versions of Bird GHI under clear skies were computed, one using precipitable water (PW) from NWP, and one using PW calculated from surface relative humidity and air temperature (Gueymard, 1993). The NWP version is more similar to what the results would be if Bird were implemented in

PATMOS-x. The Rh/Temp version conveys what increases or decreases in accuracy might be achieved if observed surface data were used to compute PW.

Results for the PW version are shown in Figure 7. A modest level of improvement in the GHI fit is apparent with the switch from the PATMOS-x SASRAB algorithm to Bird. The level of improvement is similar for most sites. The one site at which we see a large improvement by switching to Bird is DRA, Desert Rock, NV, a site at which the SASRAB algorithm has always had problems due to the bright surface. On average, using the Bird algorithm improves the slope of the fit at the seven SURFRAD sites from 0.90 to 0.92, but the intercept goes from 19.07 to 46.07 W/m^2.

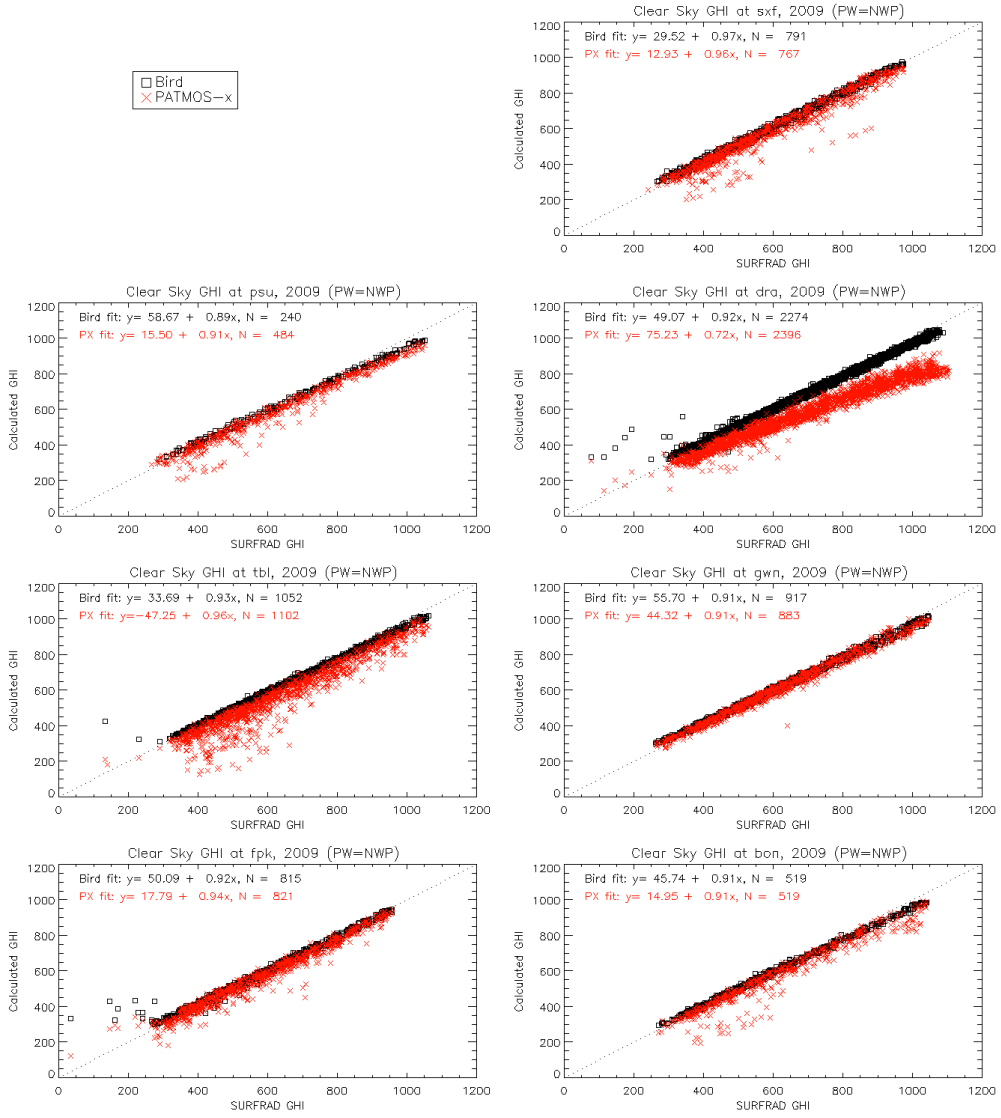

Figure 7 Clear sky GHI using Bird and PATMOS-x at seven SURFRAD sites. Units are W/m^2.

Table 3 contains the RMSE and R^2 values and Table 4 contains the mean error and mean percent error for the four methods in comparison to SURFRAD observed GHI: 1) PATMOS-x is compared to SURFRAD when SURFRAD indicates clear; 2) PATMOS-x is compared to SURFRAD when both SURFRAD and PATMOS-x indicate it is clear; 3) Bird GHI using NWP PW is compared to SURFRAD when SURFRAD indicates it is clear; and 4) Bird GHI using PW calculated from observed surface RH and air temperature is compared to SURFRAD when SURFRAD indicates it is clear. PATMOS-x shows a slight improvement

when both SURFRAD and PATMOS-x agree it is clear compared to using only SURFRAD to classify clear skies. Both Bird methods are substantially better than PATMOS-x in terms of RMSE, R^2, mean error and mean percent error. The Bird method using observed surface RH and Air temperature to compute PW is slightly better on average than that using PW from NWP.

Table 3 Statistics for three methods of computing clear sky GHI against observations at seven SURFRAD sites. Clear skies are identified from SURFRAD observations. All methods use only SURFRAD observations to identify clear skies, except for PATMOS-x Both Clear, for which skies are considered clear only if both PATMOS-x cloud fraction is zero and SURFRAD observations indicate clear. Units for RMSE are W/m^2.

	PATMOS-x		PATMOS-x Both Clear		Bird NWP		Bird Rh/Temp	
Site	RMSE	R^2	RMSE	R^2	RMSE	R^2	RMSE	R^2
BON	62.32	0.94	62.86	0.94	21.32	1.00	17.35	1.00
FPK	37.10	0.97	31.20	0.98	25.85	0.98	25.33	0.99
GWN	28.16	0.99	27.61	0.99	20.46	1.00	18.97	1.00
TBL	92.70	0.92	78.22	0.94	22.73	1.00	24.19	1.00
DRA	134.18	0.96	133.87	0.97	23.85	0.99	23.54	0.99
PSU	56.93	0.96	56.53	0.96	28.47	1.00	20.72	1.00
SXF	46.42	0.94	45.22	0.94	18.49	0.99	20.39	1.00
Average	65.40	0.95	62.22	0.96	23.02	0.99	21.50	1.00

Table 4 As above, but mean error and mean percent error, PATMOS-x or Bird minus observed SURFRAD GHI.

	PATMOS-x		PATMOS-x Both Clear		Bird NWP		Bird Rh/Temp	
Site	Mean Err	Mean % Err	Mean Err	Mean % Err	Mean Err	Mean % Err	Mean Err	Mean % Err
BON	-39	-6	-40	-6	-8	0	-2	0
FPK	-17	-2	-16	-2	6	3	8	4
GWN	-10	-1	-9	-1	0	1	3	1
TBL	-75	-12	-65	-11	-14	-2	-15	-2
DRA	-117	-16	-117	-15	-4	0	-2	1
PSU	-40	-6	-40	-6	-15	-1	-4	0
SXF	-13	-2	-12	-2	12	3	16	3
Average	-44	-6	-43	-6	-3	1	0	1

If the Bird algorithm were to be inserted into PATMOS-x, the DCOMP cloud transmission variable is available to compute GHI under cloudy skies. A method to separate the direct and diffuse components would need to be added. Data sources for correct surface albedo and aerosol optical depths at 380 and 500 nm (or converted from values at other wavelengths) would be required as well. The expected improvement, based on the averaging of results at the seven SURFRAD sites, would be a decrease in RMSE of about 42 W/m^2, an increase in correlation of 5%, a decrease in the mean error of about 40 W/m^2, and a decrease in the percent error of about 5%. The slope of the fit would increase from about 0.90 to 0.92, but the intercept would depart more from zero, from 19.07 to 46.07 W/m^2, suggesting more error at lower values of GHI. Also the conditions under which the highest error could be expected would shift away from desert areas.

6. Conclusions and Future Work

A cloud and insolation products analysis of GOES-EAST and -WEST using the SASRAB algorithm in PATMOS-x for 2012 was computed using the same version of PATMOS-x as the previous 2005-2011 data set. The analysis yielded a data set of GHI, DNI (derived) and diffuse irradiance statistically very similar to the previous analysis. In general, GHI and the diffuse irradiance show the best relationship with observations at SURFRAD sites and DNI the worst. The relationship with observations is also best under completely clear and completely cloudy skies. A real-time analysis is also being produced using an updated version of the code.

Exploring the use of the Bird and Hulstrom (1981) algorithm, indicated that improvements can be made in the clear sky GHI if ancillary data related to albedo and AOD are available for the computation. Improvements would be most significant at desert sites. This algorithm could be implemented in PAMTOS-x using the DCOMP cloud transmission variable and some method of separating the diffuse and direct components of irradiance.

Higher resolution insolation products from NOAA are possible. Even though the lower resolution GSIP is the current official product, there is a process for requesting changes to the official satellite products. The Satellite Products and Services Review Board (SPSRB) is in charge of receiving requests and making recommendations to the official products. The SPSRB web site is http://projects.osd.noaa.gov/SPSRB/index.htm. According to the document at the SPSRB web site link "SPSRB Policy for FY10 Satellite Product Development", all user requests can be submitted at the new SPSRB web page located at hnps://reguesttracker.osd.noaagov/admin_login.asp. Requests will be considered only from government employees with valid .gov or .mil email addresses and all requests need a NOAA advocate/champion." If not done so at this time, NREL should consider working with Andrew Heidinger to request improved surface radiation products for current and future GOES real time products.

7. Acknowledgements

This work was supported by Alliance for Sustainable Energy, LLC, Management and Operating Contractor for the National Renewable Energy Laboratory under subcontract AXL-3-23362-01.

8. References

Bird, R.E. and R.L. Hulstrom, 1981. A simplified clear sky model for direct and diffuse insolation on horizontal surfaces. SERI/TR-642-761, Solar Energy Research Institute, Golden, CO, USA, February 1981.

Gueymard, Christian, 1993. Assessment of the Accuracy and Computing Speed of Simplified Saturation Vapor Equations Using a New Reference Dataset. J. Appl. Meteor., 32, 1294–1300.

Heidinger, A.K., and C.C. Molling, 2011. Surface Radiation Datasets from Geostationary Satellites Subcontract AXL-0-40276-01 Final Report (November 2011 revision).

Long, C.N., and T.P. Ackerman, 2000. Identification of clear skies from broadband pyranometer measurements and calculation of downwelling shortwave cloud effects. Journal of Geophysical Research 105, D12, 15609-15626.

Molling, C., A. Heidinger, and S. Ackerman, 2013. Surface Radiation Datasets from Geostationary Satellites Subcontract AXL-0-40276-01 with 9/18/2012 Modification, Final Report. October 2013.

Sengupta, M., and P. Gotseff, 2013. Evaluation of Clear Sky Models for Satellite-Based Irradiance Estimates. NREL/TP-5D00-60735, National Renewable Energy Laboratory, Golden, CO, USA, December 2013.

Appendices

M. Sengupta requested that reports Heidinger and Molling (2011) and Molling et al. (2013) be added as appendices. However, both of these documents themselves have appendices, so the appendices in this document have non-standard lettering. Heidinger and Molling (2011) is added as Appendix AA and Molling et al. (2013) is added as Appendix BB.

Appendix AA

Surface Radiation Datasets from Geostationary Satellites
Subcontract AXL-0-40276-01

Andrew Heidinger, Christine Molling
NOAA NESDIS STAR, UW SSEC CIMSS

Status Report 5 (Final)
Date: September 2011, revised November, 2011

Abstract

The National Renewable Energy Laboratory (NREL) funded the Cooperative Institute for Meteorological Satellite Studies to compute a five-year dataset of surface radiation and ancillary information from geostationary satellites. The Global Solar Insolation Project (GSIP) code was incorporated into the PATMOS-x processing system and was run on GOES-East (GOES 10 and 11) and GOES-West (GOES 10, 12, and 13) imagery during the time span of January 2005 through December 2009. Imagery used was the northern hemisphere and northern hemisphere extended coverages every 30 minutes during each day processed, or full disk coverage when available (every 3 hours). Output consists of 9.2 Tb of level2-style hdf4 files, each containing 60 variables plus attributes at the 4km pixel level. Data were prepared for delivery to NREL via ftp, with the data transfer beginning on September 2, 2011.

Introduction

Increased prices of fossil fuels, the availability of tax credits for alternative energy sources, and a growing market for “green” energy have increased the interest in the power industry to construct solar-based power plants. In order to properly research the economics, siting, and type (photo voltaic and concentrated solar) of these plants, the industry requires knowledge of long term values and variability in Direct Normal Irradiance (DNI, or direct beam) and the Global Horizontal Irradiance (GHI, or total insolation). The currently available satellite based solar radiation datasets have been created using empirical and semi-empirical methods. In the project, the goal is to retrieve surface radiation data using

physical methods. Due the complexities of retrieving cloud properties from satellites based measurements in the visible and infrared, the creation of such a dataset requires expertise in satellite remote sensing, significant computer processing resources, including cpus for processing, disk space for file storage, and bandwidth for data transfer.

NREL funded the Cooperative Institute for Meteorological Satellite Studies (CIMSS) at the University of Wisconsin-Madison to create a surface radiation dataset using physical methods. CIMMS had the necessary expertise and resource available to create and deliver the datasets. In particular CIMMS personnel are experts in satellite based retrieval of clouds and radiation. They also have the computer resources required and a local archive of GOES data. The budget was $72,000 and the project was to be completed within one year, starting September 21, 2010.

Algorithm

The Global Solar Insolation Project (GSIP) data is currently available from NOAA's CLASS Archive (1), from January, 2009 to the present. This product consists of hourly images (northern hemisphere, northern hemisphere extended, full disk) at a $1/8^{o}$ x $1/8^{o}$ resolution (2). The algorithm used in GSIP, Satellite Algorithm for Shortwave RAdiation Budget (SASRAB [3]), is widely accepted. Therefore, this algorithm was also chosen to compute the 5 year dataset. GSIP produces GHI, but not DNI, so some modifications of the code would be required to produce both. Additional variables were also requested in order to be able to run alternative radiative transfer models using the same input data as used to produce the insolation products. Unfortunately, the GSIP code is somewhat difficult to modify to create new variables, so the decision was made to extract the portion of the SASRAB algorithm and insert it into another satellite data processing system: the same one used for AVHRR Pathfinder Atmospheres – Extended (PATMOS-x). The latest PATMOS-x is able to process imagery from GOES and MODIS, in addition to AVHRR. Advantages of using the PATMOS-x processing system include

- Ease of adding variables to or subtracting variables from output files
- Ability to produce a wide variety of cloud, atmosphere, and surface variables, some of which were not available in GSIP
- Up-to-date cloud identification and classification routines
- Ability to produce all level1(b) and level2 (4km pixel) output in a single file, with the option to process later at any coarser, gridded resolution
- Ability to use HDF4's internal compression technique to reduce file size and avoid the need to decompress files before reading
- Ability to adapt the algorithm in the future to produce insolation from other satellite instruments, such as AVHRR and MODIS

The SASRAB routine was inserted into the PATMOS-x processing package, tested, and compared to the currently available GSIP product, as well as in situ measurements. Figure 1 is an example plot comparing the three different sources for insolation along with surface observations from the SURFRAD network. Although we see in this figure that PATMOS-x produces GHI similar to NOAA-GSIP, would not expect it to be identical, due to the different time sampling, spatial resolutions, cloud properties, and other ancillary data.

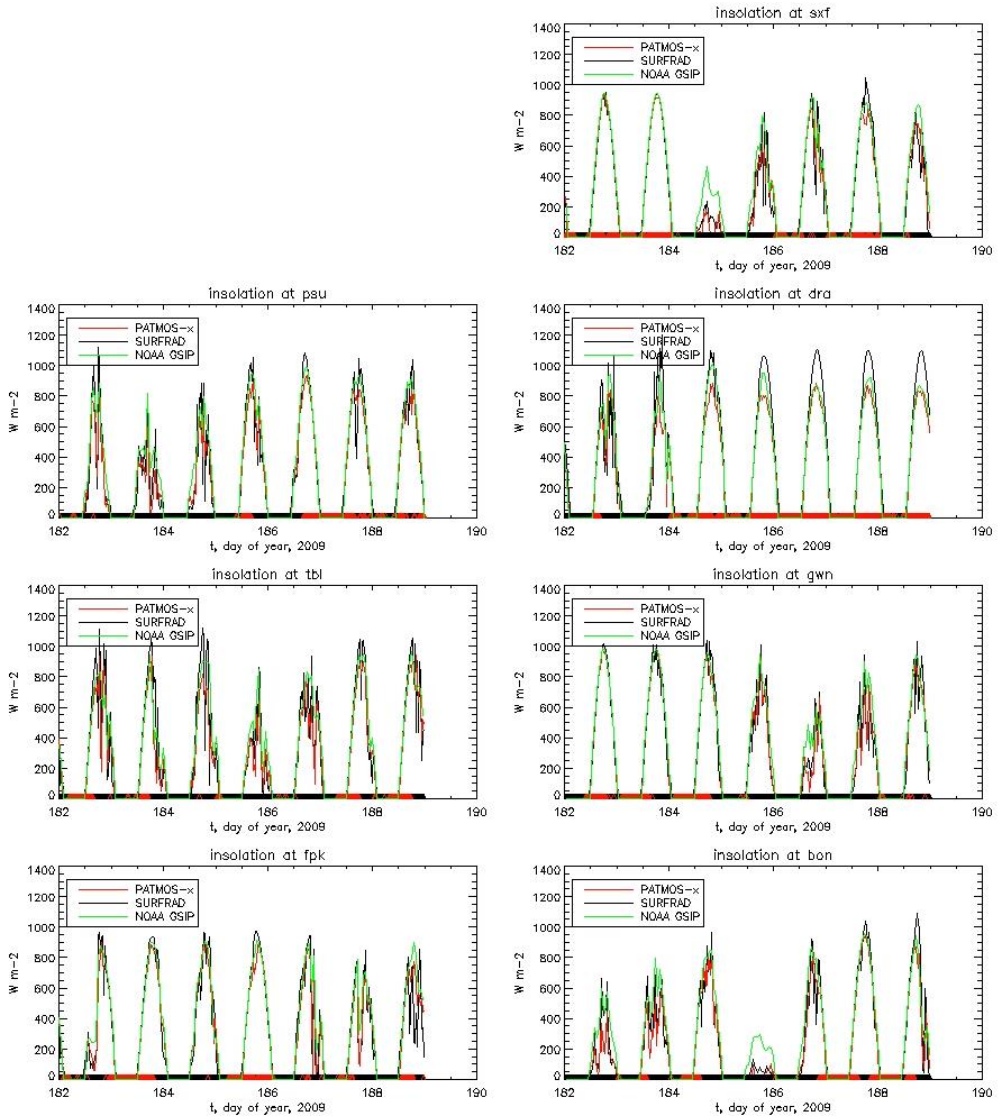

Figure 8. An example comparison of global horizontal irradiance from NOAA GSIP, SURFRAD, and PATMOS-x

Imagery and Ancillary Data

Producing insolation products from GOES imagery requires an archive of not only the GOES images themselves, but ancillary data. Table 1 describes the types, sources, uses, and amounts of data used to produce the 5 years of surface radiation.

Table 5. Inputs used to produce the 5 year insolation dataset.

Data Type	Source	Purpose	Amount (Gb)
GOES imager	CIMSS Archive	Raw counts for radiance and temperature	3824
Precipitable water; wind speed	GFS model, NOMADS archive	Radiative transfer model; requested by NREL	204
Snow and ice mask	GlobSnow, Finnish Met. Institute Archive	Cloud detection, surface properties	3
GOES dark sky_composite	CIMSS, calculated from GOES imagery	Surface albedo	334

The GOES imagery used consisted of all available Northern Hemisphere and Northern Hemisphere Extended images occurring every 30 minutes, except at times when Full Disk was scheduled. Full Disk imagery was used at those times. Table 2 lists the acquisition schedule for GOES-EAST and -WEST.

Table 6. Schedule for GOES imagery used for 5 year insolation dataset.

Imager Coverage	GOES-WEST Schedule, UTC	GOES-EAST Schedule, UTC
Northern Hemisphere GOES-WEST only) or Northern Hemisphere Extended (GOES-EAST only)	00:30, 01:00, 01:30, 02:00, 02:30, 03:30, 04:00, 04:30, 05:00, 05:30, 06:30, 07:00, 07:30, 08:00, 08:30, 09:30, 10:00, 10:30, 11:00, 11:30, 12:30, 13:00, 13:30, 14:00, 14:30, 15:30, 16:00, 16:30, 17:00, 17:30, 18:30, 19:00, 19:30, 20:00, 20:30, 21:30, 22:00, 22:30, 23:00, 23:30	00:15, 00:45, 01:15, 01:45, 02:15, 03:15, 03:45, 04:15, 04:45, 05:15, 06:15, 06:45, 07:15, 07:45, 08:15, 09:15, 09:45, 10:15, 10:45, 11:15, 12:15, 12:45, 13:15, 13:45, 14:15, 15:15, 15:45, 16:15, 16:45, 17:15, 18:15, 18:45, 19:15, 19:45, 20:15, 21:15, 21:45, 22:15, 22:45, 23:15
Full Disk	0:00, 3:00, 6:00, 9:00, 12:00, 15:00, 18:00, 21:00	2:45, 5:45, 8:45, 11:45, 14:45, 17:45, 20:45, 23:45

The PATMOS-x processing package was run on each of the GOES image files available during the period January, 2005 through December, 2009. GOES-WEST, which covers the central Pacific Ocean to the east coast of the United States, started as GOES-10, and switched to GOES-11 during 2006. GOES-EAST, which covers the eastern Pacific Ocean through the central Atlantic Ocean, was predominantly GOES-12. However, GOES-12 malfunctioned for one period during December, 2007 and again from December, 2008 through January, 2009. During this period, other satellites were used to fill in for GOES-12. Table 3 lists which satellites were used as -WEST and -EAST for the dataset.

Table 3. Satellites serving as GOES-EAST and -WEST for the 5 year insolation dataset.

Year	WEST Satellite	WEST days of service (day of year)	EAST Satellite	EAST days of service (day of year)
2005	GOES-10	1-365	GOES-12	1-365
2006	GOES-10 GOES-11	1-151 152-365	GOES-12	1-365
2007	GOES-11	1-365	GOES-12 GOES-10 GOES-12	1-338 339-351 352-365
2008	GOES-11	1-366	GOES-12 GOES-13	1-335 336-366
2009	GOES-11	1-365	GOES-13 GOES-12	1-20 21-365

Output Produced

The PATMOS-x processing routine was run on each GOES imagery file available. For each image file, one output file is produced in HDF4 format. Each file is named to indicate the satellite, date, and time. For example, the file name *goes11_2006_152_2230.level2.hdf* specifies that the data in this file comes from GOES-11 imagery acquired in 2006 on day of year 152, starting at 22:30 UTC. The data within is level 2, which is information derived from instrument counts at the thermal pixel resolution (nominally 4km x 4km at the equator). Figures 2a and b are examples of GHI from GOES-WEST on the full disk and northern hemisphere coverages. Figures 3a and b are GHI from GOES-EAST on the full disk and the northern hemisphere extended coverages.

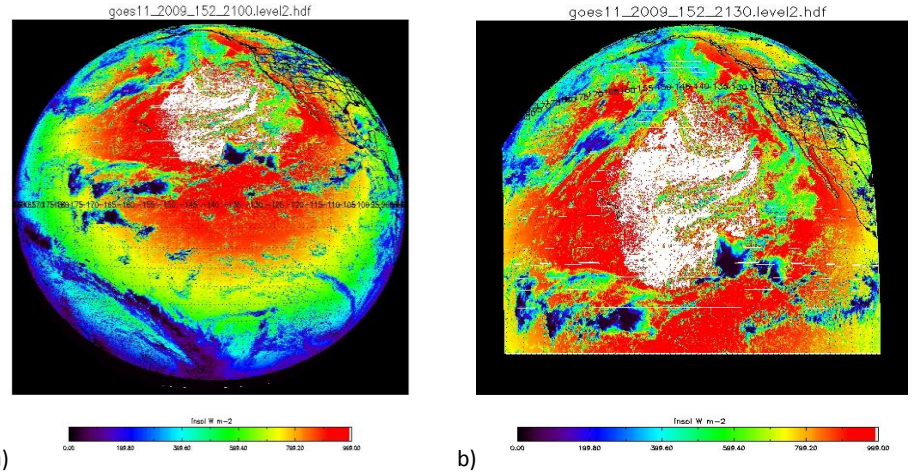

Figure 9. Examples of global horizontal irradiance calculated in the PATMOS-x framework from GOES-WEST data. Panel a) is full disk coverage and panel b is northern hemisphere coverage.

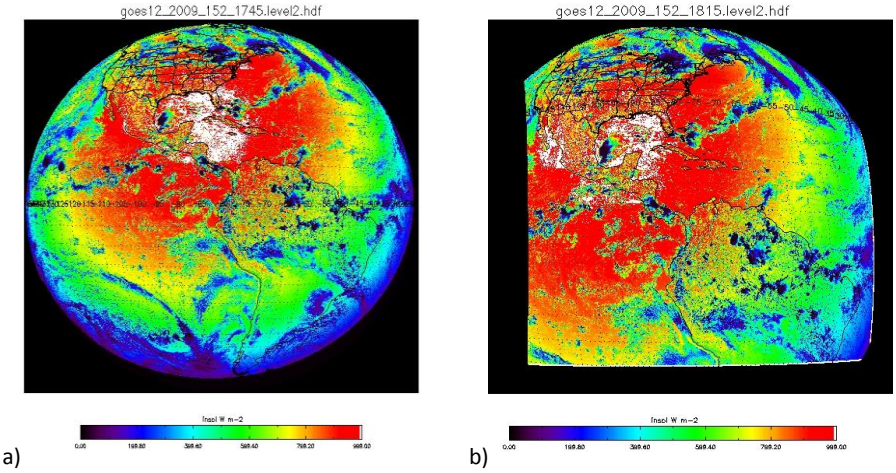

Figure 10. Examples of global horizontal irradiance calculated in the PATMOS-x framework from GOES-EAST data. Panel a) is full disk coverage and panel b is northern hemisphere extended coverage.

Each file generally contains the same variables and metadata — a total of up to 60 variables plus attributes for each variable (depends on satellite). Appendix A lists a sample header dump from one file, listing all the variable names and their attributes. All variables are produced from algorithms imbedded within the PATMOS-x processing system. Algorithms include the Bayesian cloud mask, ACHA for cloud height, and DCOMP for cloud optical properties.

The SASRAB algorithm within PATMOS-x is responsible for calculating the output variables *insolation* and *insolation_diffuse*. *Insolation* is the total surface downwelling shortwave flux, which is also known as Global Horizontal irradiance (GHI). SASRAB also produces *insolation_diffuse*, the diffuse component of the GHI. SASRAB does not calculate direct normal irradiance (DNI), and so this variable is not included in the output files. However, DNI can be easily computed using the variables *insolation*, *insolation_diffuse*, and *solar_zenith_angle*, using the equation

DNI=(insolation – insolation_diffuse)/cos(solar_zenith_angle*PI/180.)

The insolation variables are valid for solar zenith angles (SZA) from 0. (sun at zenith) to 78.4^{o} (sun 11.6^{o} above horizon). At SZAs greater than 78.4^{o}, the insolation variables are set to 0.79 – consider this minimum value to be zero. In space, or in areas where the data needed to produce insolation are missing, the insolation variables are set to the missing value, which is -999.

Notes of Caution

There are several notes of caution. Firstly, due to the differing information contained in the GOES image files over time, some variables are not contained in all files, namely *temp_12_0um_nom*, *scan_line_number*, *scan_line_time*, and *bad_scan_line_flag*. As there are different numbers of variables in the files, it is best to write any analysis software to refer to variable names, rather than indices.

Secondly, the variable *bad_scan_line_flag*, even if present, is not valid for GOES, and should be ignored. Lastly, not all non-SASRAB variables consistently have the missing value in space or when information is not present for their calculation. Each variable should be checked to determine how to identify space or non-valid values.

Analysis

Figures 4-17 are quicklook depictions of the availability of the insolation product during the 5 year period. Figures 4-9 are GOES-WEST, and figures 10-17 are GOES-EAST. A square is present for each expected image time. A **black** square indicates that no file is present for that satellite at that time. A **green** square indicates that a file is present and more than 99% of the earth pixels have a valid insolation calculation. A **yellow** square indicates that at least 95%, but less than 99% of the pixels have a valid insolation calculation. **Red** indicates that less than 95% of the pixels have a valid insolation calculation. A common pattern emerges from studying these quicklooks. Besides the semi-random nature of lower quality images due to transmission errors, satellite/instrument ageing, and malfunction, one can clearly see the large data gaps (black shapes) due to the eclipse periods in spring and fall. The limited storage of the batteries on board GOES-10 through GOES-12 cause these unrecoverable data gaps. The "wings" of red and yellow squares in fall through spring are produced by a line of missing reflectances in the southernmost row and easternmost row in the northern hemisphere and northern hemisphere extended coverages. When there are few daylight pixels, these missing pixels cause the percent of bad pixels to be large. The missing reflectances are merely due to the method used to compute the visible band average at the thermal band resolution.

GOES-WEST

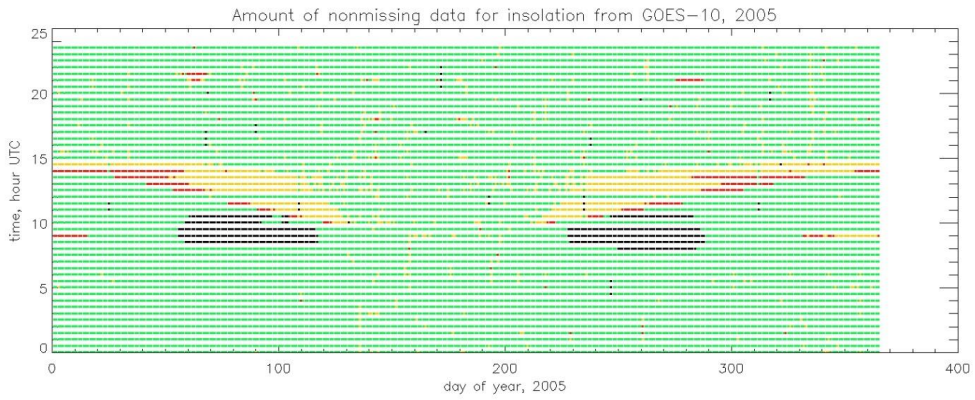

Figure 11. Availability of insolation computed from GOES-10, which served as GOES-WEST during 2005.

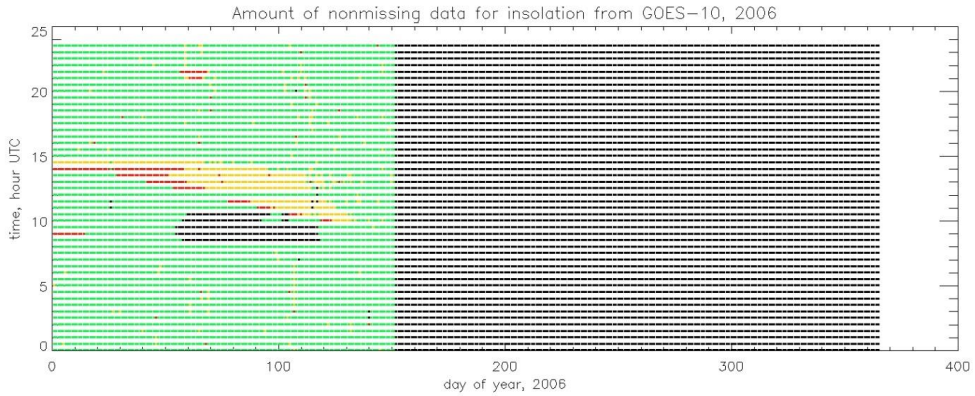

Figure 12. As above, but for GOES-10 during 2006.

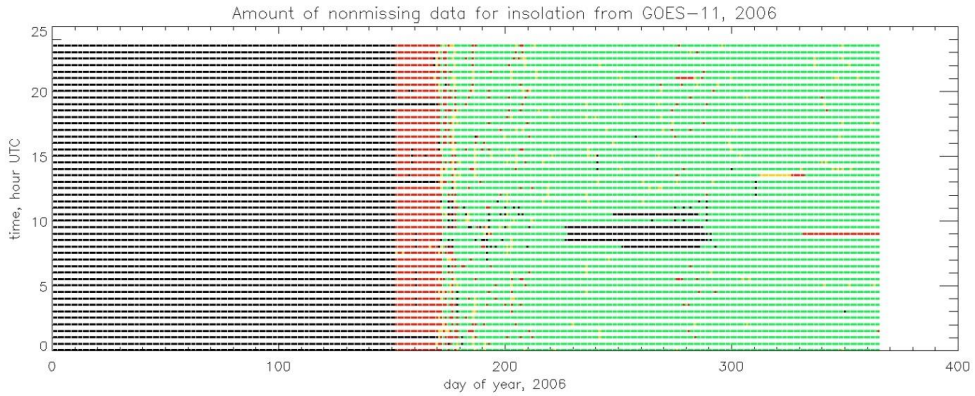

Figure 13. As above but for GOES-11 during 2006.

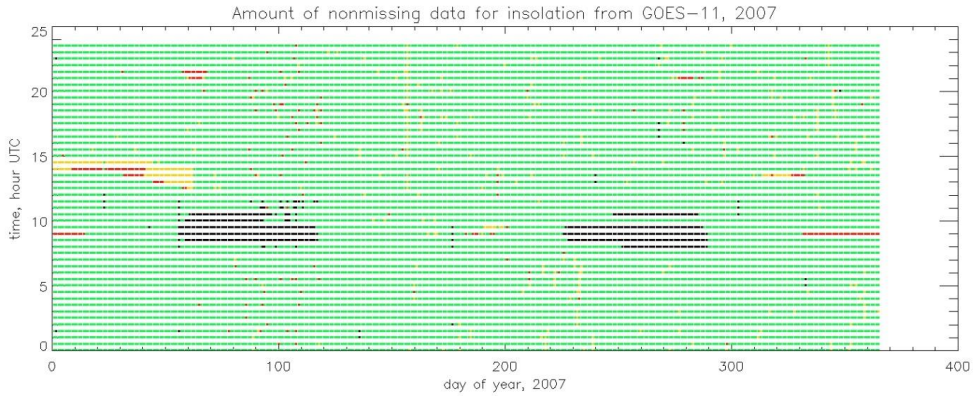

Figure 14. As above but for GOES-11 during 2007.

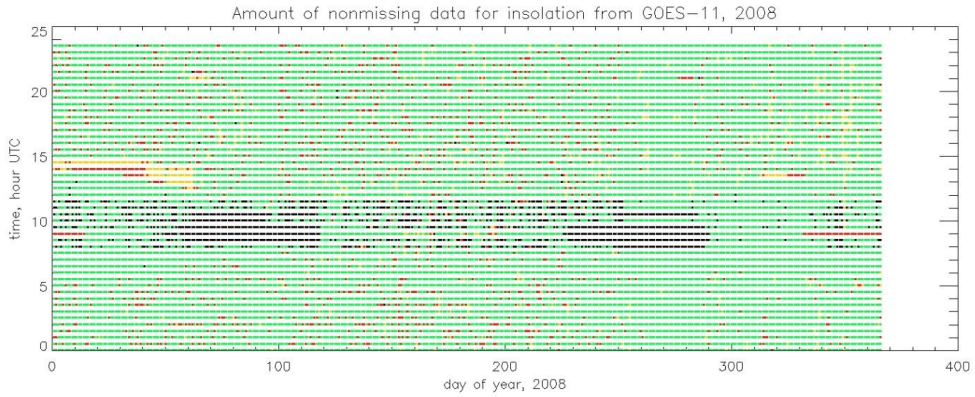

Figure 15. As above but for GOES-11 during 2008.

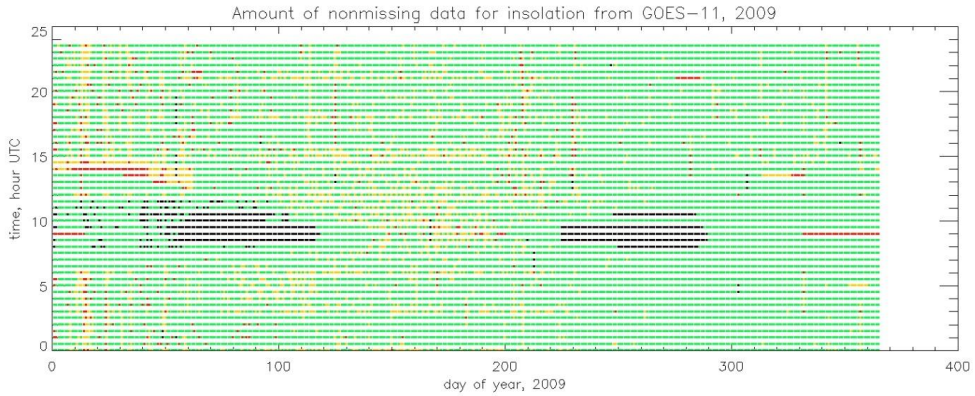

Figure 16. As above but for GOES-11 during 2009.

GOES-EAST

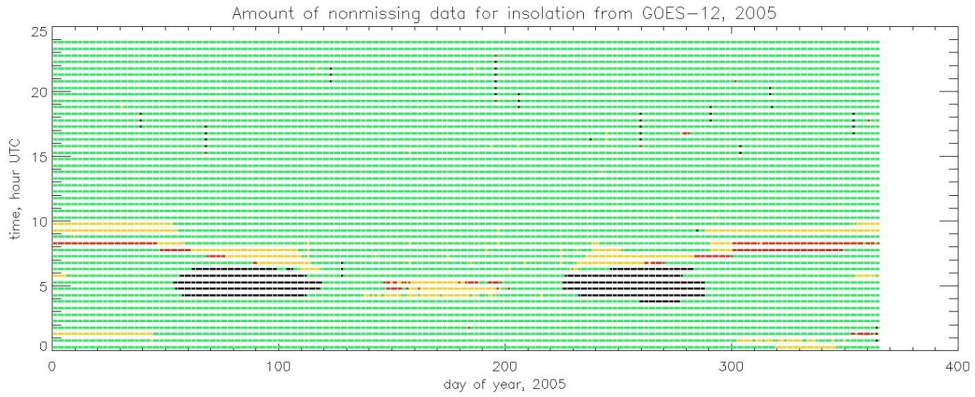

Figure 17. Availability of insolation computed from GOES-12, which served as GOES-EAST during 2005.

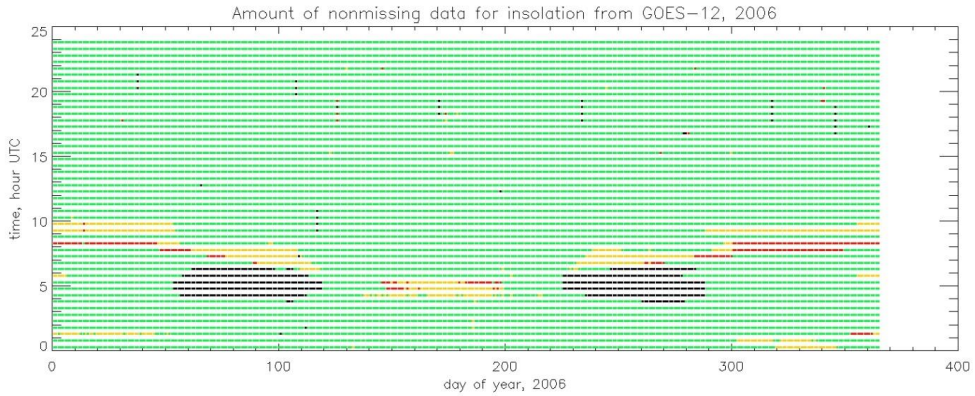

Figure 18. As above, but for GOES-12 during 2006.

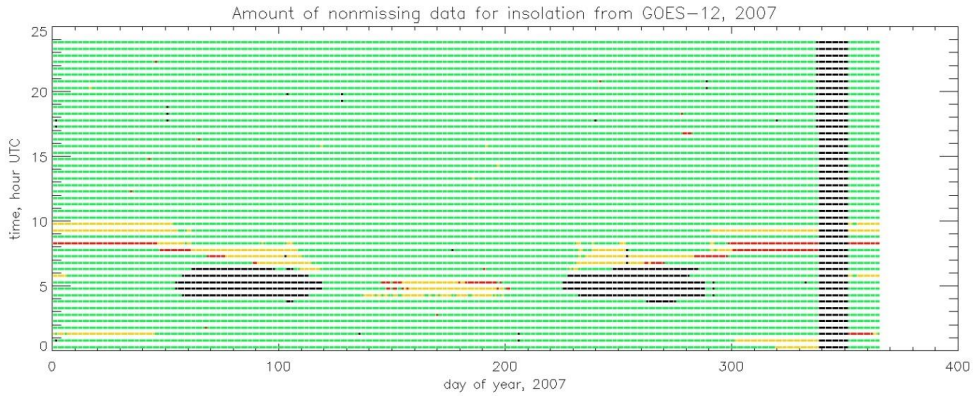

Figure 19. As above, but for GOES-12 during 2007.

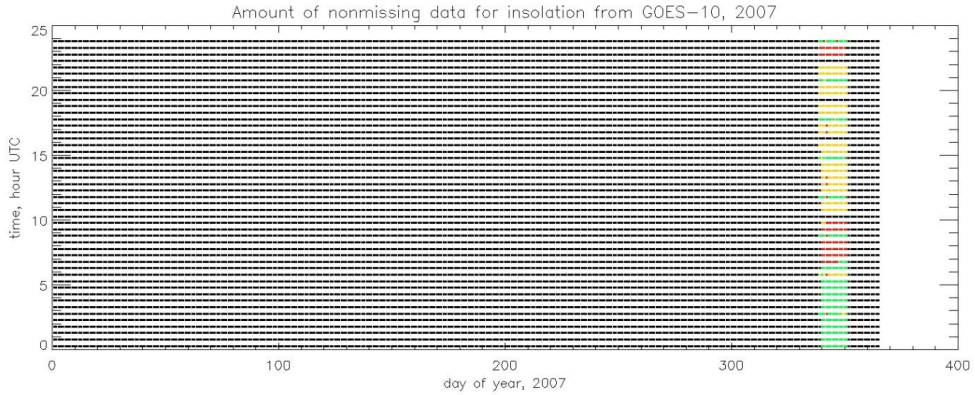

Figure 20. As above, but for GOES-10 during 2007.

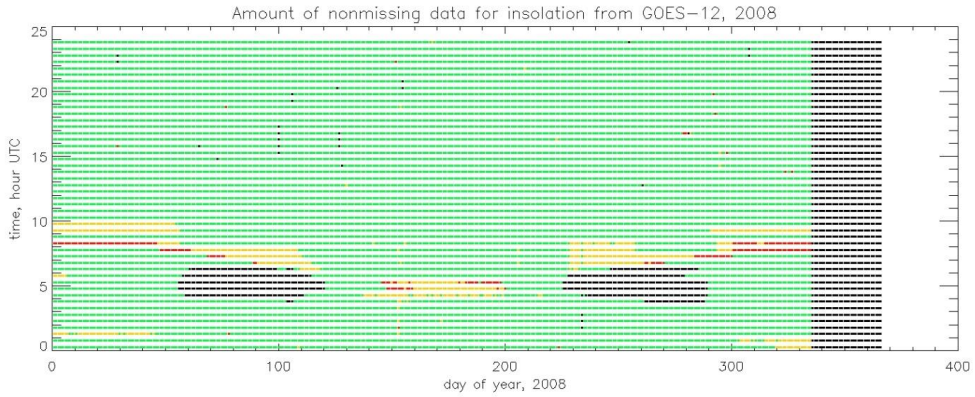

Figure 21. As above, but for GOES-12 during 2008.

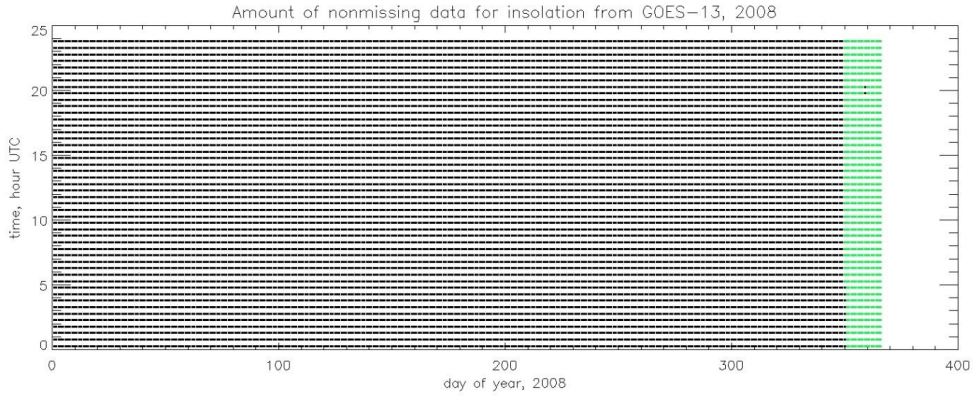

Figure 22. As above, but for GOES-13 during 2008.

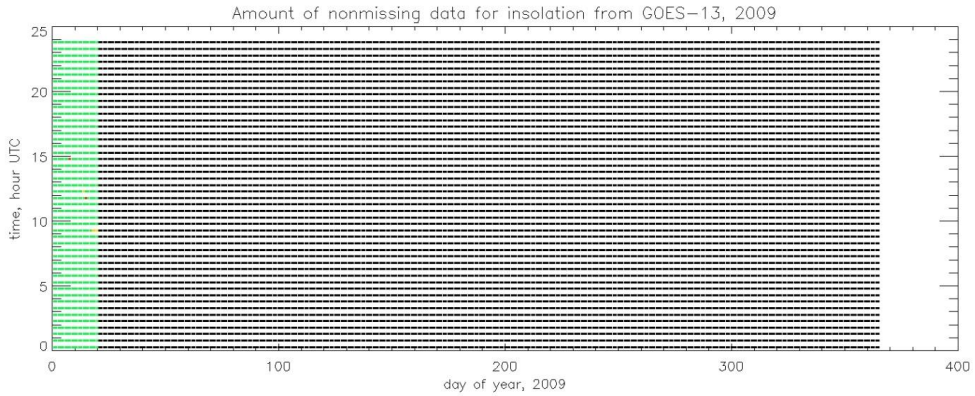

Figure 23. As above, but for GOES-13 during 2009.

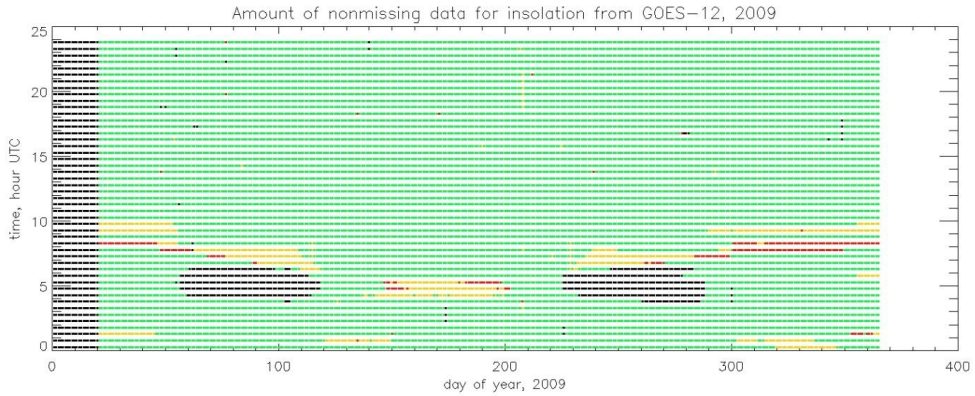

Figure 24. As above, but for GOES-12 during 2009.

To investigate the quality of the insolation calculated by SASRAB from within the PATMOS-x processing system, data were extracted from each file during selected months. These data were averages of *insolation*, *insolation_diffuse*, *solar_zenith_angle*, *surface_temperature_retrieved*, and *cloud_fraction*. The averages were of all 4km pixels within 10 km of the latitude/longitude location of seven SURFace RADiation (SURFRAD) sites (4). This radius resulted in the average of 4 to 11 pixels. The variable *scan_line_time* was also retrieved for one of the pixels, which was then used to compute a ±5 min average centered at the scan line time of *dw_psp* (GHI), *diffuse* (diffuse insolation), *direct* (DNI), and surface temperature (calculated from *uw_pir*, upwelling thermal infrared using a surface emissivity of 0.98) measured in situ. The raw SURFAD data before 2009 were 3 min averages and those from 2009 on were 1 min averages. The ±5 min averages, therefore, were actually as large as 9 min (depending on

exact scan line time) before 2009 and 11 min in 2009. PATMOS-x and SURFRAD averages were then compared.

SURFRAD locations used in the comparisons are Sioux Falls , SD (SXF, Penn State, PN (PSU), Desert Rock, NV (DRA), Table Mountain, CO (TBL), Goodwin Creek, MS (GWN), Fort Peck, MT (FPK), and Bondville, IL (BON). Based on the site photos, landscape and vegetation are shortgrass prairie and some trees at SXF, cropland and wooded low mountains at PSU, desert scrub and mountains at DRA, shortgrass prairie or desert scrub and partially forested mountains at TBL, pasture and woods at GWN, shortgrass prairie and rangeland at FPK, and pasture and crops at BON. Figure 18 shows the locations of the seven SURFRAD sites used in the comparisons. The ARMSGP site, not an official SURFRAD site, was not used. We select the appropriate GOES (WEST or EAST) by using the satellite with the smallest satellite view angle. The cutoff is 105 degrees west longitude. Data from GOES-WEST is used to compare to the SURFRAD stations FPK, TBL, and DRA. Data from GOES-EAST is used to compare to BON, GWN, PSU, and SXF.

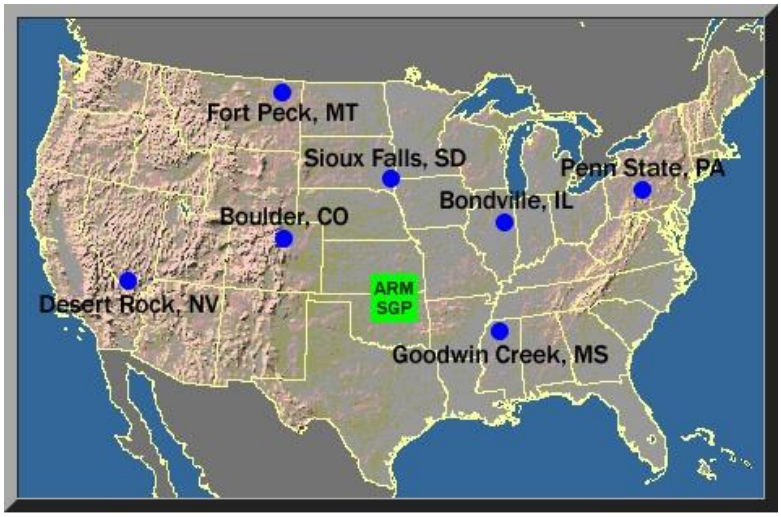

Figure 25. Locations of the seven SURFRAD sites. ARMSGP was not used. Image courtesy of SURFRAD.

The extent to which the SASRAB-based insolation agrees with the SURFRAD insolation depends on a few factors. First of all, the GOES satellites exhibit a small amount of wobble. The navigation provided in the imagery files corrects some, but not all of this wobble. The areal and time averaging of PATMOS-x insolation and SURFRAD insolation, respectively, can correct for some of this. The remaining differences are due mainly to 1) the ability of the GFS precipitable water to accurately represent the amount of water vapor in the atmosphere at the time of interest, and 2) the ability of PATMOS-x cloud algorithms to accurately represent the shadow position, fraction, height, phase, and optical depth of clouds. As precipitable water is not easily inferable from SURFRAD data, the analysis below will concentrate on the effect of accurate cloud portrayal and surface effects on insolation as derived from the GOES imagery.

In Figure 19 below, the total (direct+diffuse) insolation is shown for the seven SURFRAD sites during the first week of July, 2009. The insolation derived from SASRAB in the PATMOS-x processing system is a red line, and that from SURFRAD is a black line. Red and black symbols along the x-axis denote clear (red) skies and cloudy (black) skies as determined by the PATMOS-x cloud fraction. Clear skies are defined as average *cloud_fraction* less than or equal to 0.1, and cloudy skies are *cloud_fraction* greater than 0.9. Partly cloudy skies have no symbol on the x-axis. Looking at times when the skies are identified as clear, Figure 18 suggests that the accuracy of the PATMOS-x insolation is site specific. While the PATMOS-x insolation is a very good match to SURFRAD during clear times at SXF and GWN, it is a poor match at DRA, as the PATMOS-x peak insolation is quite low.

The relationship can be seen a little more clearly by plotting all PATMOS-x insolation values against SURFRAD values for the entire month of July, 2009 (Figure 20). In this plot, values identified as clear are marked with a red square, and those that are identified as partly cloudy or cloudy are marked with a black X. The title of each figure has the equation of the linear fit between all the daytime data. Based on the slope of the fit, the best relationship between the two sources is at SXF, and the worst at DRA.

Figures 21 through 24 are similar examples of how DNI and the diffuse component of insolation computed within PATMOS-x compare to those quantities measured *in situ* at the SURFRAD sites.

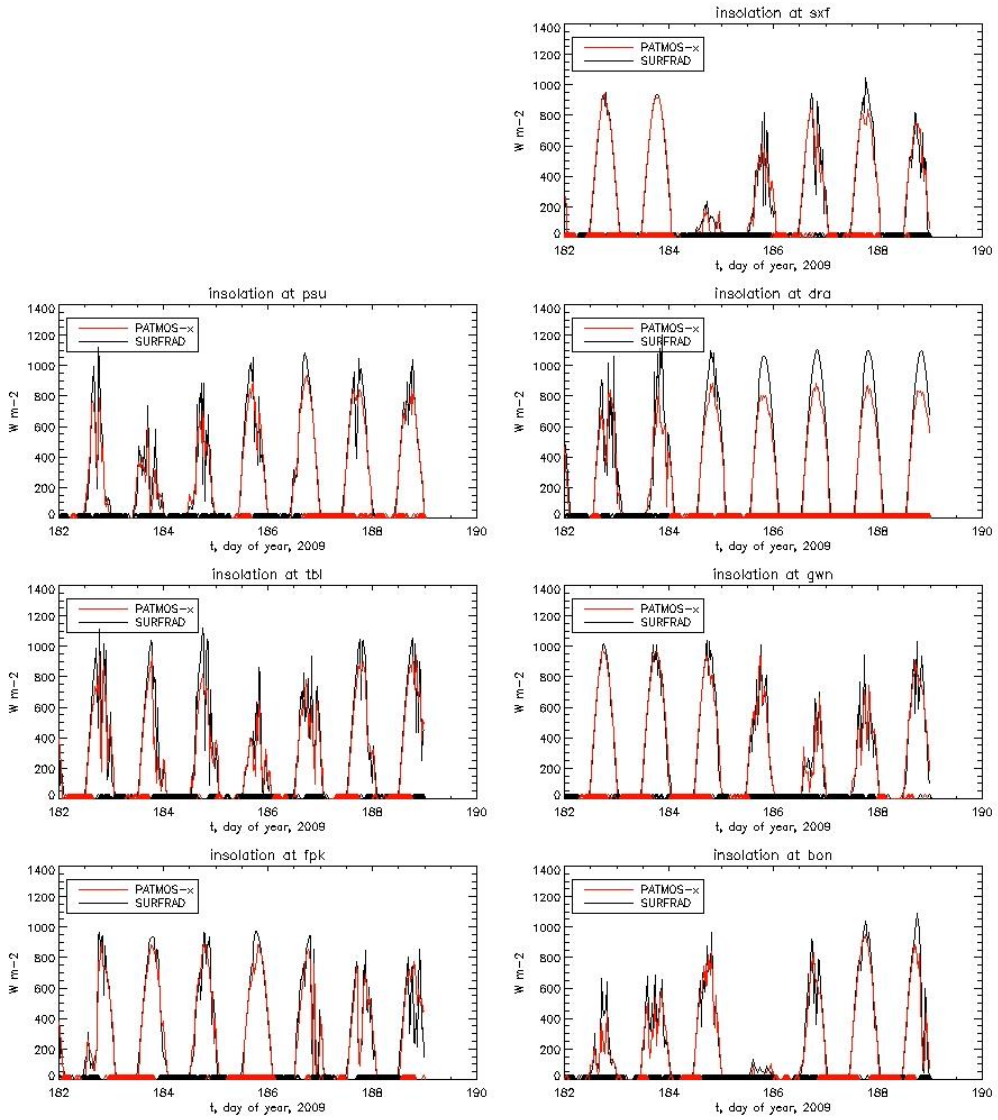

Figure 26. GHI from SURFRAD and PATMOS-x at seven SURFRAD sites for July 1-7, 2009. PATMOS-x data are derived from GOES-11 (WEST) and GOES-12 (EAST). Red symbols along the x-axis denote clear conditions, while black symbols denote cloudy. Partly cloudy conditions have no symbol.

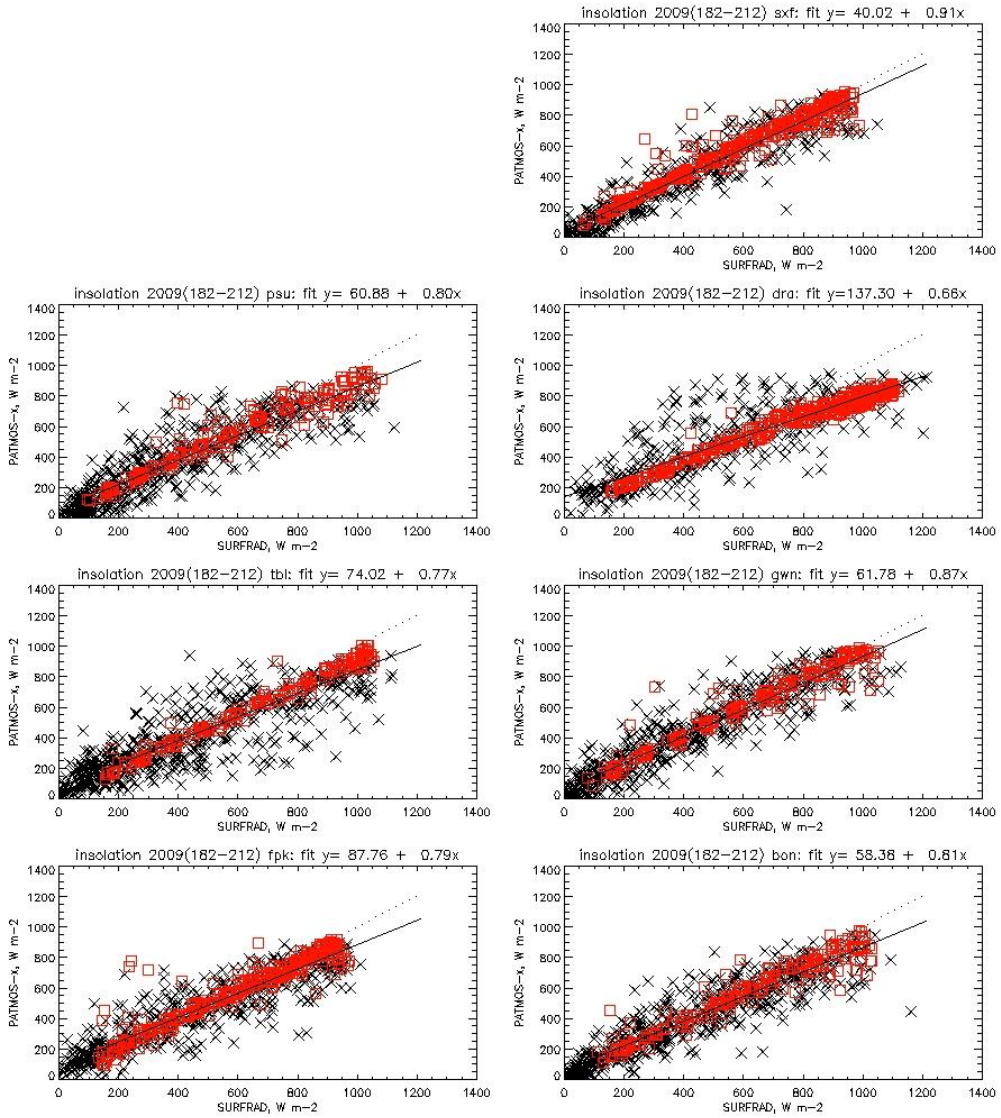

Figure 27. GHI (total insolation) from PATMOS-x and SURFRAD at seven SURFRAD sites during July, 2009. Clear conditions are depicted as red squares while cloudy or partly cloudy conditions have black Xs. The equation in the title is the linear least squares fit between the two data sources for all daytime sky conditions.

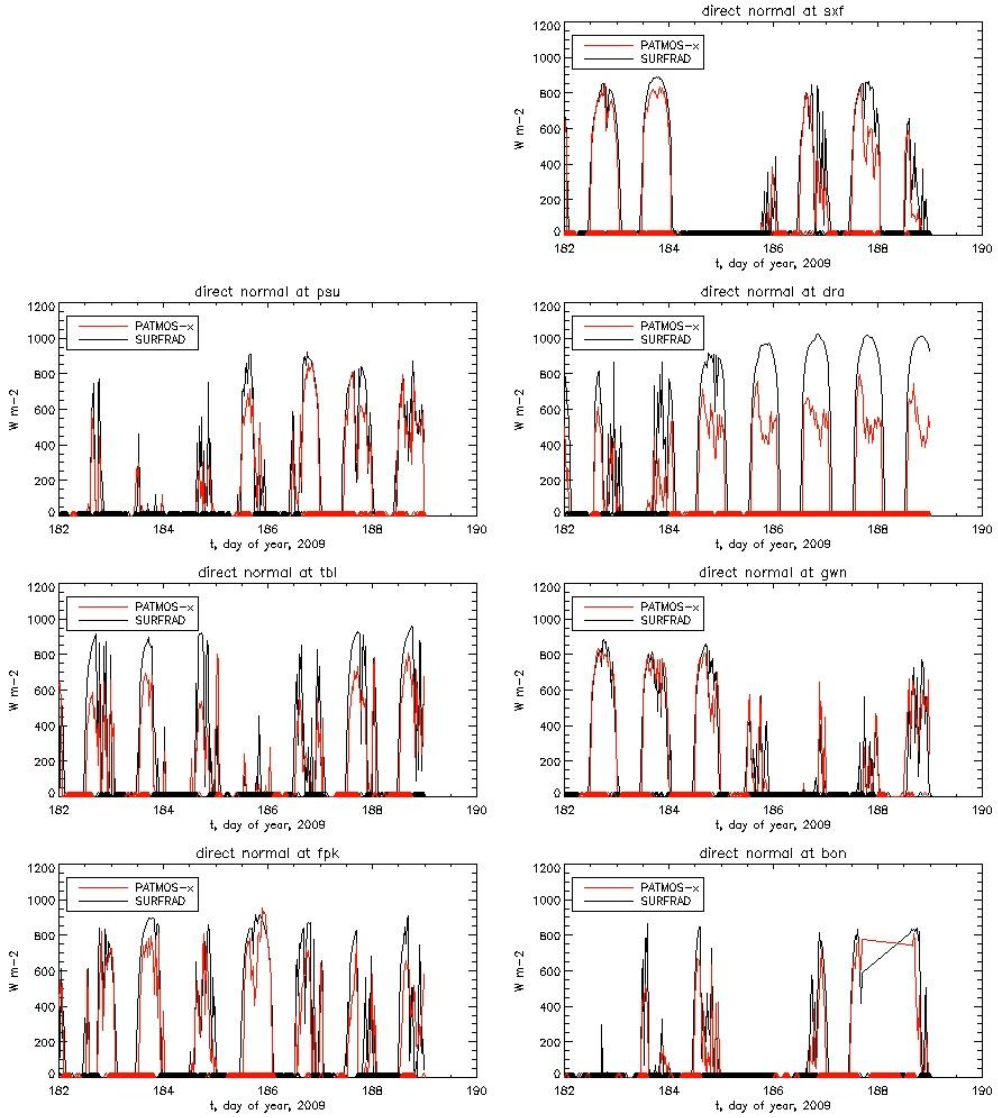

Figure 28. DNI from SURFRAD and PATMOS-x at seven SURFRAD sites for July 1-7, 2009. PATMOS-x data are derived from GOES-11 (WEST) and GOES-12 (EAST). Red symbols along the x-axis denote clear conditions, while black symbols denote cloudy. Partly cloudy conditions have no symbol. The SURFRAD site BON suffered a data outage on day 188.

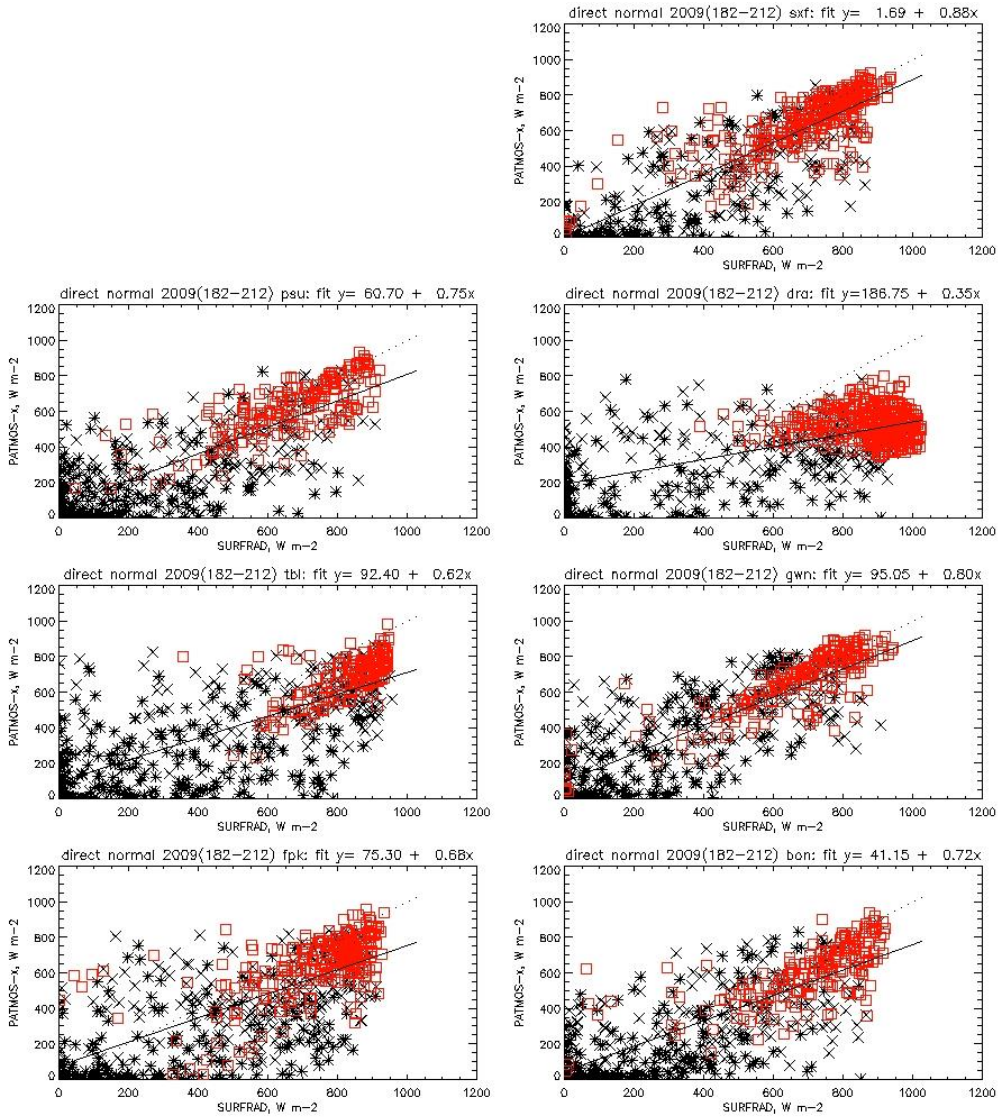

Figure 29. DNI from PATMOS-x and SURFRAD at seven SURFRAD sites during July, 2009. Clear conditions are depicted as red squares while cloudy or partly cloudy conditions have black Xs.

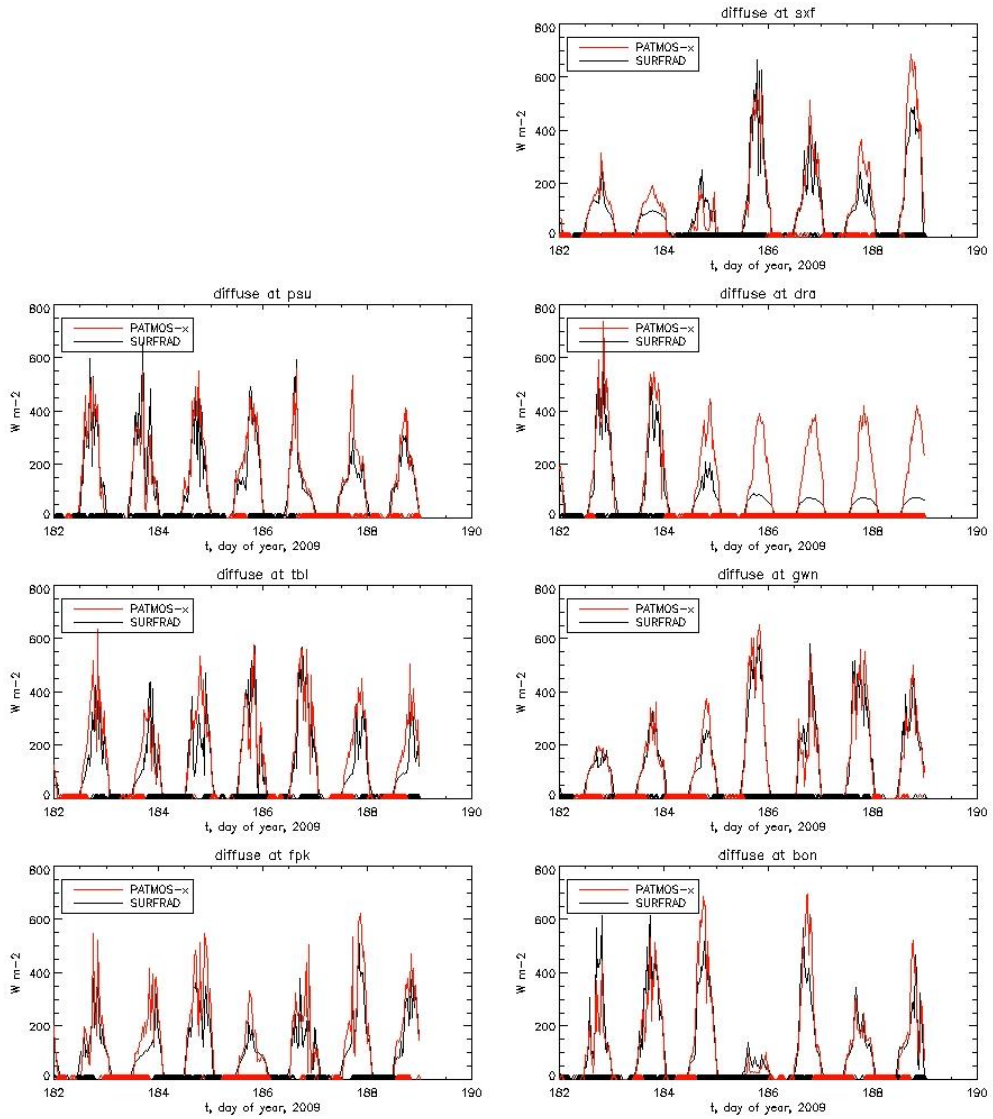

Figure 30. The diffuse component of GHI from SURFRAD and PATMOS-x at seven SURFRAD sites for July 1-7, 2009. PATMOS-x data are derived from GOES-11 (WEST) and GOES-12 (EAST). Red symbols along the x-axis denote clear conditions, while black symbols denote cloudy. Partly cloudy conditions have no symbol.

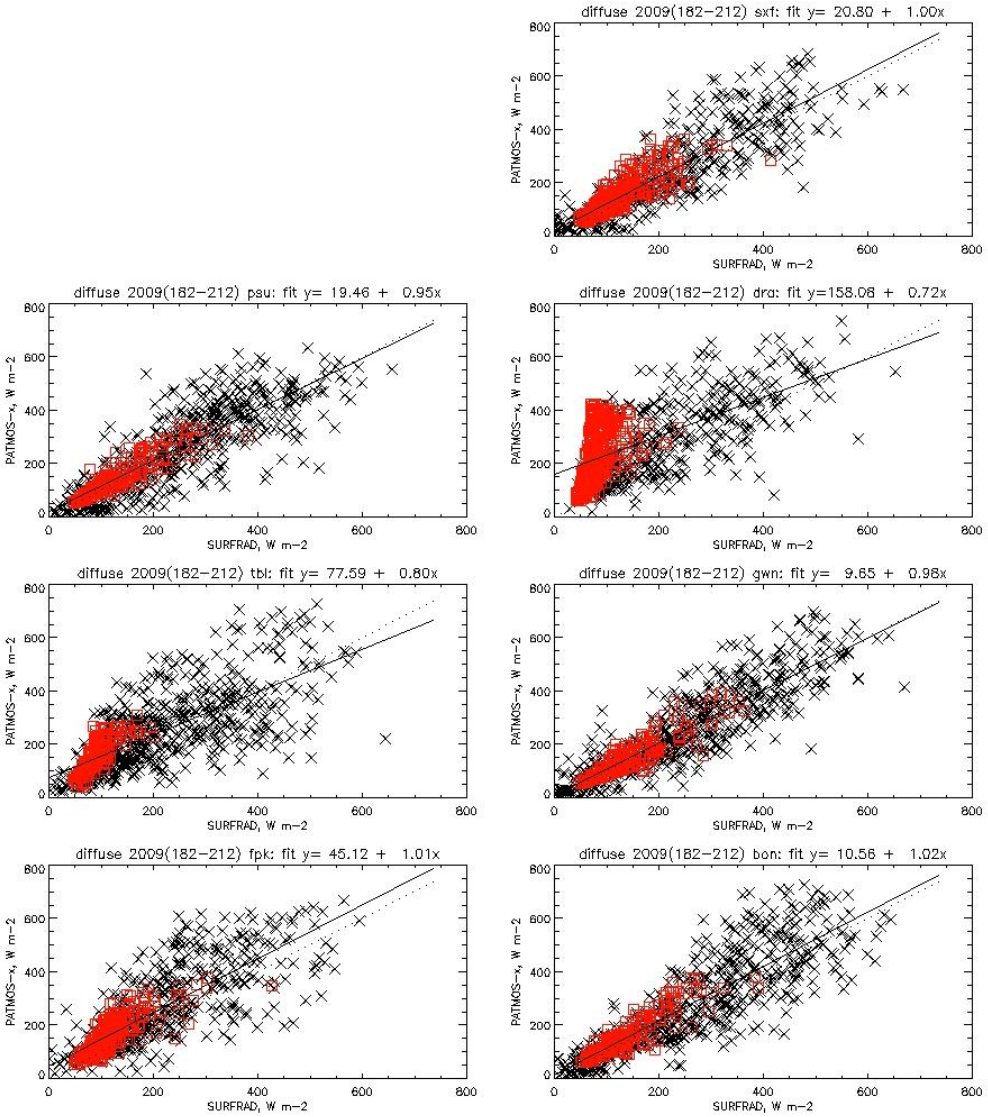

Figure 31. The diffuse component of GHI from PATMOS-x and SURFRAD at seven SURFRAD sites during July, 2009. Clear conditions are depicted as red squares while cloudy or partly cloudy conditions have black Xs.

The nature of insolation determines the kind of statistics that may prove useful in analysis of the data. If one considers that insolation ranges from zero for many hours during the night to possibly over 1000 W m^{-2} each day, the error statistic one uses may be less useful than intended. Firstly, the statistics provided in this analysis are only for values during the day time, and when the SASRAB algorithm applies (SZA less than 78.4^{o}). Secondly, for the purposes of solar power generation, one may assume that it is

more important to estimate the large values of insolation, because those generate the most power, and less important to estimate the small values. Therefore we chose to show root mean square error, which will emphasize large errors which are possible when the sun is high in the sky. Table 3 summarizes the error for GHI across all sites and sky conditions during 2009. The slope of the least squares fit line between GOES-derived and SURFRAD GHI is on average 0.78 for all sky conditions, with worst fits (farthest from 1.0) during winter months, and best fits (closest to 1.0) during spring through fall. The root mean square error, on average is 98 W m^{-2}, with the smallest error in fall. Since the diffuse and direct components are calculated separately in the SASRAB algorithm, statistics were also computed for clear (fraction cloud ≤ 0.1), partly cloudy (fraction cloud between 0.1 and 0.9), and cloudy (fraction cloud ≥0.9) sky conditions. We see that for all sites, the best fit and smallest RMSE is for clear skies, followed by cloudy skies, with partly cloudy skies having the worst fit and largest RMSE. This seems to make sense if one considers that an error in identifying clear/cloudy pixels is more likely if there are mixed conditions in the region. Cloud identification error compounds any error that SASRAB may have. The seasonal pattern is slightly different for sky conditions, however. Partly cloudy and cloudy skies have the worst fit in winter, while clear skies have the worst fit in summer.

Table 7. Statistics for GHI for all stations during 2009, broken down by month and sky condition. Slope is the slope of the linear least squares fit between GOES-derived and SURFRAD GHI. RMSE is the root mean square error between them, with units of W m^{-2}.

	All Conditions		Clear		Partly Cloudy		Cloudy	
Month	Slope	RMSE	Slope	RMSE	Slope	RMSE	Slope	RMSE
1	0.60	100	0.88	80	0.56	111	0.46	104
2	0.74	98	0.88	69	0.72	109	0.69	102
3	0.80	104	0.87	73	0.69	128	0.77	106
4	0.85	98	0.88	72	0.75	121	0.84	101
5	0.83	112	0.85	80	0.68	144	0.83	113
6	0.81	120	0.84	82	0.68	146	0.78	129
7	0.80	122	0.83	87	0.70	140	0.77	134
8	0.81	107	0.86	70	0.67	138	0.79	118
9	0.83	95	0.87	64	0.66	127	0.77	105
10	0.84	75	0.90	42	0.67	101	0.79	77
11	0.82	58	0.85	40	0.66	71	0.78	67
12	0.64	83	0.86	65	0.54	92	0.57	86
Mean	0.78	98	0.87	69	0.66	119	0.74	103

Errors in GHI vary by site as well. Figures 25 and 26 show the GHI slope and RMSE during 2009 broken down by site. Although the variation in error across months is larger than the variation in error from one site to the next, we see that not all sites have the same pattern of fit and error. The pattern of error from site to site seems to indicate that landcover determines the accuracy of insolation calculated from satellite. The worst performing sites in the winter season are those northerly enough to get snow. DRA, a site with only scrubby vegetation, has the worst performance in summer. Considering desert and

winter-condition atmopheres likely have low precipitable water, the most likely reason for these sites' poor performance is the bright surface. The more "greenly" vegetated, non-snowy site GWN has a better fit and smaller errors than other sites in winter and a better fit with lower error than DRA in summer. From these pieces of information we can hypothesize that bright scenes, like snow or bare desert, produce less accurate GHI values. This is probably a combination of mistaking snow for cloud in winter, and an inability to correctly measure degrees of brightness in pixels that are already bright. High albedo conditions such as snow and desert have often been identified being conditions difficult to simulate insolation from satellite (5). More work needs to be done in this area.

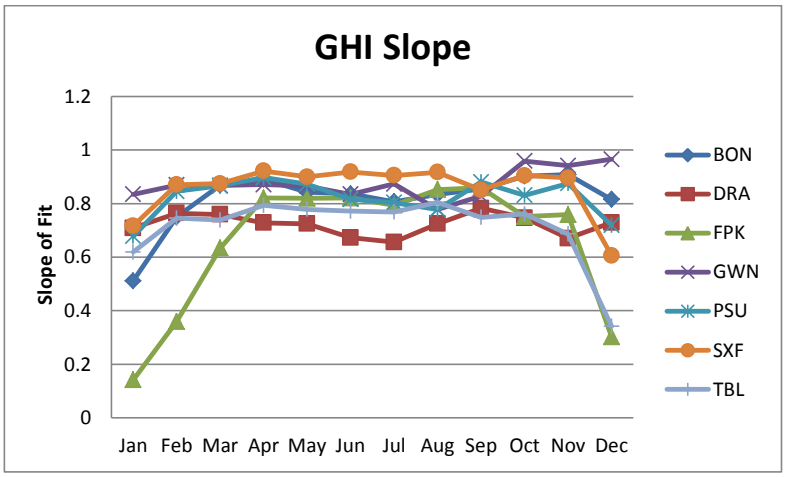

Figure 32. Slope of least squares fit, by site, between GOES-derived and SURFRAD GHI during 2009.

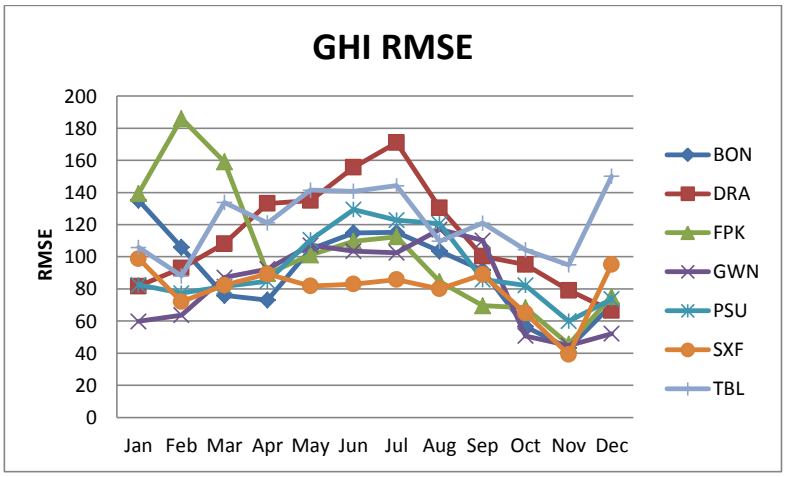

Figure 33. Root mean square error, by site, between GOES-derived and SURFRAD GHI during 2009.

We can also separate out the two components of GHI to inform whether it is the indirect or direct component of GHI that is more/less error prone. Figures 27 through 30 show the fit and RMSE for all sky conditions for the diffuse component and the direct component (*not* direct normal) of GHI. Although there is a similar annual pattern, the diffuse component tends to have a better fit than direct. The RMSE for diffuse is smaller as well, but we would expect that anyway, as the magnitude of diffuse radiation is smaller.

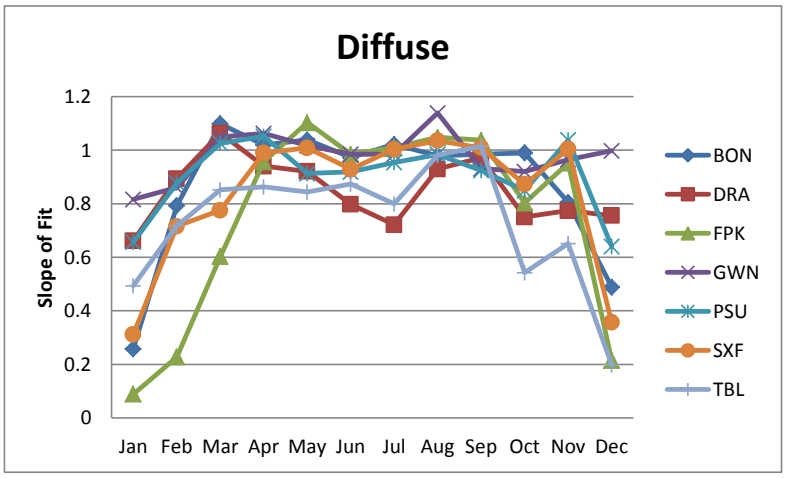

Figure 34. Same as Figure 21, but for the diffuse component of GHI.

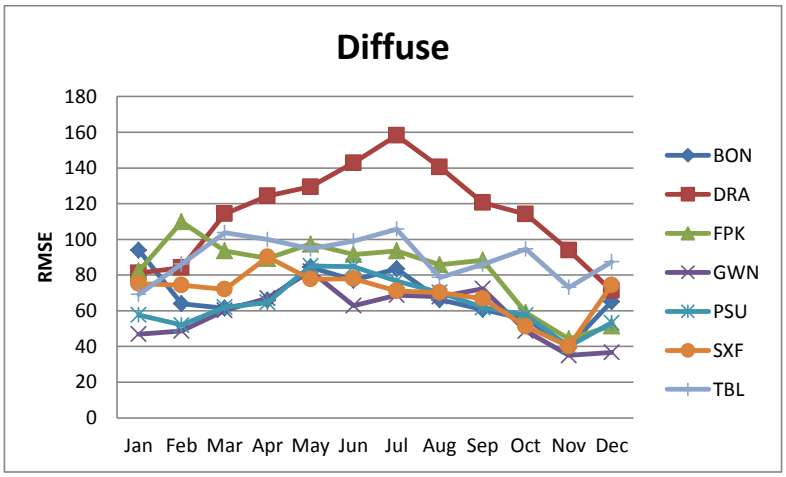

Figure 35. Same as Figure 22, but for the diffuse component of GHI.

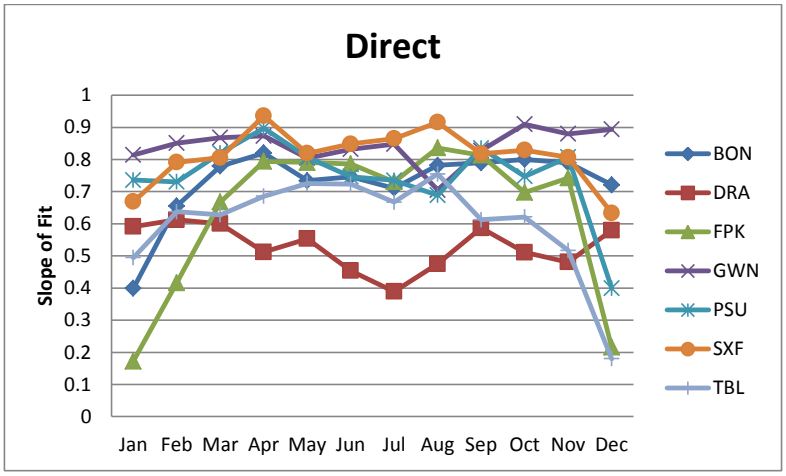

Figure 36. Same as Figure 21, but for the direct component of GHI.

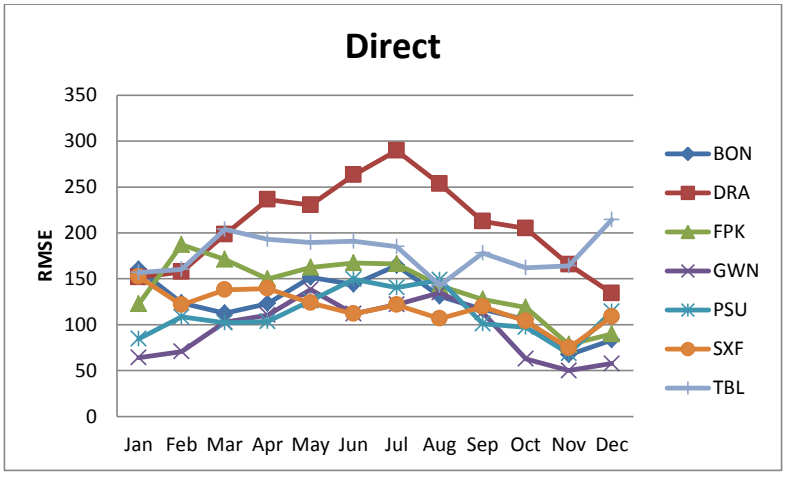

Figure 37. Same as Figure 22, but for the direct component of GHI.

Slope of fit and RMSE for DNI, which is merely the direct component divided by the cosine of the solar zenith angle, are shown in Figures 31 and 32 for 2009. Although the patterns of fit slope and RMSE remain the same, the magnitudes change due to the normalizing effects of dividing by the cosine of the SZA.

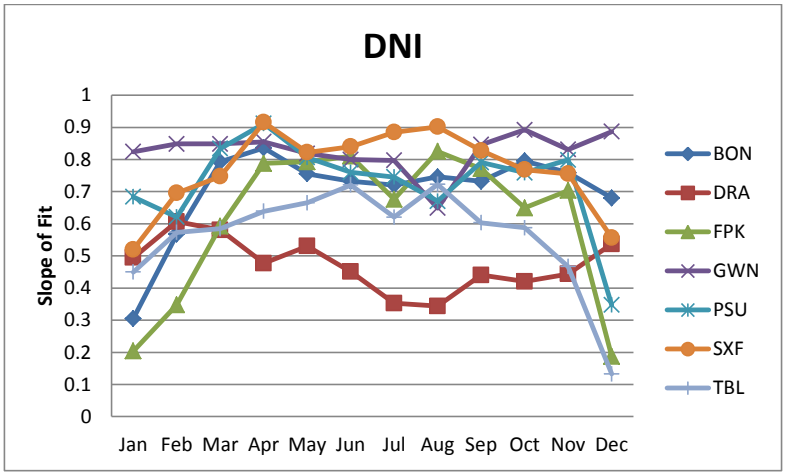

Figure 38. Same as Figure 21, but for the DNI.

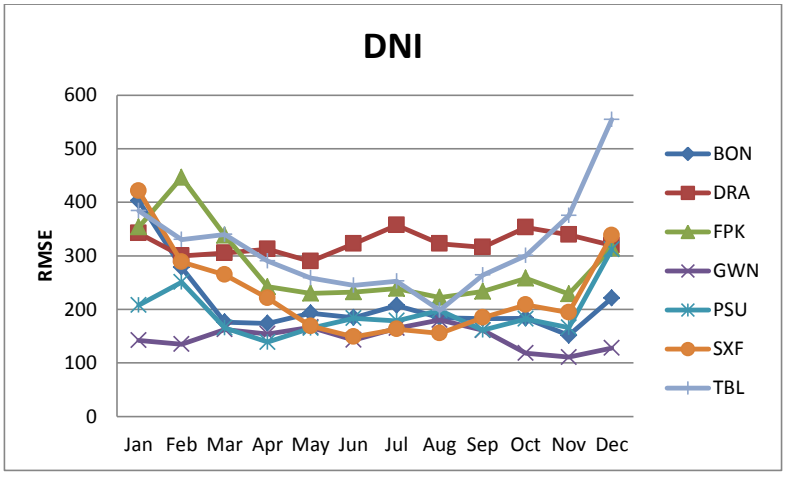

Figure 39. Same as Figure 22, but for the DNI.

A summary of the 2009 statistics for all sites is provided in Table 4. For each of the quantities, the satellite-derived data is most accurate under clear sky conditions and least accurate under partly cloudy sky conditions. This indicates that deriving surface conditions from satellite observations is best suited to uniform conditions (clear or cloudy) and least suited to mixed sky conditions. And of the uniform conditions, clear skies, which allow the satellite to actually sense the surface, result in more accurate values than cloudy skies, for which there is the additional factor of calculating the cloud's optical thickness. These statistics also indicate that diffuse radiation is better simulated by SASRAB than is direct. Additionally, if we wish to have only two categories of sky condition, we can lump partly cloudy and cloudy skies together and not interfere too much with statistics. The table provides statistics for

skin temperature as well. Skin temperature is not produced by SASRAB, but is one indicator of the quality of the cloud mask in PATMOS-x. A perfect fit of skin temperature to the surface air temperature from SURFRAD indicates that if PATMOS-x identifies pixels as clear, they really are clear. Unfortunately this sort of statistic cannot indicate when clear pixels are misidentified as cloudy.

Table 8. Summary of 2009 statistics for quantities derived from SASRAB in PATMOS-x. Slope is the slope of the linear fit between GOES-derived and SURFRAD (all sites), while RMSE is the root mean square error. Units for RMSE are Wm^{-2}, except for Skin Temp, which is in K. Skin temperature as derived from satellite is only valid under clear conditions; NA indicates not applicable. The SURFRAD quantity used in the skin temp statistic is surface temperature derived from upwelling thermal infrared.

	All Conditions		Clear		Partly Cloudy		Cloudy	
	Slope	RMSE	Slope	RMSE	Slope	RMSE	Slope	RMSE
GHI	0.78	98	0.86	69	0.66	119	0.74	103
DNI	0.67	243	0.60	214	0.30	288	0.43	230
Direct	0.70	139	0.79	116	0.48	166	0.45	139
Diffuse	0.85	78	0.98	60	0.83	82	0.89	82
Skin Temp	NA	NA	0.93	3	NA	NA	NA	NA

Statistics on GHI were also computed for selected months during 2005 through 2008. Table 5 provides the mean slope of the linear fit. Table 6 provides the RMSE. Comparing results from all months of 2009 with these selected 4 months, we see slope and RMSE are very consistent: 0.78 slope and 98 Wm^{-2} RMSE for all months of 2009 vs. 0.77 slope and 100 Wm^{-2} RMSE for the 4 months of 2009. This gives us confidence that statistics drawn from these four months are very similar to those we would calculate if all months during the period were included.

As seen from the previous analysis of all months of 2009, winter, represented here by December, has the worst fit. RMSE is largest in July, when the magnitude of GHI is largest. Interestingly, although March and September have similar GHI magnitudes, the fit is better and error smaller in September on average. Looking at the station by station statistics (not shown), FPK, SXF, and TBL match this trend, while BON, DRA, GWN, and PSU have the opposite trends on average. The Mar/Sep pattern is also not consistent at all stations for different years. Although it is possible that March snows may be the cause of worse fit compared to September, there is not enough information at this point to confirm this idea.

Year-to-year variation in both slope of fit and RMSE is very small. This is encouraging, as it suggests that difference between GHI derived from different satellites are small. And looking at the two Decembers of 2007 and 2008 where GOES-12 failed and was replaced with data from GOES-10 and -13, there appear to be only small negative effects.

Table 9. Mean slope of linear fit between GOES-derived and SURFRAD GHI (all sky conditions) for four selected months during 2005-2009.

Year	Mar	Jul	Sep	Dec	4 Months
2005	0.80	0.79	0.83	0.64	0.77
2006	0.78	0.81	0.81	0.65	0.76
2007	0.80	0.80	0.82	0.63	0.76
2008	0.82	0.79	0.83	0.56	0.75
2009	0.80	0.80	0.83	0.64	0.77
2005-2009	0.80	0.80	0.82	0.63	0.76

Table 10. Root mean square error of GOES-derived GHI (all sky conditions), by site and year, for four selected months during 2005-2009. Error is in units of W m^{-2}.

Year	Mar	Jul	Sep	Dec	4 Months
2005	100	120	88	79	97
2006	108	114	99	76	99
2007	106	119	93	87	101
2008	100	123	90	93	102
2009	104	122	95	83	101
2005-2009	104	119	93	84	100

Conclusions

The SASRAB algorithm, which is used in GSIP was inserted into the PATMOS-x processing system. PATMOS-x was used to compute insolation and cloud properties for 5 years with of GOES-WEST and GOES-EAST imagery, every 30 minutes during 2005-2009. The resulting 9.2 Tb of files contain a variety of quantities at the thermal pixel level over the Northern Hemisphere, Northern Hemisphere Extended or Full Disk coverages, according to the GOES image acquisition schedule. Comparisons with *in situ* SURFRAD observations indicate that for all sites, sky conditions, months, and years, the root mean square error for GHI is approximately 100 Wm^{-2}, with an average linear fit of 0.75. The DNI average RMSE is approximately 243 Wm-2, with an average linear fit of 0.67. Further analysis indicates that the diffuse component of insolation is slightly better calculated by SASRAB than is the direct component. Across sky conditions, GHI and DNI are most accurate under clear skies, followed by cloudy skies. Partly cloudy skies produce the least accurate GHI and DNI. Across months and sites, for those with very bright surfaces (snow, desert), SASRAB in PATMOS-x produces poor quality GHI and DNI compared to darker surfaces. Research is needed on how to compute better satellite-based insolation values over bright surfaces.

References

1. The GSIP product available via CLASS is described here: http://www.nsof.class.noaa.gov/release/glossary/GSIP.htm
2. GSIP product description can be found at: http://www.ngdc.noaa.gov/nmmrview/fgdc.jsp?id=gov.noaa.class:GSIP
3. The main SASRAB reference:
   Istvan Laszlo, Pubu Ciren, Hongqing Liu, Shobha Kondragunta, J. Dan Tarpley, Mitchell D. Goldberg. 2008: Remote sensing of aerosol and radiation from geostationary satellites. Advances in Space Research, 41 (11), 1882-1893.
4. SURFRAD site descriptions and data can be found at http://www.srrb.noaa.gov/surfrad/index.html
5. Satellite-derived insolation is of lower quality over bright surfaces like snow and desert:
   Pinker, R. T., et al. 2003: Surface radiation budgets in support of the GEWEX Continental-Scale International Project (GCIP) and the GEWEX Americas Prediction Project (GAPP), including the North American Land Data Assimilation System (NLDAS) project, J. Geophys. Res., 108(D22), 8844, doi:10.1029/2002JD003301.
   Justus, C. G. Paris, M. V. Tarpley, J. D. 1986: Satellite-measured insolation in the United States, Mexico, and South America. Remote Sensing of Environment, N.Y. 20(1), 57-83.

Appendix A

Sample header dump from one of the output files of the 5 year insolation dataset, goes11_2009_365_1930.level2.hdf. Note that though the file is in hdf4, the information appears here in the style of a netCDF header dump. The file is not in netCDF.

```
goes11_2009_365_1930.level2 {
dimensions:
        fakeDim0 = 1355 ;
        fakeDim1 = 1355 ;
        fakeDim2 = 1355 ;
        scan_lines_along_track_direction = 1355 ;
        pixel_elements_along_scan_direction = 1657 ;

variables:
        long scan_line_number(fakeDim0) ;
                scan_line_number:SCALED = '\0' ;
                scan_line_number:UNITS = "none" ;
                scan_line_number:STANDARD_NAME = "scan_line_number" ;
                scan_line_number:LONG_NAME = "scan line number" ;
                scan_line_number:RANGE_MISSING = -999.f ;
        float scan_line_time(fakeDim1) ;
                scan_line_time:SCALED = '\0' ;
                scan_line_time:UNITS = "hours" ;
                scan_line_time:LONG_NAME = "time for the scan line in fractional hours" ;
                scan_line_time:RANGE_MISSING = -999.f ;
        byte bad_scan_line_flag(fakeDim2) ;
                bad_scan_line_flag:SCALED = '\0' ;
                bad_scan_line_flag:UNITS = "none" ;
                bad_scan_line_flag:RANGE_MISSING = -128.f ;
        byte packed_pixel_meta_data(scan_lines_along_track_direction, pixel_elements_along_scan_direction) ;
                packed_pixel_meta_data:SCALED = '\0' ;
                packed_pixel_meta_data:UNITS = "none" ;
                packed_pixel_meta_data:STANDARD_NAME = "pixel_quality_flags_packed_into_one_byte" ;
                packed_pixel_meta_data:LONG_NAME = "order_and_depth:
bad_pixel_mask(1),solar_contamination_mask(1),ch6_on_pixel_mask(1),Bayes_Mask_Sfc_Type(3)" ;
                packed_pixel_meta_data:RANGE_MISSING = -128.f ;
        short latitude(scan_lines_along_track_direction, pixel_elements_along_scan_direction) ;
                latitude:SCALED = '\1' ;
                latitude:UNITS = "degrees_north" ;
                latitude:STANDARD_NAME = "latitude" ;
                latitude:LONG_NAME = "latitude for each pixel measured in degrees north" ;
                latitude:RANGE_MISSING = -999.f ;
                latitude:RANGE_MIN = -90.f ;
                latitude:RANGE_MAX = 90.f ;
                latitude:SCALED_MIN = -32767 ;
                latitude:SCALED_MAX = 32767 ;
                latitude:SCALED_MISSING = -32768 ;
                latitude:_FILLVALUE = -32768 ;
                latitude:SCALE_FACTOR = 0.0027466659f ;
                latitude:ADD_OFFSET = 0.f ;
        short longitude(scan_lines_along_track_direction, pixel_elements_along_scan_direction) ;
                longitude:SCALED = '\1' ;
                longitude:UNITS = "degrees_east" ;
                longitude:STANDARD_NAME = "longitude" ;
                longitude:LONG_NAME = "longitude for each pixel measured in degrees east" ;
```

longitude:RANGE_MISSING = -999.f ;
longitude:RANGE_MIN = -180.f ;
longitude:RANGE_MAX = 180.f ;
longitude:SCALED_MIN = -32767 ;
longitude:SCALED_MAX = 32767 ;
longitude:SCALED_MISSING = -32768 ;
longitude:_FILLVALUE = -32768 ;
longitude:SCALE_FACTOR = 0.0054933317f ;
longitude:ADD_OFFSET = 0.f ;
byte sensor_zenith_angle(scan_lines_along_track_direction, pixel_elements_along_scan_direction) ;
sensor_zenith_angle:SCALED = '\1' ;
sensor_zenith_angle:UNITS = "degrees" ;
sensor_zenith_angle:STANDARD_NAME = "sensor_zenith_angle" ;
sensor_zenith_angle:LONG_NAME = "sensor zenith for each pixel measured in degrees from nadir" ;
sensor_zenith_angle:RANGE_MISSING = -999.f ;
sensor_zenith_angle:RANGE_MIN = 0.f ;
sensor_zenith_angle:RANGE_MAX = 180.f ;
sensor_zenith_angle:SCALED_MIN = -127 ;
sensor_zenith_angle:SCALED_MAX = 127 ;
sensor_zenith_angle:SCALED_MISSING = -128 ;
sensor_zenith_angle:_FILLVALUE = -128 ;
sensor_zenith_angle:SCALE_FACTOR = 0.70866144f ;
sensor_zenith_angle:ADD_OFFSET = 90.f ;
byte solar_zenith_angle(scan_lines_along_track_direction, pixel_elements_along_scan_direction) ;
solar_zenith_angle:SCALED = '\1' ;
solar_zenith_angle:UNITS = "degrees" ;
solar_zenith_angle:STANDARD_NAME = "solar_zenith_angle" ;
solar_zenith_angle:LONG_NAME = "solar zenith for each pixel measured in degrees away from the sun (0=looking at sun)" ;
solar_zenith_angle:RANGE_MISSING = -999.f ;
solar_zenith_angle:RANGE_MIN = 0.f ;
solar_zenith_angle:RANGE_MAX = 180.f ;
solar_zenith_angle:SCALED_MIN = -127 ;
solar_zenith_angle:SCALED_MAX = 127 ;
solar_zenith_angle:SCALED_MISSING = -128 ;
solar_zenith_angle:_FILLVALUE = -128 ;
solar_zenith_angle:SCALE_FACTOR = 0.70866144f ;
solar_zenith_angle:ADD_OFFSET = 90.f ;
byte relative_azimuth_angle(scan_lines_along_track_direction, pixel_elements_along_scan_direction) ;
relative_azimuth_angle:SCALED = '\1' ;
relative_azimuth_angle:UNITS = "degrees" ;
relative_azimuth_angle:STANDARD_NAME = "relative_azimuth_angle" ;
relative_azimuth_angle:LONG_NAME = "relative azimuth angle in degrees. 0 is the principal plane looking towards sun" ;
relative_azimuth_angle:RANGE_MISSING = -999.f ;
relative_azimuth_angle:RANGE_MIN = 0.f ;
relative_azimuth_angle:RANGE_MAX = 180.f ;
relative_azimuth_angle:SCALED_MIN = -127 ;
relative_azimuth_angle:SCALED_MAX = 127 ;
relative_azimuth_angle:SCALED_MISSING = -128 ;
relative_azimuth_angle:_FILLVALUE = -128 ;
relative_azimuth_angle:SCALE_FACTOR = 0.70866144f ;
relative_azimuth_angle:ADD_OFFSET = 90.f ;
byte solar_azimuth_angle(scan_lines_along_track_direction, pixel_elements_along_scan_direction) ;
solar_azimuth_angle:SCALED = '\1' ;
solar_azimuth_angle:UNITS = "degrees" ;
solar_azimuth_angle:STANDARD_NAME = "solar_azimuth_angle" ;

solar_azimuth_angle:LONG_NAME = "solar azimuth angle in degrees from north" ;
solar_azimuth_angle:RANGE_MISSING = -999.f ;
solar_azimuth_angle:RANGE_MIN = 0.f ;
solar_azimuth_angle:RANGE_MAX = 360.f ;
solar_azimuth_angle:SCALED_MIN = -127 ;
solar_azimuth_angle:SCALED_MAX = 127 ;
solar_azimuth_angle:SCALED_MISSING = -128 ;
solar_azimuth_angle:_FILLVALUE = -128 ;
solar_azimuth_angle:SCALE_FACTOR = 1.4173229f ;
solar_azimuth_angle:ADD_OFFSET = 180.f ;
byte packed_land_cover(scan_lines_along_track_direction, pixel_elements_along_scan_direction) ;
packed_land_cover:SCALED = '\0' ;
packed_land_cover:UNITS = "none" ;
packed_land_cover:STANDARD_NAME = "packed_land_cover" ;
packed_land_cover:LONG_NAME = "land cover, snow and coast values packed into one byte, see patmos-x docs to unpack" ;
packed_land_cover:RANGE_MISSING = -128.f ;
byte land_class(scan_lines_along_track_direction, pixel_elements_along_scan_direction) ;
land_class:SCALED = '\0' ;
land_class:UNITS = "none" ;
land_class:STANDARD_NAME = "land_class" ;
land_class:LONG_NAME = "land classes and values:shallow ocean=0,land=1,coastline=2,shallow inland water=3,ephemeral water=4,deep inland water=5,moderate ocean=6,deep ocean=7" ;
land_class:RANGE_MISSING = -128.f ;
byte snow_class(scan_lines_along_track_direction, pixel_elements_along_scan_direction) ;
snow_class:SCALED = '\0' ;
snow_class:UNITS = "none" ;
snow_class:STANDARD_NAME = "snow_class" ;
snow_class:LONG_NAME = "snow classes and values:no snow/ice=1,sea_ice=2,snow=3" ;
snow_class:RANGE_MISSING = -128.f ;
short refl_0_65um_nom(scan_lines_along_track_direction, pixel_elements_along_scan_direction) ;
refl_0_65um_nom:SCALED = '\1' ;
refl_0_65um_nom:UNITS = "%" ;
refl_0_65um_nom:STANDARD_NAME = "toa_bidirectional_reflectance_0_65_micron_nominal" ;
refl_0_65um_nom:LONG_NAME = "top of atmosphere reflectance at the nominal wavelength of 0.65 microns" ;
refl_0_65um_nom:RANGE_MISSING = -999.f ;
refl_0_65um_nom:RANGE_MIN = -2.f ;
refl_0_65um_nom:RANGE_MAX = 120.f ;
refl_0_65um_nom:SCALED_MIN = -32767 ;
refl_0_65um_nom:SCALED_MAX = 32767 ;
refl_0_65um_nom:SCALED_MISSING = -32768 ;
refl_0_65um_nom:_FILLVALUE = -32768 ;
refl_0_65um_nom:SCALE_FACTOR = 0.0018616291f ;
refl_0_65um_nom:ADD_OFFSET = 59.f ;
byte refl_3_75um_nom(scan_lines_along_track_direction, pixel_elements_along_scan_direction) ;
refl_3_75um_nom:SCALED = '\1' ;
refl_3_75um_nom:UNITS = "%" ;
refl_3_75um_nom:STANDARD_NAME = "toa_bidirectional_reflectance_3_75_micron_nominal" ;
refl_3_75um_nom:LONG_NAME = "top of atmosphere reflectance at the nominal wavelength of 3.75 microns" ;
refl_3_75um_nom:RANGE_MISSING = -999.f ;
refl_3_75um_nom:RANGE_MIN = -20.f ;
refl_3_75um_nom:RANGE_MAX = 80.f ;
refl_3_75um_nom:SCALED_MIN = -127 ;
refl_3_75um_nom:SCALED_MAX = 127 ;
refl_3_75um_nom:SCALED_MISSING = -128 ;
refl_3_75um_nom:_FILLVALUE = -128 ;

refl_3_75um_nom:SCALE_FACTOR = 0.39370078f ;
refl_3_75um_nom:ADD_OFFSET = 30.f ;
short temp_3_75um_nom(scan_lines_along_track_direction, pixel_elements_along_scan_direction) ;
temp_3_75um_nom:SCALED = '\1' ;
temp_3_75um_nom:UNITS = "K" ;
temp_3_75um_nom:STANDARD_NAME = "toa_brightness_temperature_3_75_micron_nominal" ;
temp_3_75um_nom:LONG_NAME = "top of atmosphere brightness temperature at the nominal wavelength of 3.75 microns" ;
temp_3_75um_nom:RANGE_MISSING = -999.f ;
temp_3_75um_nom:RANGE_MIN = 180.f ;
temp_3_75um_nom:RANGE_MAX = 340.f ;
temp_3_75um_nom:SCALED_MIN = -32767 ;
temp_3_75um_nom:SCALED_MAX = 32767 ;
temp_3_75um_nom:SCALED_MISSING = -32768 ;
temp_3_75um_nom:_FILLVALUE = -32768 ;
temp_3_75um_nom:SCALE_FACTOR = 0.0024414808f ;
temp_3_75um_nom:ADD_OFFSET = 260.f ;
short temp_6_7um_nom(scan_lines_along_track_direction, pixel_elements_along_scan_direction) ;
temp_6_7um_nom:SCALED = '\1' ;
temp_6_7um_nom:UNITS = "K" ;
temp_6_7um_nom:STANDARD_NAME = "toa_brightness_temperature_6_7_micron_nominal" ;
temp_6_7um_nom:LONG_NAME = "top of atmosphere brightness temperature at the nominal wavelength of 6.7 microns" ;
temp_6_7um_nom:RANGE_MISSING = -999.f ;
temp_6_7um_nom:RANGE_MIN = 180.f ;
temp_6_7um_nom:RANGE_MAX = 340.f ;
temp_6_7um_nom:SCALED_MIN = -32767 ;
temp_6_7um_nom:SCALED_MAX = 32767 ;
temp_6_7um_nom:SCALED_MISSING = -32768 ;
temp_6_7um_nom:_FILLVALUE = -32768 ;
temp_6_7um_nom:SCALE_FACTOR = 0.0024414808f ;
temp_6_7um_nom:ADD_OFFSET = 260.f ;
short temp_11_0um_nom(scan_lines_along_track_direction, pixel_elements_along_scan_direction) ;
temp_11_0um_nom:SCALED = '\1' ;
temp_11_0um_nom:UNITS = "K" ;
temp_11_0um_nom:STANDARD_NAME = "toa_brightness_temperature_11_0_micron_nominal" ;
temp_11_0um_nom:LONG_NAME = "top of atmosphere brightness temperature at the nominal wavelength of 11.0 microns" ;
temp_11_0um_nom:RANGE_MISSING = -999.f ;
temp_11_0um_nom:RANGE_MIN = 180.f ;
temp_11_0um_nom:RANGE_MAX = 340.f ;
temp_11_0um_nom:SCALED_MIN = -32767 ;
temp_11_0um_nom:SCALED_MAX = 32767 ;
temp_11_0um_nom:SCALED_MISSING = -32768 ;
temp_11_0um_nom:_FILLVALUE = -32768 ;
temp_11_0um_nom:SCALE_FACTOR = 0.0024414808f ;
temp_11_0um_nom:ADD_OFFSET = 260.f ;
short temp_12_0um_nom(scan_lines_along_track_direction, pixel_elements_along_scan_direction) ;
temp_12_0um_nom:SCALED = '\1' ;
temp_12_0um_nom:UNITS = "K" ;
temp_12_0um_nom:STANDARD_NAME = "toa_brightness_temperature_12_0_micron_nominal" ;
temp_12_0um_nom:LONG_NAME = "top of atmosphere brightness temperature at the nominal wavelength of 12.0 microns" ;
temp_12_0um_nom:RANGE_MISSING = -999.f ;
temp_12_0um_nom:RANGE_MIN = 180.f ;
temp_12_0um_nom:RANGE_MAX = 340.f ;
temp_12_0um_nom:SCALED_MIN = -32767 ;
temp_12_0um_nom:SCALED_MAX = 32767 ;

temp_12_0um_nom:SCALED_MISSING = -32768 ;
temp_12_0um_nom:_FILLVALUE = -32768 ;
temp_12_0um_nom:SCALE_FACTOR = 0.0024414808f ;
temp_12_0um_nom:ADD_OFFSET = 260.f ;
byte refl_0_65um_nom_stddev_3x3(scan_lines_along_track_direction, pixel_elements_along_scan_direction) ;
refl_0_65um_nom_stddev_3x3:SCALED = '\1' ;
refl_0_65um_nom_stddev_3x3:UNITS = "%" ;
refl_0_65um_nom_stddev_3x3:STANDARD_NAME = "toa_reflectance_0_65_micron_nomimal_3x3_stddev" ;
refl_0_65um_nom_stddev_3x3:LONG_NAME = "standard deviation of the 0.63 micron reflectance computed over a 3x3 pixel array" ;
refl_0_65um_nom_stddev_3x3:RANGE_MISSING = -999.f ;
refl_0_65um_nom_stddev_3x3:RANGE_MIN = 0.f ;
refl_0_65um_nom_stddev_3x3:RANGE_MAX = 100.f ;
refl_0_65um_nom_stddev_3x3:SCALED_MIN = -127 ;
refl_0_65um_nom_stddev_3x3:SCALED_MAX = 127 ;
refl_0_65um_nom_stddev_3x3:SCALED_MISSING = -128 ;
refl_0_65um_nom_stddev_3x3:_FILLVALUE = -128 ;
refl_0_65um_nom_stddev_3x3:SCALE_FACTOR = 0.39370078f ;
refl_0_65um_nom_stddev_3x3:ADD_OFFSET = 50.f ;
byte temp_11_0um_nom_stddev_3x3(scan_lines_along_track_direction, pixel_elements_along_scan_direction) ;
temp_11_0um_nom_stddev_3x3:SCALED = '\1' ;
temp_11_0um_nom_stddev_3x3:UNITS = "K" ;
temp_11_0um_nom_stddev_3x3:STANDARD_NAME = "toa_brightness_temperature_11_micron_nominal_3x3_stddev" ;
temp_11_0um_nom_stddev_3x3:LONG_NAME = "standard deviation of the 11 micron brightness temperature computed over a 3x3 pixel array" ;
temp_11_0um_nom_stddev_3x3:RANGE_MISSING = -999.f ;
temp_11_0um_nom_stddev_3x3:RANGE_MIN = 0.f ;
temp_11_0um_nom_stddev_3x3:RANGE_MAX = 20.f ;
temp_11_0um_nom_stddev_3x3:SCALED_MIN = -127 ;
temp_11_0um_nom_stddev_3x3:SCALED_MAX = 127 ;
temp_11_0um_nom_stddev_3x3:SCALED_MISSING = -128 ;
temp_11_0um_nom_stddev_3x3:_FILLVALUE = -128 ;
temp_11_0um_nom_stddev_3x3:SCALE_FACTOR = 0.078740157f ;
temp_11_0um_nom_stddev_3x3:ADD_OFFSET = 10.f ;
byte cloud_probability(scan_lines_along_track_direction, pixel_elements_along_scan_direction) ;
cloud_probability:SCALED = '\1' ;
cloud_probability:UNITS = "none" ;
cloud_probability:STANDARD_NAME = "cloud_probability" ;
cloud_probability:LONG_NAME = "probability of a pixel being cloudy from the Bayesian cloud mask" ;
cloud_probability:RANGE_MISSING = -999.f ;
cloud_probability:RANGE_MIN = 0.f ;
cloud_probability:RANGE_MAX = 1.f ;
cloud_probability:SCALED_MIN = -127 ;
cloud_probability:SCALED_MAX = 127 ;
cloud_probability:SCALED_MISSING = -128 ;
cloud_probability:_FILLVALUE = -128 ;
cloud_probability:SCALE_FACTOR = 0.0039370079f ;
cloud_probability:ADD_OFFSET = 0.5f ;
byte cloud_mask(scan_lines_along_track_direction, pixel_elements_along_scan_direction) ;
cloud_mask:SCALED = '\0' ;
cloud_mask:UNITS = "none" ;
cloud_mask:STANDARD_NAME = "cloud_mask" ;

cloud_mask:LONG_NAME = "integer classification of the cloud mask including clear=0, probably-clear=1, probably-cloudy=2 and cloudy=3" ;
cloud_mask:RANGE_MISSING = -999.f ;
byte cloud_type(scan_lines_along_track_direction, pixel_elements_along_scan_direction) ;
cloud_type:SCALED = '\0' ;
cloud_type:UNITS = "none" ;
cloud_type:STANDARD_NAME = "cloud_type" ;
cloud_type:LONG_NAME = "integer classification of the cloud type including clear and aerosol type, see patmos-x docs for key" ;
cloud_type:RANGE_MISSING = -999.f ;
byte cld_press_acha(scan_lines_along_track_direction, pixel_elements_along_scan_direction) ;
cld_press_acha:SCALED = '\1' ;
cld_press_acha:UNITS = "hPa" ;
cld_press_acha:STANDARD_NAME = "air_pressure_at_cloud_top" ;
cld_press_acha:LONG_NAME = "cloud-top pressure computed using the AWG cloud height algorithm" ;
cld_press_acha:RANGE_MISSING = -999.f ;
cld_press_acha:RANGE_MIN = 0.f ;
cld_press_acha:RANGE_MAX = 1100.f ;
cld_press_acha:SCALED_MIN = -127 ;
cld_press_acha:SCALED_MAX = 127 ;
cld_press_acha:SCALED_MISSING = -128 ;
cld_press_acha:_FILLVALUE = -128 ;
cld_press_acha:SCALE_FACTOR = 4.3307085f ;
cld_press_acha:ADD_OFFSET = 550.f ;
byte cld_temp_acha(scan_lines_along_track_direction, pixel_elements_along_scan_direction) ;
cld_temp_acha:SCALED = '\1' ;
cld_temp_acha:UNITS = "K" ;
cld_temp_acha:STANDARD_NAME = "air_temperature_at_cloud_top" ;
cld_temp_acha:LONG_NAME = "cloud-top temperature computed using the AWG cloud height algorithm" ;
cld_temp_acha:RANGE_MISSING = -999.f ;
cld_temp_acha:RANGE_MIN = 180.f ;
cld_temp_acha:RANGE_MAX = 320.f ;
cld_temp_acha:SCALED_MIN = -127 ;
cld_temp_acha:SCALED_MAX = 127 ;
cld_temp_acha:SCALED_MISSING = -128 ;
cld_temp_acha:_FILLVALUE = -128 ;
cld_temp_acha:SCALE_FACTOR = 0.55118108f ;
cld_temp_acha:ADD_OFFSET = 250.f ;
byte cld_height_acha(scan_lines_along_track_direction, pixel_elements_along_scan_direction) ;
cld_height_acha:SCALED = '\1' ;
cld_height_acha:UNITS = "km" ;
cld_height_acha:STANDARD_NAME = "height_at_cloud_top" ;
cld_height_acha:LONG_NAME = "cloud-top height computed using the AWG cloud height algorithm" ;
cld_height_acha:RANGE_MISSING = -999.f ;
cld_height_acha:RANGE_MIN = 0.f ;
cld_height_acha:RANGE_MAX = 20.f ;
cld_height_acha:SCALED_MIN = -127 ;
cld_height_acha:SCALED_MAX = 127 ;
cld_height_acha:SCALED_MISSING = -128 ;
cld_height_acha:_FILLVALUE = -128 ;
cld_height_acha:SCALE_FACTOR = 0.078740157f ;
cld_height_acha:ADD_OFFSET = 10.f ;
byte cld_emiss_acha(scan_lines_along_track_direction, pixel_elements_along_scan_direction) ;
cld_emiss_acha:SCALED = '\1' ;
cld_emiss_acha:UNITS = "none" ;

cld_emiss_acha:STANDARD_NAME = "cloud_longwave_emissivity_11_0_micron_nominal" ;
cld_emiss_acha:LONG_NAME = "cloud emissivity at the nominal wavelength of 11 microns, determined from the AWG cloud height algorithm" ;
cld_emiss_acha:RANGE_MISSING = -999.f ;
cld_emiss_acha:RANGE_MIN = 0.f ;
cld_emiss_acha:RANGE_MAX = 1.f ;
cld_emiss_acha:SCALED_MIN = -127 ;
cld_emiss_acha:SCALED_MAX = 127 ;
cld_emiss_acha:SCALED_MISSING = -128 ;
cld_emiss_acha:_FILLVALUE = -128 ;
cld_emiss_acha:SCALE_FACTOR = 0.0039370079f ;
cld_emiss_acha:ADD_OFFSET = 0.5f ;
byte cld_beta_acha(scan_lines_along_track_direction, pixel_elements_along_scan_direction) ;
cld_beta_acha:SCALED = '\1' ;
cld_beta_acha:UNITS = "none" ;
cld_beta_acha:STANDARD_NAME = "cloud_longwave_emissivity_beta_ratio_11_0_micron_12_0_micron_nominal" ;
cld_beta_acha:LONG_NAME = "cloud 11/12 micron beta value determined from the split-window method" ;
cld_beta_acha:RANGE_MISSING = -999.f ;
cld_beta_acha:RANGE_MIN = 0.f ;
cld_beta_acha:RANGE_MAX = 2.f ;
cld_beta_acha:SCALED_MIN = -127 ;
cld_beta_acha:SCALED_MAX = 127 ;
cld_beta_acha:SCALED_MISSING = -128 ;
cld_beta_acha:_FILLVALUE = -128 ;
cld_beta_acha:SCALE_FACTOR = 0.0078740157f ;
cld_beta_acha:ADD_OFFSET = 1.f ;
byte cld_height_uncer_acha(scan_lines_along_track_direction, pixel_elements_along_scan_direction) ;
cld_height_uncer_acha:SCALED = '\1' ;
cld_height_uncer_acha:UNITS = "km" ;
cld_height_uncer_acha:STANDARD_NAME = "cloud_height_uncertainty" ;
cld_height_uncer_acha:LONG_NAME = "cloud height uncertainty computed using the AWG cloud height algorithm" ;
cld_height_uncer_acha:RANGE_MISSING = -999.f ;
cld_height_uncer_acha:RANGE_MIN = 0.f ;
cld_height_uncer_acha:RANGE_MAX = 10.f ;
cld_height_uncer_acha:SCALED_MIN = -127 ;
cld_height_uncer_acha:SCALED_MAX = 127 ;
cld_height_uncer_acha:SCALED_MISSING = -128 ;
cld_height_uncer_acha:_FILLVALUE = -128 ;
cld_height_uncer_acha:SCALE_FACTOR = 0.039370079f ;
cld_height_uncer_acha:ADD_OFFSET = 5.f ;
byte cld_temp_acha_qf(scan_lines_along_track_direction, pixel_elements_along_scan_direction) ;
cld_temp_acha_qf:SCALED = '\0' ;
cld_temp_acha_qf:UNITS = "none" ;
cld_temp_acha_qf:STANDARD_NAME = "cld_temp_acha_qf" ;
cld_temp_acha_qf:LONG_NAME = "quality flag for cloud-top temperature from ACHA not attempted=0, failed=1, low quality=2, high quality=3" ;
cld_temp_acha_qf:RANGE_MISSING = -128.f ;
byte cld_emiss_acha_qf(scan_lines_along_track_direction, pixel_elements_along_scan_direction) ;
cld_emiss_acha_qf:SCALED = '\0' ;
cld_emiss_acha_qf:UNITS = "none" ;
cld_emiss_acha_qf:STANDARD_NAME = "cld_emiss_acha_qf" ;
cld_emiss_acha_qf:LONG_NAME = "quality flag for 11 micron cloud emissivity from ACHA not attempted=0, failed=1, low quality=2, high quality=3" ;
cld_emiss_acha_qf:RANGE_MISSING = -128.f ;
byte cld_beta_acha_qf(scan_lines_along_track_direction, pixel_elements_along_scan_direction) ;

cld_beta_acha_qf:SCALED = '\0' ;
cld_beta_acha_qf:UNITS = "none" ;
cld_beta_acha_qf:STANDARD_NAME = "cld_beta_acha_qf" ;
cld_beta_acha_qf:LONG_NAME = "quality flag for cloud 11/12 micron beta from ACHA not attempted=0, failed=1, low quality=2, high quality=3" ;
cld_beta_acha_qf:RANGE_MISSING = -128.f ;
short cld_opd_dcomp(scan_lines_along_track_direction, pixel_elements_along_scan_direction) ;
cld_opd_dcomp:SCALED = '\1' ;
cld_opd_dcomp:UNITS = "none" ;
cld_opd_dcomp:STANDARD_NAME = "atmosphere_optical_thickness_due_to_cloud" ;
cld_opd_dcomp:LONG_NAME = "cloud optical depth at the nominal wavelength of 0.65 microns, determined from DCOMP" ;
cld_opd_dcomp:RANGE_MISSING = -999.f ;
cld_opd_dcomp:RANGE_MIN = -0.2f ;
cld_opd_dcomp:RANGE_MAX = 160.f ;
cld_opd_dcomp:SCALED_MIN = -32767 ;
cld_opd_dcomp:SCALED_MAX = 32767 ;
cld_opd_dcomp:SCALED_MISSING = -32768 ;
cld_opd_dcomp:_FILLVALUE = -32768 ;
cld_opd_dcomp:SCALE_FACTOR = 0.0024445325f ;
cld_opd_dcomp:ADD_OFFSET = 79.900002f ;
short cld_reff_dcomp(scan_lines_along_track_direction, pixel_elements_along_scan_direction) ;
cld_reff_dcomp:SCALED = '\1' ;
cld_reff_dcomp:UNITS = "micron" ;
cld_reff_dcomp:STANDARD_NAME = "effective_radius_of_cloud_particle" ;
cld_reff_dcomp:LONG_NAME = "effective radius of cloud particles determined from DCOMP; see attributes for channels used" ;
cld_reff_dcomp:RANGE_MISSING = -999.f ;
cld_reff_dcomp:RANGE_MIN = 0.f ;
cld_reff_dcomp:RANGE_MAX = 160.f ;
cld_reff_dcomp:SCALED_MIN = -32767 ;
cld_reff_dcomp:SCALED_MAX = 32767 ;
cld_reff_dcomp:SCALED_MISSING = -32768 ;
cld_reff_dcomp:_FILLVALUE = -32768 ;
cld_reff_dcomp:SCALE_FACTOR = 0.0024414808f ;
cld_reff_dcomp:ADD_OFFSET = 80.f ;
short cld_opd_dcomp_unc(scan_lines_along_track_direction, pixel_elements_along_scan_direction) ;
cld_opd_dcomp_unc:SCALED = '\1' ;
cld_opd_dcomp_unc:UNITS = "none" ;
cld_opd_dcomp_unc:STANDARD_NAME = "atmosphere_optical_thickness_due_to_cloud" ;
cld_opd_dcomp_unc:LONG_NAME = "uncertainty in cloud optical depth at the nominal wavelength of 0.63 microns, determined from DCOMP" ;
cld_opd_dcomp_unc:RANGE_MISSING = -999.f ;
cld_opd_dcomp_unc:RANGE_MIN = -0.2f ;
cld_opd_dcomp_unc:RANGE_MAX = 160.f ;
cld_opd_dcomp_unc:SCALED_MIN = -32767 ;
cld_opd_dcomp_unc:SCALED_MAX = 32767 ;
cld_opd_dcomp_unc:SCALED_MISSING = -32768 ;
cld_opd_dcomp_unc:_FILLVALUE = -32768 ;
cld_opd_dcomp_unc:SCALE_FACTOR = 0.0024445325f ;
cld_opd_dcomp_unc:ADD_OFFSET = 79.900002f ;
short cld_reff_dcomp_unc(scan_lines_along_track_direction, pixel_elements_along_scan_direction) ;
cld_reff_dcomp_unc:SCALED = '\1' ;
cld_reff_dcomp_unc:UNITS = "micron" ;
cld_reff_dcomp_unc:STANDARD_NAME = "effective_radius_of_cloud_particle" ;
cld_reff_dcomp_unc:LONG_NAME = "effective radius of cloud particle determined from DCOMP; see attributes for channels used" ;
cld_reff_dcomp_unc:RANGE_MISSING = -999.f ;

cld_reff_dcomp_unc:RANGE_MIN = 0.f ;
cld_reff_dcomp_unc:RANGE_MAX = 160.f ;
cld_reff_dcomp_unc:SCALED_MIN = -32767 ;
cld_reff_dcomp_unc:SCALED_MAX = 32767 ;
cld_reff_dcomp_unc:SCALED_MISSING = -32768 ;
cld_reff_dcomp_unc:_FILLVALUE = -32768 ;
cld_reff_dcomp_unc:SCALE_FACTOR = 0.0024414808f ;
cld_reff_dcomp_unc:ADD_OFFSET = 80.f ;
byte cld_opd_dcomp_qf(scan_lines_along_track_direction, pixel_elements_along_scan_direction) ;
cld_opd_dcomp_qf:SCALED = '\0' ;
cld_opd_dcomp_qf:UNITS = "none" ;
cld_opd_dcomp_qf:STANDARD_NAME = "cld_opd_dcomp_qf" ;
cld_opd_dcomp_qf:LONG_NAME = "quality flag for cloud optical depth from DCOMP not attempted=0, failed=1, low quality=2, high quality=3" ;
cld_opd_dcomp_qf:RANGE_MISSING = -128.f ;
byte cld_reff_dcomp_qf(scan_lines_along_track_direction, pixel_elements_along_scan_direction) ;
cld_reff_dcomp_qf:SCALED = '\0' ;
cld_reff_dcomp_qf:UNITS = "none" ;
cld_reff_dcomp_qf:STANDARD_NAME = "cld_reff_dcomp_qf" ;
cld_reff_dcomp_qf:LONG_NAME = "quality flag for cloud effective radius from DCOMP not attempted=0, failed=1, low quality=2, high quality=3" ;
cld_reff_dcomp_qf:RANGE_MISSING = -128.f ;
byte cloud_albedo_0_65um_nom(scan_lines_along_track_direction, pixel_elements_along_scan_direction) ;
cloud_albedo_0_65um_nom:SCALED = '\1' ;
cloud_albedo_0_65um_nom:UNITS = "none" ;
cloud_albedo_0_65um_nom:STANDARD_NAME = "cloud_albedo_0_65um_nominal" ;
cloud_albedo_0_65um_nom:LONG_NAME = "cloud albedo at 0.65 microns nominal from DCOMP" ;
cloud_albedo_0_65um_nom:RANGE_MISSING = -999.f ;
cloud_albedo_0_65um_nom:RANGE_MIN = 0.f ;
cloud_albedo_0_65um_nom:RANGE_MAX = 1.f ;
cloud_albedo_0_65um_nom:SCALED_MIN = -127 ;
cloud_albedo_0_65um_nom:SCALED_MAX = 127 ;
cloud_albedo_0_65um_nom:SCALED_MISSING = -128 ;
cloud_albedo_0_65um_nom:_FILLVALUE = -128 ;
cloud_albedo_0_65um_nom:SCALE_FACTOR = 0.0039370079f ;
cloud_albedo_0_65um_nom:ADD_OFFSET = 0.5f ;
byte cloud_transmission_0_65um_nom(scan_lines_along_track_direction, pixel_elements_along_scan_direction) ;
cloud_transmission_0_65um_nom:SCALED = '\1' ;
cloud_transmission_0_65um_nom:UNITS = "none" ;
cloud_transmission_0_65um_nom:STANDARD_NAME = "cloud_transmission_0_65um_nominal" ;
cloud_transmission_0_65um_nom:LONG_NAME = "cloud transmission 0.65 microns nominal from DCOMP" ;
cloud_transmission_0_65um_nom:RANGE_MISSING = -999.f ;
cloud_transmission_0_65um_nom:RANGE_MIN = 0.f ;
cloud_transmission_0_65um_nom:RANGE_MAX = 1.f ;
cloud_transmission_0_65um_nom:SCALED_MIN = -127 ;
cloud_transmission_0_65um_nom:SCALED_MAX = 127 ;
cloud_transmission_0_65um_nom:SCALED_MISSING = -128 ;
cloud_transmission_0_65um_nom:_FILLVALUE = -128 ;
cloud_transmission_0_65um_nom:SCALE_FACTOR = 0.0039370079f ;
cloud_transmission_0_65um_nom:ADD_OFFSET = 0.5f ;
byte cloud_fraction(scan_lines_along_track_direction, pixel_elements_along_scan_direction) ;
cloud_fraction:SCALED = '\1' ;
cloud_fraction:UNITS = "none" ;
cloud_fraction:STANDARD_NAME = "cloud_fraction" ;

cloud_fraction:LONG_NAME = "cloud fraction computed over a 3x3 pixel array at the native resolution centered on this pixel" ;
cloud_fraction:RANGE_MISSING = -999.f ;
cloud_fraction:RANGE_MIN = 0.f ;
cloud_fraction:RANGE_MAX = 1.f ;
cloud_fraction:SCALED_MIN = -127 ;
cloud_fraction:SCALED_MAX = 127 ;
cloud_fraction:SCALED_MISSING = -128 ;
cloud_fraction:_FILLVALUE = -128 ;
cloud_fraction:SCALE_FACTOR = 0.0039370079f ;
cloud_fraction:ADD_OFFSET = 0.5f ;
byte cloud_fraction_uncertainty(scan_lines_along_track_direction, pixel_elements_along_scan_direction) ;
cloud_fraction_uncertainty:SCALED = '\1' ;
cloud_fraction_uncertainty:UNITS = "none" ;
cloud_fraction_uncertainty:STANDARD_NAME = "cloud_fraction_uncertainty" ;
cloud_fraction_uncertainty:LONG_NAME = "cloud fraction uncertainty computed over a 3x3 array" ;
cloud_fraction_uncertainty:RANGE_MISSING = -999.f ;
cloud_fraction_uncertainty:RANGE_MIN = 0.f ;
cloud_fraction_uncertainty:RANGE_MAX = 1.f ;
cloud_fraction_uncertainty:SCALED_MIN = -127 ;
cloud_fraction_uncertainty:SCALED_MAX = 127 ;
cloud_fraction_uncertainty:SCALED_MISSING = -128 ;
cloud_fraction_uncertainty:_FILLVALUE = -128 ;
cloud_fraction_uncertainty:SCALE_FACTOR = 0.0039370079f ;
cloud_fraction_uncertainty:ADD_OFFSET = 0.5f ;
short aot_0_65um_nom(scan_lines_along_track_direction, pixel_elements_along_scan_direction) ;
aot_0_65um_nom:SCALED = '\1' ;
aot_0_65um_nom:UNITS = "none" ;
aot_0_65um_nom:STANDARD_NAME = "optical_thickness_of_atmosphere_layer_due_to_aerosol_0.65_micron nominal" ;
aot_0_65um_nom:LONG_NAME = "optical thickness of atmosphere layer due to aerosol at the nominal wavelength of 0.65 microns" ;
aot_0_65um_nom:RANGE_MISSING = -999.f ;
aot_0_65um_nom:RANGE_MIN = -0.2f ;
aot_0_65um_nom:RANGE_MAX = 5.f ;
aot_0_65um_nom:SCALED_MIN = -32767 ;
aot_0_65um_nom:SCALED_MAX = 32767 ;
aot_0_65um_nom:SCALED_MISSING = -32768 ;
aot_0_65um_nom:_FILLVALUE = -32768 ;
aot_0_65um_nom:SCALE_FACTOR = 7.9348123e-05f ;
aot_0_65um_nom:ADD_OFFSET = 2.3999999f ;
byte olr(scan_lines_along_track_direction, pixel_elements_along_scan_direction) ;
olr:SCALED = '\1' ;
olr:UNITS = "W m-2" ;
olr:STANDARD_NAME = "toa_outgoing_longwave_flux" ;
olr:LONG_NAME = "top of atmosphere outgoing longwave radiation" ;
olr:RANGE_MISSING = -999.f ;
olr:RANGE_MIN = 50.f ;
olr:RANGE_MAX = 350.f ;
olr:SCALED_MIN = -127 ;
olr:SCALED_MAX = 127 ;
olr:SCALED_MISSING = -128 ;
olr:_FILLVALUE = -128 ;
olr:SCALE_FACTOR = 1.1811024f ;
olr:ADD_OFFSET = 200.f ;
byte insolation(scan_lines_along_track_direction, pixel_elements_along_scan_direction) ;
insolation:SCALED = '\1' ;

insolation:UNITS = "W m-2" ;
insolation:STANDARD_NAME = "surface_downwelling_shortwave_flux" ;
insolation:LONG_NAME = "surface downwelling shortwave flux computed from the SASRAB routine" ;
insolation:RANGE_MISSING = -999.f ;
insolation:RANGE_MIN = -100.f ;
insolation:RANGE_MAX = 1500.f ;
insolation:SCALED_MIN = -127 ;
insolation:SCALED_MAX = 127 ;
insolation:SCALED_MISSING = -128 ;
insolation:_FILLVALUE = -128 ;
insolation:SCALE_FACTOR = 6.2992125f ;
insolation:ADD_OFFSET = 700.f ;
byte insolation_diffuse(scan_lines_along_track_direction, pixel_elements_along_scan_direction) ;
insolation_diffuse:SCALED = '\1' ;
insolation_diffuse:UNITS = "W m-2" ;
insolation_diffuse:STANDARD_NAME = "surface_downwelling_shortwave_flux_diffuse" ;
insolation_diffuse:LONG_NAME = "diffuse component of the surface downwelling shortwave flux computed from the SASRAB routine" ;
insolation_diffuse:RANGE_MISSING = -999.f ;
insolation_diffuse:RANGE_MIN = -100.f ;
insolation_diffuse:RANGE_MAX = 1500.f ;
insolation_diffuse:SCALED_MIN = -127 ;
insolation_diffuse:SCALED_MAX = 127 ;
insolation_diffuse:SCALED_MISSING = -128 ;
insolation_diffuse:_FILLVALUE = -128 ;
insolation_diffuse:SCALE_FACTOR = 6.2992125f ;
insolation_diffuse:ADD_OFFSET = 700.f ;
byte ndvi_sfc(scan_lines_along_track_direction, pixel_elements_along_scan_direction) ;
ndvi_sfc:SCALED = '\1' ;
ndvi_sfc:UNITS = "none" ;
ndvi_sfc:STANDARD_NAME = "normalized_difference_vegetation_index_at_surface" ;
ndvi_sfc:LONG_NAME = "normalized difference vegetation index, atmospherically corrected" ;
ndvi_sfc:RANGE_MISSING = -999.f ;
ndvi_sfc:RANGE_MIN = -0.5f ;
ndvi_sfc:RANGE_MAX = 1.f ;
ndvi_sfc:SCALED_MIN = -127 ;
ndvi_sfc:SCALED_MAX = 127 ;
ndvi_sfc:SCALED_MISSING = -128 ;
ndvi_sfc:_FILLVALUE = -128 ;
ndvi_sfc:SCALE_FACTOR = 0.0059055118f ;
ndvi_sfc:ADD_OFFSET = 0.25f ;
byte surface_temperature_retrieved(scan_lines_along_track_direction, pixel_elements_along_scan_direction) ;
surface_temperature_retrieved:SCALED = '\1' ;
surface_temperature_retrieved:UNITS = "K" ;
surface_temperature_retrieved:STANDARD_NAME = "surface_temperature_retrieved" ;
surface_temperature_retrieved:LONG_NAME = "surface temperature retrieved using atmosherically corrected 11 micron radiance" ;
surface_temperature_retrieved:RANGE_MISSING = -999.f ;
surface_temperature_retrieved:RANGE_MIN = 220.f ;
surface_temperature_retrieved:RANGE_MAX = 340.f ;
surface_temperature_retrieved:SCALED_MIN = -127 ;
surface_temperature_retrieved:SCALED_MAX = 127 ;
surface_temperature_retrieved:SCALED_MISSING = -128 ;
surface_temperature_retrieved:_FILLVALUE = -128 ;
surface_temperature_retrieved:SCALE_FACTOR = 0.47244096f ;
surface_temperature_retrieved:ADD_OFFSET = 280.f ;

byte tropopause_temperature(scan_lines_along_track_direction, pixel_elements_along_scan_direction) ;
tropopause_temperature:SCALED = '\1' ;
tropopause_temperature:UNITS = "K" ;
tropopause_temperature:STANDARD_NAME = "tropopause_temperature" ;
tropopause_temperature:LONG_NAME = "tropopause temperature from numerical weather prediction ancillary data" ;
tropopause_temperature:RANGE_MISSING = -999.f ;
tropopause_temperature:RANGE_MIN = 160.f ;
tropopause_temperature:RANGE_MAX = 260.f ;
tropopause_temperature:SCALED_MIN = -127 ;
tropopause_temperature:SCALED_MAX = 127 ;
tropopause_temperature:SCALED_MISSING = -128 ;
tropopause_temperature:_FILLVALUE = -128 ;
tropopause_temperature:SCALE_FACTOR = 0.39370078f ;
tropopause_temperature:ADD_OFFSET = 210.f ;
byte quality_flags_1(scan_lines_along_track_direction, pixel_elements_along_scan_direction) ;
quality_flags_1:SCALED = '\0' ;
quality_flags_1:UNITS = "none" ;
quality_flags_1:STANDARD_NAME = "quality_flags_1" ;
quality_flags_1:LONG_NAME = "first set of packed quality flags, see documentation to unpack" ;
quality_flags_1:RANGE_MISSING = -128.f ;
byte quality_flags_2(scan_lines_along_track_direction, pixel_elements_along_scan_direction) ;
quality_flags_2:SCALED = '\0' ;
quality_flags_2:UNITS = "none" ;
quality_flags_2:STANDARD_NAME = "quality_flags_2" ;
quality_flags_2:LONG_NAME = "second set of packed quality flags, see documention to unpack" ;
quality_flags_2:RANGE_MISSING = -128.f ;
byte total_precipitable_water(scan_lines_along_track_direction, pixel_elements_along_scan_direction) ;
total_precipitable_water:SCALED = '\1' ;
total_precipitable_water:UNITS = "cm" ;
total_precipitable_water:STANDARD_NAME = "total_precipitable_water_from_nwp_ancillary_data" ;
total_precipitable_water:LONG_NAME = "total precipitable water from numerical weather prediction ancillary data" ;
total_precipitable_water:RANGE_MISSING = -999.f ;
total_precipitable_water:RANGE_MIN = 0.f ;
total_precipitable_water:RANGE_MAX = 10.f ;
total_precipitable_water:SCALED_MIN = -127 ;
total_precipitable_water:SCALED_MAX = 127 ;
total_precipitable_water:SCALED_MISSING = -128 ;
total_precipitable_water:_FILLVALUE = -128 ;
total_precipitable_water:SCALE_FACTOR = 0.039370079f ;
total_precipitable_water:ADD_OFFSET = 5.f ;
short refl_0_65um_nom_unnormalized(scan_lines_along_track_direction, pixel_elements_along_scan_direction) ;
refl_0_65um_nom_unnormalized:SCALED = '\1' ;
refl_0_65um_nom_unnormalized:UNITS = "%" ;
refl_0_65um_nom_unnormalized:STANDARD_NAME = "toa_bidirectional_reflectance_0_65_micron_nominal_unormalized_to_solar_zenith" ;
refl_0_65um_nom_unnormalized:LONG_NAME = "top of atmosphere reflectance at the nominal wavelength of 0.65 microns unnormalized to the cosine of the solar zenith angle" ;
refl_0_65um_nom_unnormalized:RANGE_MISSING = -999.f ;
refl_0_65um_nom_unnormalized:RANGE_MIN = -2.f ;
refl_0_65um_nom_unnormalized:RANGE_MAX = 120.f ;
refl_0_65um_nom_unnormalized:SCALED_MIN = -32767 ;
refl_0_65um_nom_unnormalized:SCALED_MAX = 32767 ;
refl_0_65um_nom_unnormalized:SCALED_MISSING = -32768 ;
refl_0_65um_nom_unnormalized:_FILLVALUE = -32768 ;

refl_0_65um_nom_unnormalized:SCALE_FACTOR = 0.0018616291f ;
refl_0_65um_nom_unnormalized:ADD_OFFSET = 59.f ;
short refl_0_65um_nom_clear_sky(scan_lines_along_track_direction,
pixel_elements_along_scan_direction) ;
refl_0_65um_nom_clear_sky:SCALED = '\1' ;
refl_0_65um_nom_clear_sky:UNITS = "%" ;
refl_0_65um_nom_clear_sky:STANDARD_NAME =
"toa_bidirectional_reflectance_assuming_clear_sky_0_65_micron_nominal" ;
refl_0_65um_nom_clear_sky:LONG_NAME = "top of atmosphere bidirectional reflectance
modeled assuming clear skies at the nominal wavelength of 0.65 microns" ;
refl_0_65um_nom_clear_sky:RANGE_MISSING = -999.f ;
refl_0_65um_nom_clear_sky:RANGE_MIN = -2.f ;
refl_0_65um_nom_clear_sky:RANGE_MAX = 120.f ;
refl_0_65um_nom_clear_sky:SCALED_MIN = -32767 ;
refl_0_65um_nom_clear_sky:SCALED_MAX = 32767 ;
refl_0_65um_nom_clear_sky:SCALED_MISSING = -32768 ;
refl_0_65um_nom_clear_sky:_FILLVALUE = -32768 ;
refl_0_65um_nom_clear_sky:SCALE_FACTOR = 0.0018616291f ;
refl_0_65um_nom_clear_sky:ADD_OFFSET = 59.f ;
short refl_0_65um_nom_mean_3x3(scan_lines_along_track_direction,
pixel_elements_along_scan_direction) ;
refl_0_65um_nom_mean_3x3:SCALED = '\1' ;
refl_0_65um_nom_mean_3x3:UNITS = "%" ;
refl_0_65um_nom_mean_3x3:STANDARD_NAME =
"toa_reflectance_0_65_micron_nomimal_3x3_mean" ;
refl_0_65um_nom_mean_3x3:LONG_NAME = "mean of the 0.65 micron nominal reflectance
computed over a 3x3 pixel array" ;
refl_0_65um_nom_mean_3x3:RANGE_MISSING = -999.f ;
refl_0_65um_nom_mean_3x3:RANGE_MIN = -2.f ;
refl_0_65um_nom_mean_3x3:RANGE_MAX = 120.f ;
refl_0_65um_nom_mean_3x3:SCALED_MIN = -32767 ;
refl_0_65um_nom_mean_3x3:SCALED_MAX = 32767 ;
refl_0_65um_nom_mean_3x3:SCALED_MISSING = -32768 ;
refl_0_65um_nom_mean_3x3:_FILLVALUE = -32768 ;
refl_0_65um_nom_mean_3x3:SCALE_FACTOR = 0.0018616291f ;
refl_0_65um_nom_mean_3x3:ADD_OFFSET = 59.f ;
byte pixel_sst_unmasked(scan_lines_along_track_direction, pixel_elements_along_scan_direction) ;
pixel_sst_unmasked:SCALED = '\1' ;
pixel_sst_unmasked:UNITS = "K" ;
pixel_sst_unmasked:STANDARD_NAME = "sea_surface_skin_temperature_unmasked" ;
pixel_sst_unmasked:LONG_NAME = "sea surface skin temperature at the pixel with land mask
applied and cloud mask not applied" ;
pixel_sst_unmasked:RANGE_MISSING = -999.f ;
pixel_sst_unmasked:RANGE_MIN = 265.f ;
pixel_sst_unmasked:RANGE_MAX = 315.f ;
pixel_sst_unmasked:SCALED_MIN = -127 ;
pixel_sst_unmasked:SCALED_MAX = 127 ;
pixel_sst_unmasked:SCALED_MISSING = -128 ;
pixel_sst_unmasked:_FILLVALUE = -128 ;
pixel_sst_unmasked:SCALE_FACTOR = 0.19685039f ;
pixel_sst_unmasked:ADD_OFFSET = 290.f ;
byte wind_speed_10m(scan_lines_along_track_direction, pixel_elements_along_scan_direction) ;
wind_speed_10m:SCALED = '\1' ;
wind_speed_10m:UNITS = "m/s" ;
wind_speed_10m:STANDARD_NAME = "wind_speed_10m_above_ground" ;
wind_speed_10m:LONG_NAME = "wind speed from the NWP ancillary data at 10m above ground
level" ;
wind_speed_10m:RANGE_MISSING = -999.f ;

wind_speed_10m:RANGE_MIN = 0.f ;
wind_speed_10m:RANGE_MAX = 50.f ;
wind_speed_10m:SCALED_MIN = -127 ;
wind_speed_10m:SCALED_MAX = 127 ;
wind_speed_10m:SCALED_MISSING = -128 ;
wind_speed_10m:_FILLVALUE = -128 ;
wind_speed_10m:SCALE_FACTOR = 0.19685039f ;
wind_speed_10m:ADD_OFFSET = 25.f ;
byte wind_direction_10m(scan_lines_along_track_direction, pixel_elements_along_scan_direction) ;
wind_direction_10m:SCALED = '\1' ;
wind_direction_10m:UNITS = "degrees" ;
wind_direction_10m:STANDARD_NAME = "wind_direction_10m_above_ground" ;
wind_direction_10m:LONG_NAME = "wind direction from the NWP ancillary data at 10m above ground level" ;
wind_direction_10m:RANGE_MISSING = -999.f ;
wind_direction_10m:RANGE_MIN = 0.f ;
wind_direction_10m:RANGE_MAX = 360.f ;
wind_direction_10m:SCALED_MIN = -127 ;
wind_direction_10m:SCALED_MAX = 127 ;
wind_direction_10m:SCALED_MISSING = -128 ;
wind_direction_10m:_FILLVALUE = -128 ;
wind_direction_10m:SCALE_FACTOR = 1.4173229f ;
wind_direction_10m:ADD_OFFSET = 180.f ;
short refl_0_65um_nom_dark(scan_lines_along_track_direction, pixel_elements_along_scan_direction) ;
refl_0_65um_nom_dark:SCALED = '\1' ;
refl_0_65um_nom_dark:UNITS = "%" ;
refl_0_65um_nom_dark:STANDARD_NAME = "toa_bidirectional_reflectance_0_65_micron_nominal_dark_sky_composite" ;
refl_0_65um_nom_dark:LONG_NAME = "top of atmosphere reflectance at the nominal wavelength of 0.65 microns generated from a dark-sky compositing method" ;
refl_0_65um_nom_dark:RANGE_MISSING = -999.f ;
refl_0_65um_nom_dark:RANGE_MIN = -2.f ;
refl_0_65um_nom_dark:RANGE_MAX = 120.f ;
refl_0_65um_nom_dark:SCALED_MIN = -32767 ;
refl_0_65um_nom_dark:SCALED_MAX = 32767 ;
refl_0_65um_nom_dark:SCALED_MISSING = -32768 ;
refl_0_65um_nom_dark:_FILLVALUE = -32768 ;
refl_0_65um_nom_dark:SCALE_FACTOR = 0.0018616291f ;
refl_0_65um_nom_dark:ADD_OFFSET = 59.f ;
byte cloud_water_path(scan_lines_along_track_direction, pixel_elements_along_scan_direction) ;
cloud_water_path:SCALED = '\1' ;
cloud_water_path:UNITS = "g m-2" ;
cloud_water_path:STANDARD_NAME = "cloud_water_path" ;
cloud_water_path:LONG_NAME = "integrated total cloud water over whole column" ;
cloud_water_path:RANGE_MISSING = -999.f ;
cloud_water_path:RANGE_MIN = 0.f ;
cloud_water_path:RANGE_MAX = 1200.f ;
cloud_water_path:SCALED_MIN = -127 ;
cloud_water_path:SCALED_MAX = 127 ;
cloud_water_path:SCALED_MISSING = -128 ;
cloud_water_path:_FILLVALUE = -128 ;
cloud_water_path:SCALE_FACTOR = 4.7244096f ;
cloud_water_path:ADD_OFFSET = 600.f ;

// global attributes:
:PROCESSOR = "CLAVR-x + PATMOS-x 6.2.0" ;
:CREATED = "2011-07-26T15:26:44-05:00" ;
:HDF_LIB_VERSION = "HDF Version 4.2 Release 4, January 25, 2009" ;

:MACHINE = "saga" ;
:PROGLANG = "F90" ;
:FILENAME = "goes11_2009_365_1930.level2.hdf" ;
:L1B = "goes11_2009_365_1930" ;
:START_YEAR = 2009s ;
:START_DAY = 365s ;
:START_TIME = 19.5f ;
:END_YEAR = 2009s ;
:END_DAY = 365s ;
:END_TIME = 19.5f ;
:SPACECRAFT_ID = 25 ;
:ACHA_MODE = 5 ;
:DCOMP_MODE = 3 ;
:WMO_SATELLITE_CODE = 255 ;
:SENSOR_NAME = "GOES-11 : Imager   " ;
:DATA_TYPE = "PIXEL" ;
:USE_1B_THERMAL_CALIBRATION_FLAG = 0 ;
:USE_1B_REFLECTANCE_CALIBRATION_FLAG = 0 ;
:RENAVIGATION_FLAG = 2 ;
:USE_SST_ANALYSIS_FLAG = 1 ;
:CLOUD_TYPING_FLAG = 0 ;
:SST_ANALYSIS_SOURCE_FLAG = 0 ;
:NWP_FLAG = 3 ;
:MODIS_CLEAR_SKY_REFLECTANCE_FLAG = 1 ;
:CH1_GAIN_LOW = 0.f ;
:CH1_GAIN_HIGH = 0.f ;
:CH1_SWITCH_COUNT = 0.f ;
:CH1_DARK_COUNT = 0.f ;
:CH2_GAIN_LOW = 0.f ;
:CH2_GAIN_HIGH = 0.f ;
:CH2_SWITCH_COUNT = 0.f ;
:CH2_DARK_COUNT = 0.f ;
:CH3A_GAIN_LOW = 0.f ;
:CH3A_GAIN_HIGH = 0.f ;
:CH3A_SWITCH_COUNT = 0.f ;
:CH3A_DARK_COUNT = 0.f ;
:SUN_EARTH_DISTANCE = 0.98331589f ;
:C1 = 1.191062e-05f ;
:C2 = 1.4387863f ;
:A_20 = -0.64474517f ;
:B_20 = 1.0007721f ;
:NU_20 = 2562.084f ;
:A_31 = -0.57256413f ;
:B_31 = 1.0015252f ;
:NU_31 = 933.49097f ;
:A_32 = -0.3507058f ;
:B_32 = 1.001025f ;
:NU_32 = 833.46735f ;
:SOLAR_20_NU = 14.580327f ;
:TIME_ERROR_SECONDS = 0.f ;
:NUMBER_OF_ELEMENTS = 1657 ;
:NUMBER_OF_SCANS_LEVEL1B = 1355 ;
:NUMBER_OF_SCANS_LEVEL2 = 1355 ;
}

Appendix BB

Surface Radiation Datasets from Geostationary Satellites

Subcontract AXL-0-40276-01
with 9/18/2012 Modification

Christine Molling[1], Andrew Heidinger[2], Steve Ackerman[1]
1. UW SSEC CIMSS, 2. NOAA NESDIS STAR

Final Report
Date: October 2013

Abstract

An improved version of the Pathfinder Atmospheres – Extended (PATMOS-x) processing system was used to reprocess GOES-WEST and -EAST data for years 2005-2009; and to process years 2010 and 2011. By using 2009 statistics as representative of the expected changes for the 2005-2009 reanalysis, the annual root mean square error for all sky conditions and all sites global horizontal irradiance (GHI), direct normal irradiance (DNI), and diffuse irradiance changed very little from the original processing. The least squares fit slope changed from 0.83, 0.69, and 0.91 for GHI, DNI, and diffuse, to 0.83, 0.67, and 0.90, respectively. The root mean squared error changed very little as well. Analysis of 2010 and 2011 produced irradiance products with a similar level of accuracy.

9. Introduction

In September, 2010, a subcontract agreement was made between the National Renewable Energy Laboratory and the University of Wisconsin – Madison in order to compute cloud and surface products from Geostationary Operational Environmental Satellite (GOES) Imager data for the years 2005 through 2009. This data set was computed by inserting the Global Solar Insolation Project (GSIP) algorithm Satellite Algorithm for Shortwave RAdiation Budget (SASRAB) into the Pathfinder Atmospheres – Extended (PATMOS-x) processing system in order to compute the desired surface products of global horizontal irradiance (GHI) and direct normal irradiance (DNI) and cloud products at a higher resolution than was available from GSIP. The data set consisted of 9.2 Tb of files, each containing about 60 different data variables at the resolution of the GOES Imager thermal data (4km at the equator). This data set was delivered in 2011 (Heidinger and Molling, 2011).

A subsequent modification to the subcontact was signed in 2012 to support the production of another 2 years of analysis plus a reanalysis of 2005-2009. This report covers the work supported by the subcontract modification.

Funds under this subcontract were used for labor (salary, fringe benefits and indirect costs), a trip to NREL, and to purchase a computer disk (Dell MD1200, serial number 4W5LYV1, property number F0034005).

10. Algorithm

The version of PATMOS-x used to create the data set is the development branch version tagged "nrel_2010-11_and_2005-9_reanalysis" and dated March 23, 2013. The main differences between the version of PATMOS-x used for this analysis and the previous version are related to tuning of the cloud detection and products algorithms. In particular cloud detection was tuned to better identify low, thin cloud and fog. SASRAB code was not changed. All other processing was identical to that described in Heidinger and Molling (2011), except for the following:

- Updated calibration tables for operational GOES Imagers (11, 12, 13)
- Use of Climate Forecast System Reanalysis (CFSR) ancillary data instead of Global Forecast System (GFS).

Any differences between the 2005-2009 reanalysis and the old analysis are due to the PATMOS-x algorithm changes, calibration changes, and ancillary data changes listed above.

11. Results

Level2 files (data products at the thermal pixel resolution) were computed for 2005-2011. 2005-2011 output was about 16.2 Tb. When processed at the thermal resolution, the 1km visible image is subsampled once per thermal pixel. The pixel selected is the most northwest in the box covered by the thermal pixel.

11.1. Files

File format is HDF4 and is similar to the previous analysis. Some attributes have changed names and/or capitalization, and additional global attributes are present. There is one level2 file every 30 minutes when available, with WEST having files 00 and 30 minutes after the hour and EAST 15 and 45 minutes after the hour. Files are Northern Hemisphere (WEST) or Northern Hemisphere Extended (EAST) for most times, and Full Disk, when a Full Disk image is available (every 3 hours beginning 0000 UTC for WEST and 0245 for EAST). Below are plots showing data availability for years 2010 and 2011. The same files as in the 2005-2009 original processing were reprocessed using the new algorithm. Please refer Heidinger and Molling (2011) for figures depicting these years.

A **black** square indicates that no file is present for that satellite at that time. A **green** square indicates that a file is present and more than 99% of the earth pixels have a valid insolation calculation. A **yellow** square indicates that at least 95%, but less than 99% of the pixels have a valid insolation calculation. **Red** indicates that less than 95% of the pixels have a valid insolation calculation. A common pattern emerges from studying these quicklooks. Besides the semi-random nature of lower quality images due to transmission errors, satellite/instrument ageing, and malfunction, one can clearly see the large data gaps (black shapes) due to the eclipse periods in spring and fall. The limited storage of the batteries on board GOES cause these unrecoverable data gaps. Yellow squares usually indicate data loss in the source imagery, while red typically indicates there was some difficulty in computing the dark sky composite. The red shapes at the same time of year as the eclipse period occur because the rapidly changing availabilty of the small number of illuminated pixels from one day to the next causes the dark sky composite code to fail. If no dark sky composite was available, insolation products were not calculated. GOES-13 had an extended period of dark sky compositing failure at the beginning of operations in 2010 because its orbital position was changing as it was maneuvered into the EAST operational position.

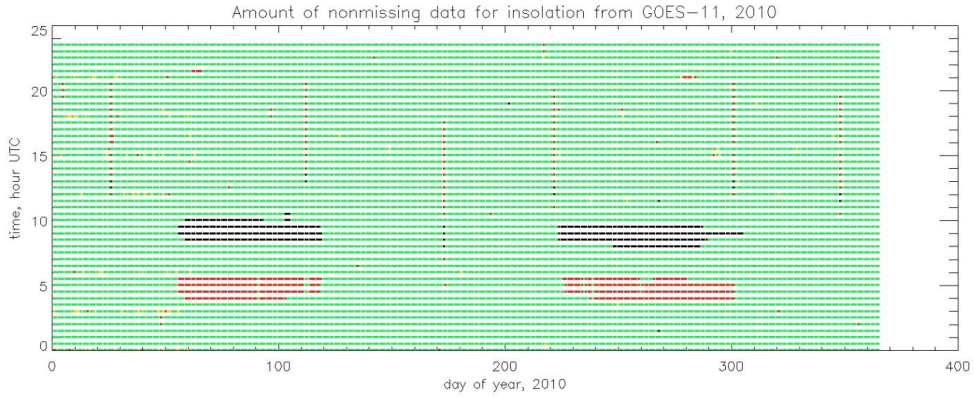

Figure 0.1 Amount of non-missing insolation data for GOES-11 (WEST) processed during 2010.

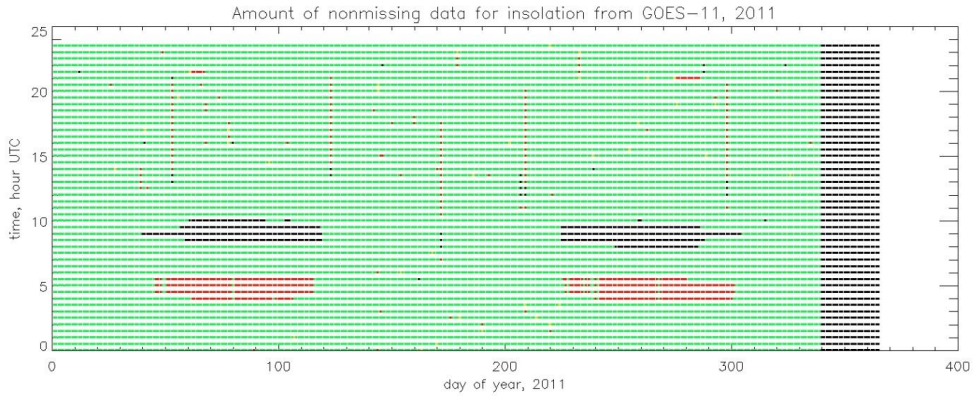

Figure 0.2 As above, but for GOES-11 (WEST), 2011.

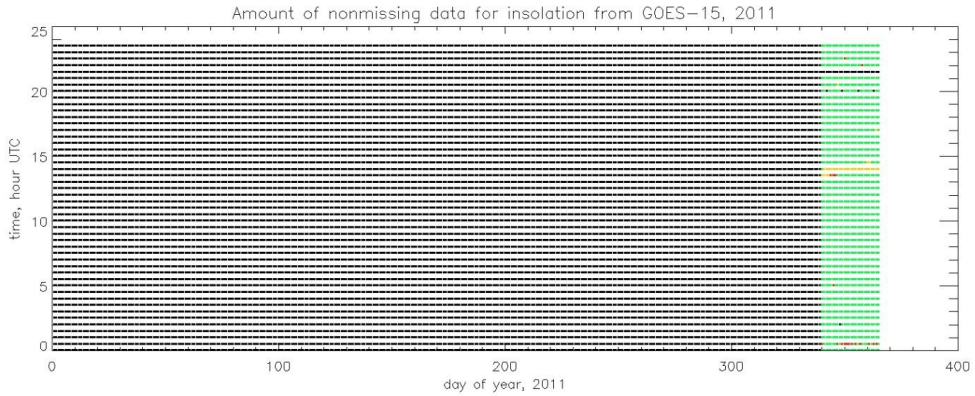

Figure 0.3 As above, but for GOES-15 (WEST), 2011.

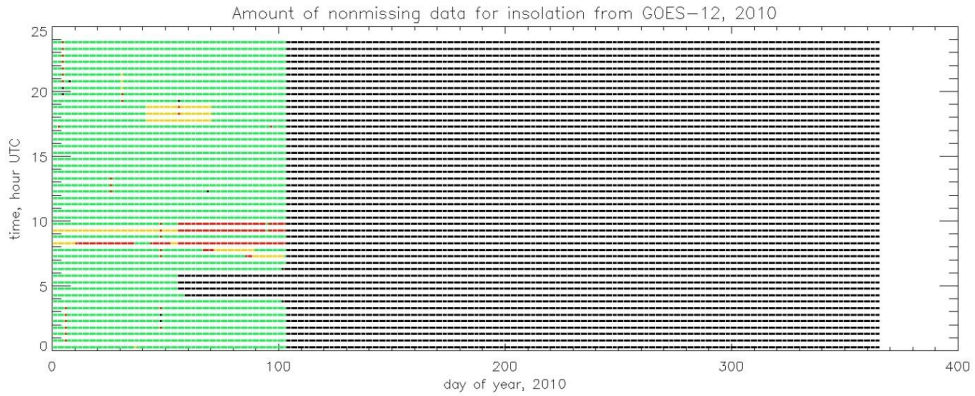

Figure 0.4 As above, but for GOES-12 (EAST), 2010.

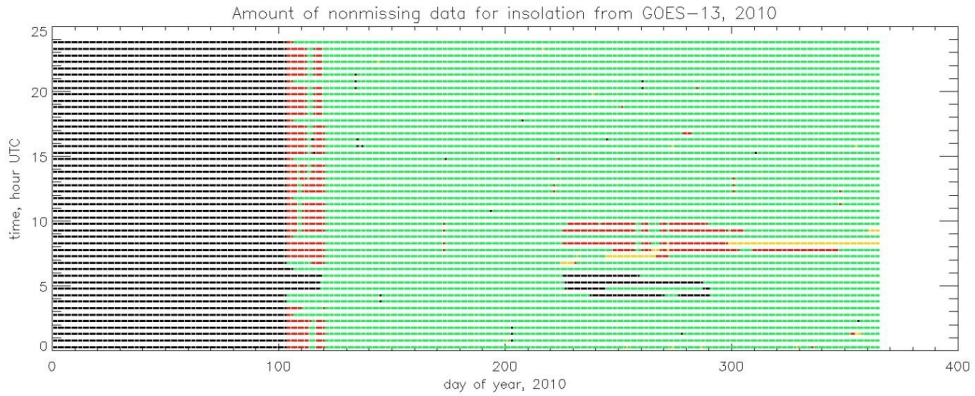

Figure 0.5 As above, but for GOES-13 (EAST), 2010.

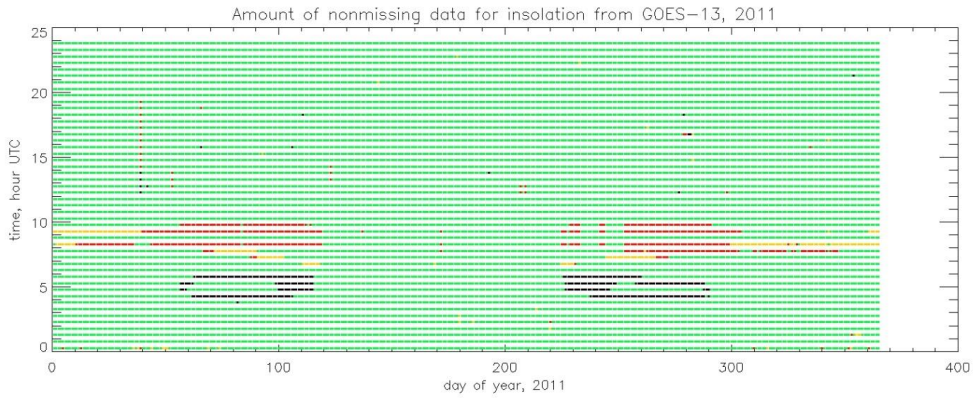

Figure 0.6 As above, but for GOES-13 (EAST), 2011.

Each file contains approximately 60 observed and computed products. See Appendix A for a header list that contains product names and other metadata.

11.2. Statistics

The statistics for a linear least squares fit and the root mean squared error (RMSE) were computed between the PATMOS-x and SURFRAD quantities of global horizontal irradiance (GHI, known as insolation in the level2 files), direct normal irradiance (DNI, computed from insolation, diffuse, and solar zenith angle in the level2 files) and diffuse irradiance. GOES-WEST data are compared to SURFRAD observations at sites Fort Peck, MT (fpk), Boulder, CO (tbl), and Desert Rock, NV (dra). GOES-EAST data are compared to sites Bondville, IL (bon), Goodwin Creek, MS (gwn), Penn State, PA (psu), and Sioux Falls, SD (sxf). SURFRAD observations used were a mean of all data within 5 minutes of the satellite pixel acquisition time at the site. Skies are considered clear if the average cloud fraction in PATMOS-x within 10km of the SURFRAD sites is less than 0.1, and cloudy skies if the cloud fraction is greater than 0.9. Table 1 contains the all-site average statistics of slope and RMSE for years 2009 through 2011. The statistics for the older analysis are also provided for 2009. Please note that the statistics in the table for the old 2009 analysis are not identical to those provided in the previous report, as those statistics were the mean of 12 monthly statistics. The values in Table 1 below are single statistics for all data during the entire year. Note that all sky condition slope statistics for diffuse are worse than for individual sky conditions, as there are some sites that have very poor statistics that average out to a slope near 1.

Table 11 Statistics for seven SURFRAD sites for entire year under different sky conditions. Slope is the least squares fit slope between the PATMOS-x computed quantity and that observed at the SURFRAD sites. RMSE is the root mean squared error

(Wm^{-2}) between the PATMOS-x computed quantity and that observed at the SURFRAD sites. A * indicates statistics for the previous 2005-2009 analysis.

		All Conditions		Clear		Partly Cloudy		Cloudy	
Quantity	Year	Slope	RMSE	Slope	RMSE	Slope	RMSE	Slope	RMSE
GHI	2009*	0.83	104	0.87	73	0.73	130	0.79	109
GHI	2009	0.83	104	0.83	104	0.74	128	0.81	108
GHI	2010	0.82	106	0.87	71	0.71	134	0.79	112
GHI	2011	0.82	103	0.88	75	0.73	126	0.78	110
DNI	2009*	0.69	239	0.58	212	0.31	286	0.44	231
DNI	2009	0.67	242	0.67	242	0.34	280	0.51	225
DNI	2010	0.66	244	0.50	222	0.30	289	0.51	225
DNI	2011	0.67	246	0.53	240	0.36	277	0.53	219
Diffuse	2009*	0.91	82	1.03	63	0.99	88	0.96	86
Diffuse	2009	0.90	85	1.00	65	0.97	92	0.96	86
Diffuse	2010	0.85	88	0.94	69	0.92	95	0.89	90
Diffuse	2011	0.85	85	0.96	68	0.90	89	0.89	87

Figure 0.7 and Figure 0.8 show the fit of all sky condition data for the old and new analyses for 2009, with clear, partly cloudy, and cloudy symbols. Changes are subtle.

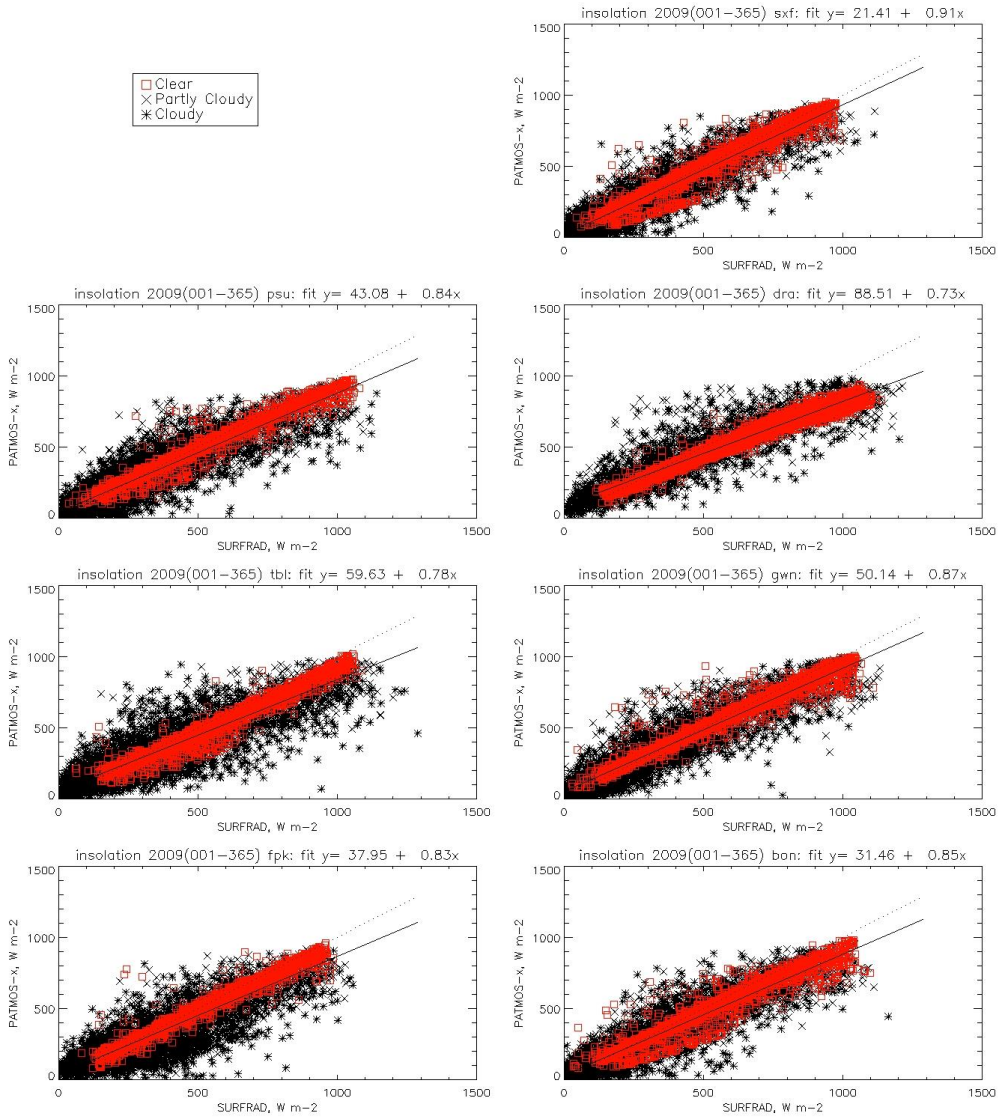

Figure 0.7 Relationship between PATMOS-x calculated GHI and SURFRAD observed by site for 2009 from the old analysis. Solid line is the line of least squares fit. Dotted line is the 1:1 line.

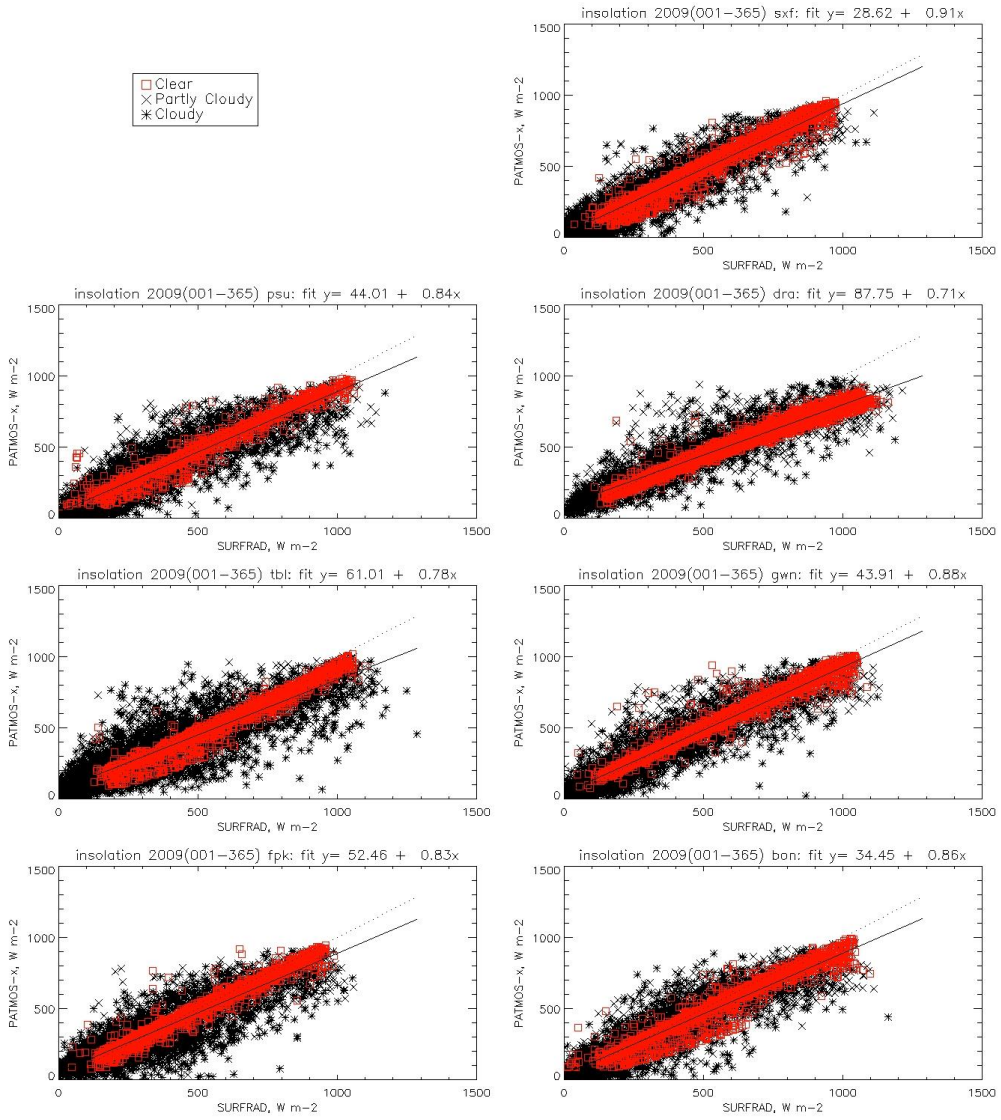

Figure 0.8 As above, but from the new analysis.

As in the previous analysis, statistics for different sky conditions reveal that the best relationship is achieved under completely clear and completely cloudy skies. This is an expected finding, as not only is it easier to identify completely clear and completely cloudy scenes, but it is also easier to model the transmission in a completely clear or cloudy sky. The SASRAB algorithm still fails, however, to capture

the highest values of GHI (and DNI). The best fits tend to be at wetter (darker surface) sites and the worst at drier (brighter surface) sites. This is fairly consistent from one year to the next.

Table 12 Slope of least squares fit and RMSE (Wm^{-2}) by site for all sky conditions during years 2009-2011.

		2009		2010		2011		2009-2011 Average	
Quantity	Site	Slope	RMSE	Slope	RMSE	Slope	RMSE	Slope	RMSE
GHI	bon	0.86	97	0.85	97	0.86	86	0.86	93
GHI	fpk	0.83	100	0.81	109	0.81	118	0.82	109
GHI	gwn	0.88	90	0.86	89	0.89	80	0.88	87
GHI	tbl	0.78	127	0.78	123	0.77	129	0.78	127
GHI	dra	0.71	131	0.71	132	0.72	123	0.72	129
GHI	psu	0.84	100	0.84	101	0.83	95	0.84	99
GHI	sxf	0.91	81	0.86	94	0.85	93	0.87	89
DNI	bon	0.71	209	0.73	210	0.79	182	0.75	200
DNI	fpk	0.74	241	0.70	248	0.67	274	0.70	254
DNI	gwn	0.84	152	0.79	159	0.81	161	0.81	158
DNI	tbl	0.51	326	0.52	315	0.44	355	0.49	332
DNI	dra	0.44	353	0.44	366	0.44	361	0.44	360
DNI	psu	0.71	198	0.70	209	0.77	191	0.73	199
DNI	sxf	0.77	215	0.75	203	0.78	196	0.76	205
Diffuse	bon	0.96	73	0.87	78	0.91	69	0.91	73
Diffuse	fpk	0.90	85	0.80	97	0.65	101	0.78	95
Diffuse	gwn	1.01	64	0.99	58	0.96	54	0.99	59
Diffuse	tbl	0.77	95	0.74	94	0.77	97	0.76	96
Diffuse	dra	0.85	131	0.80	138	0.80	133	0.82	134
Diffuse	psu	0.92	71	0.92	71	0.98	66	0.94	69
Diffuse	sxf	0.92	74	0.79	81	0.85	75	0.85	77

12. Conclusions and Future Work

A cloud and insolation products reanalysis of GOES-EAST and -WEST using SASRAB for 2005 through 2009 was computed using a newer version of PATMOS-x 2010 and 2011 data were also processed with this new version, resulting in a seven year data set. The reanalysis yielded a data set of GHI, DNI (derived) and diffuse irradiance statistically very similar to the previous analysis, based on statistics from 2009. In general, GHI and the diffuse irradiance show the best relationship with observations at SURFRAD sites and DNI the worst. The relationship with observations is also best under completely clear and completely cloudy skies.

Further improvements in PATMOS-x cloud products may be able to reduce the RMSE in comparison with SURFRAD observations, particularly for partly cloudy conditions. Other small improvements can be

expected in 2010 and 2011 irradiance products after the newest GOES (-13 and -15) have a longer calibration period. In order to improve the slope of the linear fit, however, a model better than the current SASRAB would need to be used. This is particularly needful for high quality estimates of DNI.

13. Acknowledgements

This work was supported by Alliance for Sustainable Energy, LLC, Management and Operating Contractor for the National Renewable Energy Laboratory under subcontract AXL-0-40276-01.

14. References

Heidinger, A.K., and C.C. Molling, 2011. Surface Radiation Datasets from Geostationary Satellites Subcontract AXL-0-40276-01 Final Report (November 2011 revision).

15. Appendices

Appendix A

Sample header from a GOES-15 (WEST) level2 file. Output format is in NetCDF style (for readability), even though the file is in HDF4. Attributes are in a mix of upper and lower case in order to satisfy various processing packages.

```
goes15_2011_365_2330.level2 {
dimensions:
      fakeDim0 = 1355 ;
      fakeDim1 = 1355 ;
      scan_lines_along_track_direction = 1355 ;
      pixel_elements_along_scan_direction = 1656 ;
      test_number = 32 ;

variables:
      long scan_line_number(fakeDim0) ;
            scan_line_number:SCALED = '\0' ;
            scan_line_number:units = "none" ;
            scan_line_number:standard_name = "scan_line_number" ;
            scan_line_number:long_name = "scan line number" ;
            scan_line_number:RANGE_MISSING = -999.f ;
            scan_line_number:_FillValue = -999 ;
      float scan_line_time(fakeDim1) ;
            scan_line_time:SCALED = '\0' ;
            scan_line_time:units = "hours" ;
            scan_line_time:long_name = "time for the scan line in
fractional hours" ;
            scan_line_time:RANGE_MISSING = -999.f ;
            scan_line_time:_FillValue = -999.f ;
```

```
      byte bad_pixel_mask(scan_lines_along_track_direction,
pixel_elements_along_scan_direction) ;
            bad_pixel_mask:SCALED = '\0' ;
            bad_pixel_mask:units = "none" ;
            bad_pixel_mask:standard_name = "bad_pixel_mask" ;
            bad_pixel_mask:long_name = "mask that distinguishes good(0)
from bad(1) pixels" ;
            bad_pixel_mask:coordinates = "longitude latitude" ;
            bad_pixel_mask:RANGE_MISSING = -128.f ;
            bad_pixel_mask:valid_range = '\201', '\177' ;
            bad_pixel_mask:_FillValue = '\200' ;
      float total_ozone(scan_lines_along_track_direction,
pixel_elements_along_scan_direction) ;
            total_ozone:SCALED = '\0' ;
            total_ozone:units = "Dobson" ;
            total_ozone:standard_name = "total_ozone" ;
            total_ozone:long_name = "Total ozone from NWP" ;
            total_ozone:coordinates = "longitude latitude" ;
            total_ozone:RANGE_MISSING = -999.f ;
            total_ozone:valid_range = 0.f, 0.f ;
            total_ozone:_FillValue = -999.f ;
      byte packed_pixel_meta_data(scan_lines_along_track_direction,
pixel_elements_along_scan_direction) ;
            packed_pixel_meta_data:SCALED = '\0' ;
            packed_pixel_meta_data:units = "none" ;
            packed_pixel_meta_data:standard_name =
"pixel_quality_flags_packed_into_one_byte" ;
            packed_pixel_meta_data:long_name = "order_and_depth:
bad_pixel_mask(1),solar_contamination_mask(1),ch6_on_pixel_mask(1),Bayes_M
ask_Sfc_Type(3)" ;
            packed_pixel_meta_data:coordinates = "longitude latitude" ;
            packed_pixel_meta_data:RANGE_MISSING = -888.f ;
      short latitude(scan_lines_along_track_direction,
pixel_elements_along_scan_direction) ;
            latitude:SCALED = '\1' ;
            latitude:units = "degrees_north" ;
            latitude:standard_name = "latitude" ;
            latitude:long_name = "latitude" ;
            latitude:RANGE_MISSING = -999.f ;
            latitude:valid_range = -32767s, 32767s ;
            latitude:_FillValue = -32768s ;
            latitude:RANGE_MIN = -90.f ;
            latitude:RANGE_MAX = 90.f ;
            latitude:SCALED_MISSING = -32768 ;
            latitude:SCALED_MIN = -32767 ;
            latitude:SCALED_MAX = 32767 ;
            latitude:add_offset = 0.f ;
            latitude:scale_factor = 0.0027466659f ;
      short longitude(scan_lines_along_track_direction,
pixel_elements_along_scan_direction) ;
            longitude:SCALED = '\1' ;
            longitude:units = "degrees_east" ;
            longitude:standard_name = "longitude" ;
            longitude:long_name = "longitude" ;
```

```
            longitude:RANGE_MISSING = -999.f ;
            longitude:valid_range = -32767s, 32767s ;
            longitude:_FillValue = -32768s ;
            longitude:RANGE_MIN = -180.f ;
            longitude:RANGE_MAX = 180.f ;
            longitude:SCALED_MISSING = -32768 ;
            longitude:SCALED_MIN = -32767 ;
            longitude:SCALED_MAX = 32767 ;
            longitude:add_offset = 0.f ;
            longitude:scale_factor = 0.0054933317f ;
      byte sensor_zenith_angle(scan_lines_along_track_direction,
pixel_elements_along_scan_direction) ;
            sensor_zenith_angle:SCALED = '\1' ;
            sensor_zenith_angle:units = "degrees" ;
            sensor_zenith_angle:standard_name = "sensor_zenith_angle" ;
            sensor_zenith_angle:long_name = "sensor zenith for each pixel
measured in degrees from nadir" ;
            sensor_zenith_angle:coordinates = "longitude latitude" ;
            sensor_zenith_angle:RANGE_MISSING = -999.f ;
            sensor_zenith_angle:valid_range = '\201', '\177' ;
            sensor_zenith_angle:_FillValue = '\200' ;
            sensor_zenith_angle:RANGE_MIN = 0.f ;
            sensor_zenith_angle:RANGE_MAX = 180.f ;
            sensor_zenith_angle:SCALED_MISSING = -128 ;
            sensor_zenith_angle:SCALED_MIN = -127 ;
            sensor_zenith_angle:SCALED_MAX = 127 ;
            sensor_zenith_angle:add_offset = 90.f ;
            sensor_zenith_angle:scale_factor = 0.70866144f ;
      byte solar_zenith_angle(scan_lines_along_track_direction,
pixel_elements_along_scan_direction) ;
            solar_zenith_angle:SCALED = '\1' ;
            solar_zenith_angle:units = "degrees" ;
            solar_zenith_angle:standard_name = "solar_zenith_angle" ;
            solar_zenith_angle:long_name = "solar zenith for each pixel
measured in degrees away from the sun (0=looking at sun)" ;
            solar_zenith_angle:coordinates = "longitude latitude" ;
            solar_zenith_angle:RANGE_MISSING = -999.f ;
            solar_zenith_angle:valid_range = '\201', '\177' ;
            solar_zenith_angle:_FillValue = '\200' ;
            solar_zenith_angle:RANGE_MIN = 0.f ;
            solar_zenith_angle:RANGE_MAX = 180.f ;
            solar_zenith_angle:SCALED_MISSING = -128 ;
            solar_zenith_angle:SCALED_MIN = -127 ;
            solar_zenith_angle:SCALED_MAX = 127 ;
            solar_zenith_angle:add_offset = 90.f ;
            solar_zenith_angle:scale_factor = 0.70866144f ;
      byte relative_azimuth_angle(scan_lines_along_track_direction,
pixel_elements_along_scan_direction) ;
            relative_azimuth_angle:SCALED = '\1' ;
            relative_azimuth_angle:units = "degrees" ;
            relative_azimuth_angle:standard_name =
"relative_azimuth_angle" ;
            relative_azimuth_angle:long_name = "relative azimuth angle in
degrees. 0 is the principal plane looking towards sun" ;
```

```
            relative_azimuth_angle:coordinates = "longitude latitude" ;
            relative_azimuth_angle:RANGE_MISSING = -999.f ;
            relative_azimuth_angle:valid_range = '\201', '\177' ;
            relative_azimuth_angle:_FillValue = '\200' ;
            relative_azimuth_angle:RANGE_MIN = 0.f ;
            relative_azimuth_angle:RANGE_MAX = 180.f ;
            relative_azimuth_angle:SCALED_MISSING = -128 ;
            relative_azimuth_angle:SCALED_MIN = -127 ;
            relative_azimuth_angle:SCALED_MAX = 127 ;
            relative_azimuth_angle:add_offset = 90.f ;
            relative_azimuth_angle:scale_factor = 0.70866144f ;
      byte solar_azimuth_angle(scan_lines_along_track_direction,
pixel_elements_along_scan_direction) ;
            solar_azimuth_angle:SCALED = '\1' ;
            solar_azimuth_angle:units = "degrees" ;
            solar_azimuth_angle:standard_name = "solar_azimuth_angle" ;
            solar_azimuth_angle:long_name = "solar azimuth angle in
degrees from north" ;
            solar_azimuth_angle:coordinates = "longitude latitude" ;
            solar_azimuth_angle:RANGE_MISSING = -999.f ;
            solar_azimuth_angle:valid_range = '\201', '\177' ;
            solar_azimuth_angle:_FillValue = '\200' ;
            solar_azimuth_angle:RANGE_MIN = 0.f ;
            solar_azimuth_angle:RANGE_MAX = 360.f ;
            solar_azimuth_angle:SCALED_MISSING = -128 ;
            solar_azimuth_angle:SCALED_MIN = -127 ;
            solar_azimuth_angle:SCALED_MAX = 127 ;
            solar_azimuth_angle:add_offset = 180.f ;
            solar_azimuth_angle:scale_factor = 1.4173229f ;
      byte glint_mask(scan_lines_along_track_direction,
pixel_elements_along_scan_direction) ;
            glint_mask:SCALED = '\0' ;
            glint_mask:units = "none" ;
            glint_mask:standard_name = "glint_mask" ;
            glint_mask:long_name = "glint mask (0=no) (1=yes)" ;
            glint_mask:coordinates = "longitude latitude" ;
            glint_mask:RANGE_MISSING = -128.f ;
            glint_mask:valid_range = '\201', '\177' ;
            glint_mask:_FillValue = '\200' ;
      byte coast_mask(scan_lines_along_track_direction,
pixel_elements_along_scan_direction) ;
            coast_mask:SCALED = '\0' ;
            coast_mask:units = "none" ;
            coast_mask:standard_name = "coast_mask" ;
            coast_mask:long_name = "coast mask (0=no) (1=yes)" ;
            coast_mask:coordinates = "longitude latitude" ;
            coast_mask:RANGE_MISSING = -128.f ;
            coast_mask:valid_range = '\201', '\177' ;
            coast_mask:_FillValue = '\200' ;
      byte surface_type(scan_lines_along_track_direction,
pixel_elements_along_scan_direction) ;
            surface_type:SCALED = '\0' ;
            surface_type:units = "none" ;
            surface_type:standard_name = "surface_type" ;
```

```
            surface_type:long_name = "UMD surface type:
water=0,evergreen_needle=1,evergreen_broad=2,deciduous_needle=3,deciduous_
broad=4,mixed_forest=5,woodlands=6,wooded_grass=7closed_shrubs=8,open_shru
bs=9,grasses=10,croplands=11,bare=12,urban=13" ;
            surface_type:coordinates = "longitude latitude" ;
            surface_type:RANGE_MISSING = -128.f ;
            surface_type:valid_range = '\201', '\177' ;
            surface_type:_FillValue = '\200' ;
      byte land_class(scan_lines_along_track_direction,
pixel_elements_along_scan_direction) ;
            land_class:SCALED = '\0' ;
            land_class:units = "none" ;
            land_class:standard_name = "land_class" ;
            land_class:long_name = "land classes and values:shallow
ocean=0,land=1,coastline=2,shallow inland water=3,ephemeral water=4,deep
inland water=5,moderate ocean=6,deep ocean=7" ;
            land_class:coordinates = "longitude latitude" ;
            land_class:RANGE_MISSING = -128.f ;
            land_class:valid_range = '\201', '\177' ;
            land_class:_FillValue = '\200' ;
      byte snow_class(scan_lines_along_track_direction,
pixel_elements_along_scan_direction) ;
            snow_class:SCALED = '\0' ;
            snow_class:units = "none" ;
            snow_class:standard_name = "snow_class" ;
            snow_class:long_name = "snow classes and values:no
snow/ice=1,sea_ice=2,snow=3" ;
            snow_class:coordinates = "longitude latitude" ;
            snow_class:RANGE_MISSING = -128.f ;
            snow_class:valid_range = '\201', '\177' ;
            snow_class:_FillValue = '\200' ;
      short surface_elevation(scan_lines_along_track_direction,
pixel_elements_along_scan_direction) ;
            surface_elevation:SCALED = '\1' ;
            surface_elevation:units = "meters" ;
            surface_elevation:standard_name = "surface_elevation" ;
            surface_elevation:long_name = "surface elevation above mean
sea level" ;
            surface_elevation:coordinates = "longitude latitude" ;
            surface_elevation:RANGE_MISSING = -999.f ;
            surface_elevation:valid_range = -32767s, 32767s ;
            surface_elevation:_FillValue = -32768s ;
            surface_elevation:RANGE_MIN = -500.f ;
            surface_elevation:RANGE_MAX = 10000.f ;
            surface_elevation:SCALED_MISSING = -32768 ;
            surface_elevation:SCALED_MIN = -32767 ;
            surface_elevation:SCALED_MAX = 32767 ;
            surface_elevation:add_offset = 4750.f ;
            surface_elevation:scale_factor = 0.16022217f ;
      short refl_0_65um_nom(scan_lines_along_track_direction,
pixel_elements_along_scan_direction) ;
            refl_0_65um_nom:SCALED = '\1' ;
            refl_0_65um_nom:units = "%" ;
```

```
            refl_0_65um_nom:standard_name =
"toa_bidirectional_reflectance_0_65_micron_nominal" ;
            refl_0_65um_nom:long_name = "top of atmosphere reflectance at
the nominal wavelength of 0.65 microns" ;
            refl_0_65um_nom:coordinates = "longitude latitude" ;
            refl_0_65um_nom:RANGE_MISSING = -999.f ;
            refl_0_65um_nom:valid_range = -32767s, 32767s ;
            refl_0_65um_nom:_FillValue = -32768s ;
            refl_0_65um_nom:RANGE_MIN = -2.f ;
            refl_0_65um_nom:RANGE_MAX = 120.f ;
            refl_0_65um_nom:SCALED_MISSING = -32768 ;
            refl_0_65um_nom:SCALED_MIN = -32767 ;
            refl_0_65um_nom:SCALED_MAX = 32767 ;
            refl_0_65um_nom:add_offset = 59.f ;
            refl_0_65um_nom:scale_factor = 0.0018616291f ;
      byte refl_3_75um_nom(scan_lines_along_track_direction,
pixel_elements_along_scan_direction) ;
            refl_3_75um_nom:SCALED = '\1' ;
            refl_3_75um_nom:units = "%" ;
            refl_3_75um_nom:standard_name =
"toa_bidirectional_reflectance_3_75_micron_nominal" ;
            refl_3_75um_nom:long_name = "top of atmosphere reflectance at
the nominal wavelength of 3.75 microns" ;
            refl_3_75um_nom:coordinates = "longitude latitude" ;
            refl_3_75um_nom:RANGE_MISSING = -999.f ;
            refl_3_75um_nom:valid_range = '\201', '\177' ;
            refl_3_75um_nom:_FillValue = '\200' ;
            refl_3_75um_nom:RANGE_MIN = -20.f ;
            refl_3_75um_nom:RANGE_MAX = 80.f ;
            refl_3_75um_nom:SCALED_MISSING = -128 ;
            refl_3_75um_nom:SCALED_MIN = -127 ;
            refl_3_75um_nom:SCALED_MAX = 127 ;
            refl_3_75um_nom:add_offset = 30.f ;
            refl_3_75um_nom:scale_factor = 0.39370078f ;
      short temp_3_75um_nom(scan_lines_along_track_direction,
pixel_elements_along_scan_direction) ;
            temp_3_75um_nom:SCALED = '\1' ;
            temp_3_75um_nom:units = "K" ;
            temp_3_75um_nom:standard_name =
"toa_brightness_temperature_3_75_micron_nominal" ;
            temp_3_75um_nom:long_name = "top of atmosphere brightness
temperature at the nominal wavelength of 3.75 microns" ;
            temp_3_75um_nom:coordinates = "longitude latitude" ;
            temp_3_75um_nom:RANGE_MISSING = -999.f ;
            temp_3_75um_nom:valid_range = -32767s, 32767s ;
            temp_3_75um_nom:_FillValue = -32768s ;
            temp_3_75um_nom:RANGE_MIN = 180.f ;
            temp_3_75um_nom:RANGE_MAX = 340.f ;
            temp_3_75um_nom:SCALED_MISSING = -32768 ;
            temp_3_75um_nom:SCALED_MIN = -32767 ;
            temp_3_75um_nom:SCALED_MAX = 32767 ;
            temp_3_75um_nom:add_offset = 260.f ;
            temp_3_75um_nom:scale_factor = 0.0024414808f ;
```

```
      short temp_6_7um_nom(scan_lines_along_track_direction,
pixel_elements_along_scan_direction) ;
            temp_6_7um_nom:SCALED = '\1' ;
            temp_6_7um_nom:units = "K" ;
            temp_6_7um_nom:standard_name =
"toa_brightness_temperature_6_7_micron_nominal" ;
            temp_6_7um_nom:long_name = "top of atmosphere brightness
temperature at the nominal wavelength of 6.7 microns" ;
            temp_6_7um_nom:coordinates = "longitude latitude" ;
            temp_6_7um_nom:RANGE_MISSING = -999.f ;
            temp_6_7um_nom:valid_range = -32767s, 32767s ;
            temp_6_7um_nom:_FillValue = -32768s ;
            temp_6_7um_nom:RANGE_MIN = 180.f ;
            temp_6_7um_nom:RANGE_MAX = 340.f ;
            temp_6_7um_nom:SCALED_MISSING = -32768 ;
            temp_6_7um_nom:SCALED_MIN = -32767 ;
            temp_6_7um_nom:SCALED_MAX = 32767 ;
            temp_6_7um_nom:add_offset = 260.f ;
            temp_6_7um_nom:scale_factor = 0.0024414808f ;
      short temp_11_0um_nom(scan_lines_along_track_direction,
pixel_elements_along_scan_direction) ;
            temp_11_0um_nom:SCALED = '\1' ;
            temp_11_0um_nom:units = "K" ;
            temp_11_0um_nom:standard_name =
"toa_brightness_temperature_11_0_micron_nominal" ;
            temp_11_0um_nom:long_name = "top of atmosphere brightness
temperature at the nominal wavelength of 11.0 microns" ;
            temp_11_0um_nom:coordinates = "longitude latitude" ;
            temp_11_0um_nom:RANGE_MISSING = -999.f ;
            temp_11_0um_nom:valid_range = -32767s, 32767s ;
            temp_11_0um_nom:_FillValue = -32768s ;
            temp_11_0um_nom:RANGE_MIN = 180.f ;
            temp_11_0um_nom:RANGE_MAX = 340.f ;
            temp_11_0um_nom:SCALED_MISSING = -32768 ;
            temp_11_0um_nom:SCALED_MIN = -32767 ;
            temp_11_0um_nom:SCALED_MAX = 32767 ;
            temp_11_0um_nom:add_offset = 260.f ;
            temp_11_0um_nom:scale_factor = 0.0024414808f ;
      short temp_13_3um_nom(scan_lines_along_track_direction,
pixel_elements_along_scan_direction) ;
            temp_13_3um_nom:SCALED = '\1' ;
            temp_13_3um_nom:units = "K" ;
            temp_13_3um_nom:standard_name =
"toa_brightness_temperature_13_3_micron_nominal" ;
            temp_13_3um_nom:long_name = "top of atmosphere brightness
temperature at the nominal wavelength of 13.3 microns" ;
            temp_13_3um_nom:coordinates = "longitude latitude" ;
            temp_13_3um_nom:RANGE_MISSING = -999.f ;
            temp_13_3um_nom:valid_range = -32767s, 32767s ;
            temp_13_3um_nom:_FillValue = -32768s ;
            temp_13_3um_nom:RANGE_MIN = 180.f ;
            temp_13_3um_nom:RANGE_MAX = 340.f ;
            temp_13_3um_nom:SCALED_MISSING = -32768 ;
            temp_13_3um_nom:SCALED_MIN = -32767 ;
```

```
            temp_13_3um_nom:SCALED_MAX = 32767 ;
            temp_13_3um_nom:add_offset = 260.f ;
            temp_13_3um_nom:scale_factor = 0.0024414808f ;
      byte refl_0_65um_nom_stddev_3x3(scan_lines_along_track_direction,
pixel_elements_along_scan_direction) ;
            refl_0_65um_nom_stddev_3x3:SCALED = '\1' ;
            refl_0_65um_nom_stddev_3x3:units = "%" ;
            refl_0_65um_nom_stddev_3x3:standard_name =
"toa_reflectance_0_65_micron_nomimal_3x3_stddev" ;
            refl_0_65um_nom_stddev_3x3:long_name = "standard deviation of
the 0.63 micron reflectance computed over a 3x3 pixel array" ;
            refl_0_65um_nom_stddev_3x3:coordinates = "longitude latitude"
;
            refl_0_65um_nom_stddev_3x3:RANGE_MISSING = -999.f ;
            refl_0_65um_nom_stddev_3x3:valid_range = '\201', '\177' ;
            refl_0_65um_nom_stddev_3x3:_FillValue = '\200' ;
            refl_0_65um_nom_stddev_3x3:RANGE_MIN = 0.f ;
            refl_0_65um_nom_stddev_3x3:RANGE_MAX = 20.f ;
            refl_0_65um_nom_stddev_3x3:SCALED_MISSING = -128 ;
            refl_0_65um_nom_stddev_3x3:SCALED_MIN = -127 ;
            refl_0_65um_nom_stddev_3x3:SCALED_MAX = 127 ;
            refl_0_65um_nom_stddev_3x3:add_offset = 10.f ;
            refl_0_65um_nom_stddev_3x3:scale_factor = 0.078740157f ;
      byte temp_11_0um_nom_stddev_3x3(scan_lines_along_track_direction,
pixel_elements_along_scan_direction) ;
            temp_11_0um_nom_stddev_3x3:SCALED = '\1' ;
            temp_11_0um_nom_stddev_3x3:units = "K" ;
            temp_11_0um_nom_stddev_3x3:standard_name =
"toa_brightness_temperature_11_micron_nominal_3x3_stddev" ;
            temp_11_0um_nom_stddev_3x3:long_name = "standard deviation of
the 11 micron brightness temperature computed over a 3x3 pixel array" ;
            temp_11_0um_nom_stddev_3x3:coordinates = "longitude latitude"
;
            temp_11_0um_nom_stddev_3x3:RANGE_MISSING = -999.f ;
            temp_11_0um_nom_stddev_3x3:valid_range = '\201', '\177' ;
            temp_11_0um_nom_stddev_3x3:_FillValue = '\200' ;
            temp_11_0um_nom_stddev_3x3:RANGE_MIN = 0.f ;
            temp_11_0um_nom_stddev_3x3:RANGE_MAX = 20.f ;
            temp_11_0um_nom_stddev_3x3:SCALED_MISSING = -128 ;
            temp_11_0um_nom_stddev_3x3:SCALED_MIN = -127 ;
            temp_11_0um_nom_stddev_3x3:SCALED_MAX = 127 ;
            temp_11_0um_nom_stddev_3x3:add_offset = 10.f ;
            temp_11_0um_nom_stddev_3x3:scale_factor = 0.078740157f ;
      byte cloud_probability(scan_lines_along_track_direction,
pixel_elements_along_scan_direction) ;
            cloud_probability:SCALED = '\1' ;
            cloud_probability:units = "none" ;
            cloud_probability:standard_name = "cloud_probability" ;
            cloud_probability:long_name = "probability of a pixel being
cloudy from the Bayesian cloud mask" ;
            cloud_probability:coordinates = "longitude latitude" ;
            cloud_probability:RANGE_MISSING = -999.f ;
            cloud_probability:valid_range = '\201', '\177' ;
            cloud_probability:_FillValue = '\200' ;
```

```
            cloud_probability:RANGE_MIN = 0.f ;
            cloud_probability:RANGE_MAX = 1.f ;
            cloud_probability:SCALED_MISSING = -128 ;
            cloud_probability:SCALED_MIN = -127 ;
            cloud_probability:SCALED_MAX = 127 ;
            cloud_probability:add_offset = 0.5f ;
            cloud_probability:scale_factor = 0.0039370079f ;
      byte cloud_mask(scan_lines_along_track_direction,
pixel_elements_along_scan_direction) ;
            cloud_mask:SCALED = '\0' ;
            cloud_mask:units = "none" ;
            cloud_mask:standard_name = "cloud_mask" ;
            cloud_mask:long_name = "integer classification of the cloud
mask including clear=0, probably-clear=1, probably-cloudy=2, cloudy=3" ;
            cloud_mask:coordinates = "longitude latitude" ;
            cloud_mask:RANGE_MISSING = -128.f ;
            cloud_mask:valid_range = '\201', '\177' ;
            cloud_mask:_FillValue = '\200' ;
      byte cloud_mask_test_results(scan_lines_along_track_direction,
pixel_elements_along_scan_direction, test_number) ;
            cloud_mask_test_results:SCALED = '\0' ;
            cloud_mask_test_results:units = "none" ;
            cloud_mask_test_results:standard_name =
"cloud_mask_test_results" ;
            cloud_mask_test_results:long_name = "individual cloud mask
test results" ;
            cloud_mask_test_results:RANGE_MISSING = -128.f ;
            cloud_mask_test_results:valid_range = '\201', '\177' ;
            cloud_mask_test_results:_FillValue = '\200' ;
      byte cloud_type(scan_lines_along_track_direction,
pixel_elements_along_scan_direction) ;
            cloud_type:SCALED = '\0' ;
            cloud_type:units = "none" ;
            cloud_type:standard_name = "cloud_type" ;
            cloud_type:long_name = "integer classification of the cloud
type including clear and aerosol type,0=clear,1=probably
clear,2=fog,3=water,4=supercooled
water,5=mixed,6=opaque_ice,7=cirrus,8=overlapping,9=overshooting,10=unknow
n,11=dust,12=smoke" ;
            cloud_type:coordinates = "longitude latitude" ;
            cloud_type:RANGE_MISSING = -128.f ;
            cloud_type:valid_range = '\201', '\177' ;
            cloud_type:_FillValue = '\200' ;
      byte cloud_phase(scan_lines_along_track_direction,
pixel_elements_along_scan_direction) ;
            cloud_phase:SCALED = '\0' ;
            cloud_phase:units = "none" ;
            cloud_phase:standard_name = "cloud_phase" ;
            cloud_phase:long_name = "integer classification of the cloud
phase including clear and aerosol type,0=clear,1=water,2=supercooled
water,3=mixed,4=ice,5=unknown" ;
            cloud_phase:coordinates = "longitude latitude" ;
            cloud_phase:RANGE_MISSING = -128.f ;
            cloud_phase:valid_range = '\201', '\177' ;
```

```
            cloud_phase:_FillValue = '\200' ;
      byte cld_press_acha(scan_lines_along_track_direction,
pixel_elements_along_scan_direction) ;
            cld_press_acha:SCALED = '\1' ;
            cld_press_acha:units = "hPa" ;
            cld_press_acha:standard_name = "air_pressure_at_cloud_top" ;
            cld_press_acha:long_name = "cloud-top pressure computed using
the AWG cloud height algorithm" ;
            cld_press_acha:coordinates = "longitude latitude" ;
            cld_press_acha:RANGE_MISSING = -999.f ;
            cld_press_acha:valid_range = '\201', '\177' ;
            cld_press_acha:_FillValue = '\200' ;
            cld_press_acha:RANGE_MIN = 0.f ;
            cld_press_acha:RANGE_MAX = 1100.f ;
            cld_press_acha:SCALED_MISSING = -128 ;
            cld_press_acha:SCALED_MIN = -127 ;
            cld_press_acha:SCALED_MAX = 127 ;
            cld_press_acha:add_offset = 550.f ;
            cld_press_acha:scale_factor = 4.3307085f ;
      short cld_temp_acha(scan_lines_along_track_direction,
pixel_elements_along_scan_direction) ;
            cld_temp_acha:SCALED = '\1' ;
            cld_temp_acha:units = "K" ;
            cld_temp_acha:standard_name = "air_temperature_at_cloud_top" ;
            cld_temp_acha:long_name = "cloud-top temperature computed
using the AWG cloud height algorithm" ;
            cld_temp_acha:coordinates = "longitude latitude" ;
            cld_temp_acha:RANGE_MISSING = -999.f ;
            cld_temp_acha:valid_range = -32767s, 32767s ;
            cld_temp_acha:_FillValue = -32768s ;
            cld_temp_acha:RANGE_MIN = 180.f ;
            cld_temp_acha:RANGE_MAX = 320.f ;
            cld_temp_acha:SCALED_MISSING = -32768 ;
            cld_temp_acha:SCALED_MIN = -32767 ;
            cld_temp_acha:SCALED_MAX = 32767 ;
            cld_temp_acha:add_offset = 250.f ;
            cld_temp_acha:scale_factor = 0.0021362957f ;
      byte cld_height_acha(scan_lines_along_track_direction,
pixel_elements_along_scan_direction) ;
            cld_height_acha:SCALED = '\1' ;
            cld_height_acha:units = "km" ;
            cld_height_acha:standard_name = "height_of_cloud" ;
            cld_height_acha:long_name = "cloud height computed using the
AWG cloud height algorithm" ;
            cld_height_acha:coordinates = "longitude latitude" ;
            cld_height_acha:RANGE_MISSING = -999.f ;
            cld_height_acha:valid_range = '\201', '\177' ;
            cld_height_acha:_FillValue = '\200' ;
            cld_height_acha:RANGE_MIN = 0.f ;
            cld_height_acha:RANGE_MAX = 20.f ;
            cld_height_acha:SCALED_MISSING = -128 ;
            cld_height_acha:SCALED_MIN = -127 ;
            cld_height_acha:SCALED_MAX = 127 ;
            cld_height_acha:add_offset = 10.f ;
```

```
            cld_height_acha:scale_factor = 0.078740157f ;
      byte cld_emiss_acha(scan_lines_along_track_direction,
pixel_elements_along_scan_direction) ;
            cld_emiss_acha:SCALED = '\1' ;
            cld_emiss_acha:units = "none" ;
            cld_emiss_acha:standard_name =
"cloud_longwave_emissivity_11_0_micron_nominal" ;
            cld_emiss_acha:long_name = "cloud emissivity at the nominal
wavelength of 11 microns, determined from the AWG cloud height algorithm"
;
            cld_emiss_acha:coordinates = "longitude latitude" ;
            cld_emiss_acha:RANGE_MISSING = -999.f ;
            cld_emiss_acha:valid_range = '\201', '\177' ;
            cld_emiss_acha:_FillValue = '\200' ;
            cld_emiss_acha:RANGE_MIN = 0.f ;
            cld_emiss_acha:RANGE_MAX = 1.f ;
            cld_emiss_acha:SCALED_MISSING = -128 ;
            cld_emiss_acha:SCALED_MIN = -127 ;
            cld_emiss_acha:SCALED_MAX = 127 ;
            cld_emiss_acha:add_offset = 0.5f ;
            cld_emiss_acha:scale_factor = 0.0039370079f ;
      byte cld_height_uncer_acha(scan_lines_along_track_direction,
pixel_elements_along_scan_direction) ;
            cld_height_uncer_acha:SCALED = '\1' ;
            cld_height_uncer_acha:units = "km" ;
            cld_height_uncer_acha:standard_name =
"cloud_height_uncertainty" ;
            cld_height_uncer_acha:long_name = "cloud height uncertainty
computed using the AWG cloud height algorithm" ;
            cld_height_uncer_acha:coordinates = "longitude latitude" ;
            cld_height_uncer_acha:RANGE_MISSING = -999.f ;
            cld_height_uncer_acha:valid_range = '\201', '\177' ;
            cld_height_uncer_acha:_FillValue = '\200' ;
            cld_height_uncer_acha:RANGE_MIN = 0.f ;
            cld_height_uncer_acha:RANGE_MAX = 10.f ;
            cld_height_uncer_acha:SCALED_MISSING = -128 ;
            cld_height_uncer_acha:SCALED_MIN = -127 ;
            cld_height_uncer_acha:SCALED_MAX = 127 ;
            cld_height_uncer_acha:add_offset = 5.f ;
            cld_height_uncer_acha:scale_factor = 0.039370079f ;
      byte cld_emiss_acha_qf(scan_lines_along_track_direction,
pixel_elements_along_scan_direction) ;
            cld_emiss_acha_qf:SCALED = '\0' ;
            cld_emiss_acha_qf:units = "none" ;
            cld_emiss_acha_qf:standard_name = "cld_emiss_acha_qf" ;
            cld_emiss_acha_qf:long_name = "quality flag for 11.0 micron
cloud emissivity from ACHA not attempted=0, failed=1, low quality=2, high
quality=3" ;
            cld_emiss_acha_qf:coordinates = "longitude latitude" ;
            cld_emiss_acha_qf:RANGE_MISSING = -128.f ;
            cld_emiss_acha_qf:valid_range = '\201', '\177' ;
            cld_emiss_acha_qf:_FillValue = '\200' ;
      byte acha_quality(scan_lines_along_track_direction,
pixel_elements_along_scan_direction) ;
```

```
            acha_quality:SCALED = '\0' ;
            acha_quality:units = "none" ;
            acha_quality:standard_name = "acha_quality" ;
            acha_quality:long_name = "quality flags for ACHA products
1:Processed (0=no,1=yes) 2:valid Tc retrieval (1=yes,0=no) 3:valid ec
retrieval (1=yes,0=no) 4:valid beta retrieval (1=yes,0=no) 5:degraded Tc
retrieval (1=yes,0=no) 6:degraded ec retrieval (1=yes,0=no) 7:degraded
beta retrieval (1=yes,0=no)" ;
            acha_quality:coordinates = "longitude latitude" ;
            acha_quality:RANGE_MISSING = -888.f ;
      short cld_opd_dcomp(scan_lines_along_track_direction,
pixel_elements_along_scan_direction) ;
            cld_opd_dcomp:SCALED = '\1' ;
            cld_opd_dcomp:units = "none" ;
            cld_opd_dcomp:standard_name =
"atmosphere_optical_thickness_due_to_cloud" ;
            cld_opd_dcomp:long_name = "cloud optical depth at the nominal
wavelength of 0.65 microns, determined from DCOMP" ;
            cld_opd_dcomp:coordinates = "longitude latitude" ;
            cld_opd_dcomp:RANGE_MISSING = -999.f ;
            cld_opd_dcomp:valid_range = -32767s, 32767s ;
            cld_opd_dcomp:_FillValue = -32768s ;
            cld_opd_dcomp:RANGE_MIN = -0.2f ;
            cld_opd_dcomp:RANGE_MAX = 160.f ;
            cld_opd_dcomp:SCALED_MISSING = -32768 ;
            cld_opd_dcomp:SCALED_MIN = -32767 ;
            cld_opd_dcomp:SCALED_MAX = 32767 ;
            cld_opd_dcomp:add_offset = 79.900002f ;
            cld_opd_dcomp:scale_factor = 0.0024445325f ;
      short cld_reff_dcomp(scan_lines_along_track_direction,
pixel_elements_along_scan_direction) ;
            cld_reff_dcomp:SCALED = '\1' ;
            cld_reff_dcomp:units = "micron" ;
            cld_reff_dcomp:standard_name =
"effective_radius_of_cloud_particle" ;
            cld_reff_dcomp:long_name = "effective radius of cloud
particles determined from DCOMP; see attributes for channels used" ;
            cld_reff_dcomp:coordinates = "longitude latitude" ;
            cld_reff_dcomp:RANGE_MISSING = -999.f ;
            cld_reff_dcomp:valid_range = -32767s, 32767s ;
            cld_reff_dcomp:_FillValue = -32768s ;
            cld_reff_dcomp:RANGE_MIN = 0.f ;
            cld_reff_dcomp:RANGE_MAX = 160.f ;
            cld_reff_dcomp:SCALED_MISSING = -32768 ;
            cld_reff_dcomp:SCALED_MIN = -32767 ;
            cld_reff_dcomp:SCALED_MAX = 32767 ;
            cld_reff_dcomp:add_offset = 80.f ;
            cld_reff_dcomp:scale_factor = 0.0024414808f ;
      short cld_opd_dcomp_unc(scan_lines_along_track_direction,
pixel_elements_along_scan_direction) ;
            cld_opd_dcomp_unc:SCALED = '\1' ;
            cld_opd_dcomp_unc:units = "none" ;
            cld_opd_dcomp_unc:standard_name =
"atmosphere_optical_thickness_due_to_cloud" ;
```

```
            cld_opd_dcomp_unc:long_name = "uncertainty in cloud optical
depth at the nominal wavelength of 0.65 microns, determined from DCOMP" ;
            cld_opd_dcomp_unc:coordinates = "longitude latitude" ;
            cld_opd_dcomp_unc:RANGE_MISSING = -999.f ;
            cld_opd_dcomp_unc:valid_range = -32767s, 32767s ;
            cld_opd_dcomp_unc:_FillValue = -32768s ;
            cld_opd_dcomp_unc:RANGE_MIN = -0.2f ;
            cld_opd_dcomp_unc:RANGE_MAX = 160.f ;
            cld_opd_dcomp_unc:SCALED_MISSING = -32768 ;
            cld_opd_dcomp_unc:SCALED_MIN = -32767 ;
            cld_opd_dcomp_unc:SCALED_MAX = 32767 ;
            cld_opd_dcomp_unc:add_offset = 79.900002f ;
            cld_opd_dcomp_unc:scale_factor = 0.0024445325f ;
      short cld_reff_dcomp_unc(scan_lines_along_track_direction,
pixel_elements_along_scan_direction) ;
            cld_reff_dcomp_unc:SCALED = '\1' ;
            cld_reff_dcomp_unc:units = "micron" ;
            cld_reff_dcomp_unc:standard_name =
"effective_radius_of_cloud_particle" ;
            cld_reff_dcomp_unc:long_name = "effective radius of cloud
particle determined from DCOMP; see attributes for channels used" ;
            cld_reff_dcomp_unc:coordinates = "longitude latitude" ;
            cld_reff_dcomp_unc:RANGE_MISSING = -999.f ;
            cld_reff_dcomp_unc:valid_range = -32767s, 32767s ;
            cld_reff_dcomp_unc:_FillValue = -32768s ;
            cld_reff_dcomp_unc:RANGE_MIN = 0.f ;
            cld_reff_dcomp_unc:RANGE_MAX = 160.f ;
            cld_reff_dcomp_unc:SCALED_MISSING = -32768 ;
            cld_reff_dcomp_unc:SCALED_MIN = -32767 ;
            cld_reff_dcomp_unc:SCALED_MAX = 32767 ;
            cld_reff_dcomp_unc:add_offset = 80.f ;
            cld_reff_dcomp_unc:scale_factor = 0.0024414808f ;
      byte cld_opd_dcomp_qf(scan_lines_along_track_direction,
pixel_elements_along_scan_direction) ;
            cld_opd_dcomp_qf:SCALED = '\0' ;
            cld_opd_dcomp_qf:units = "none" ;
            cld_opd_dcomp_qf:standard_name = "cld_opd_dcomp_qf" ;
            cld_opd_dcomp_qf:long_name = "quality flag for cloud optical
depth from DCOMP not attempted=0, failed=1, low quality=2, high quality=3"
;
            cld_opd_dcomp_qf:coordinates = "longitude latitude" ;
            cld_opd_dcomp_qf:RANGE_MISSING = -128.f ;
            cld_opd_dcomp_qf:valid_range = '\201', '\177' ;
            cld_opd_dcomp_qf:_FillValue = '\200' ;
      byte cld_reff_dcomp_qf(scan_lines_along_track_direction,
pixel_elements_along_scan_direction) ;
            cld_reff_dcomp_qf:SCALED = '\0' ;
            cld_reff_dcomp_qf:units = "none" ;
            cld_reff_dcomp_qf:standard_name = "cld_reff_dcomp_qf" ;
            cld_reff_dcomp_qf:long_name = "quality flag for cloud
effective radius from DCOMP not attempted=0, failed=1, low quality=2, high
quality=3" ;
            cld_reff_dcomp_qf:coordinates = "longitude latitude" ;
            cld_reff_dcomp_qf:RANGE_MISSING = -128.f ;
```

```
            cld_reff_dcomp_qf:valid_range = '\201', '\177' ;
            cld_reff_dcomp_qf:_FillValue = '\200' ;
      byte cloud_transmission_0_65um_nom(scan_lines_along_track_direction,
pixel_elements_along_scan_direction) ;
            cloud_transmission_0_65um_nom:SCALED = '\1' ;
            cloud_transmission_0_65um_nom:units = "none" ;
            cloud_transmission_0_65um_nom:standard_name =
"cloud_transmission_0_65um_nominal" ;
            cloud_transmission_0_65um_nom:long_name = "cloud transmission
0.65 microns nominal from DCOMP" ;
            cloud_transmission_0_65um_nom:coordinates = "longitude
latitude" ;
            cloud_transmission_0_65um_nom:RANGE_MISSING = -999.f ;
            cloud_transmission_0_65um_nom:valid_range = '\201', '\177' ;
            cloud_transmission_0_65um_nom:_FillValue = '\200' ;
            cloud_transmission_0_65um_nom:RANGE_MIN = 0.f ;
            cloud_transmission_0_65um_nom:RANGE_MAX = 1.f ;
            cloud_transmission_0_65um_nom:SCALED_MISSING = -128 ;
            cloud_transmission_0_65um_nom:SCALED_MIN = -127 ;
            cloud_transmission_0_65um_nom:SCALED_MAX = 127 ;
            cloud_transmission_0_65um_nom:add_offset = 0.5f ;
            cloud_transmission_0_65um_nom:scale_factor = 0.0039370079f ;
      byte cloud_fraction(scan_lines_along_track_direction,
pixel_elements_along_scan_direction) ;
            cloud_fraction:SCALED = '\1' ;
            cloud_fraction:units = "none" ;
            cloud_fraction:standard_name = "cloud_fraction" ;
            cloud_fraction:long_name = "cloud fraction computed over a 3x3
pixel array at the native resolution centered on this pixel" ;
            cloud_fraction:coordinates = "longitude latitude" ;
            cloud_fraction:RANGE_MISSING = -999.f ;
            cloud_fraction:valid_range = '\201', '\177' ;
            cloud_fraction:_FillValue = '\200' ;
            cloud_fraction:RANGE_MIN = 0.f ;
            cloud_fraction:RANGE_MAX = 1.f ;
            cloud_fraction:SCALED_MISSING = -128 ;
            cloud_fraction:SCALED_MIN = -127 ;
            cloud_fraction:SCALED_MAX = 127 ;
            cloud_fraction:add_offset = 0.5f ;
            cloud_fraction:scale_factor = 0.0039370079f ;
      byte cloud_fraction_uncertainty(scan_lines_along_track_direction,
pixel_elements_along_scan_direction) ;
            cloud_fraction_uncertainty:SCALED = '\1' ;
            cloud_fraction_uncertainty:units = "none" ;
            cloud_fraction_uncertainty:standard_name =
"cloud_fraction_uncertainty" ;
            cloud_fraction_uncertainty:long_name = "cloud fraction
uncertainty computed over a 3x3 array" ;
            cloud_fraction_uncertainty:coordinates = "longitude latitude"
;
            cloud_fraction_uncertainty:RANGE_MISSING = -999.f ;
            cloud_fraction_uncertainty:valid_range = '\201', '\177' ;
            cloud_fraction_uncertainty:_FillValue = '\200' ;
            cloud_fraction_uncertainty:RANGE_MIN = 0.f ;
```

```
            cloud_fraction_uncertainty:RANGE_MAX = 1.f ;
            cloud_fraction_uncertainty:SCALED_MISSING = -128 ;
            cloud_fraction_uncertainty:SCALED_MIN = -127 ;
            cloud_fraction_uncertainty:SCALED_MAX = 127 ;
            cloud_fraction_uncertainty:add_offset = 0.5f ;
            cloud_fraction_uncertainty:scale_factor = 0.0039370079f ;
      short insolation(scan_lines_along_track_direction,
pixel_elements_along_scan_direction) ;
            insolation:SCALED = '\1' ;
            insolation:units = "W m-2" ;
            insolation:standard_name =
"surface_downwelling_shortwave_flux" ;
            insolation:long_name = "surface downwelling shortwave flux
computed from the SASRAB routine" ;
            insolation:coordinates = "longitude latitude" ;
            insolation:RANGE_MISSING = -999.f ;
            insolation:valid_range = -32767s, 32767s ;
            insolation:_FillValue = -32768s ;
            insolation:RANGE_MIN = 0.f ;
            insolation:RANGE_MAX = 1500.f ;
            insolation:SCALED_MISSING = -32768 ;
            insolation:SCALED_MIN = -32767 ;
            insolation:SCALED_MAX = 32767 ;
            insolation:add_offset = 750.f ;
            insolation:scale_factor = 0.022888882f ;
      short insolation_diffuse(scan_lines_along_track_direction,
pixel_elements_along_scan_direction) ;
            insolation_diffuse:SCALED = '\1' ;
            insolation_diffuse:units = "W m-2" ;
            insolation_diffuse:standard_name =
"surface_downwelling_shortwave_flux_diffuse" ;
            insolation_diffuse:long_name = "diffuse component of the
surface downwelling shortwave flux computed from the SASRAB routine" ;
            insolation_diffuse:coordinates = "longitude latitude" ;
            insolation_diffuse:RANGE_MISSING = -999.f ;
            insolation_diffuse:valid_range = -32767s, 32767s ;
            insolation_diffuse:_FillValue = -32768s ;
            insolation_diffuse:RANGE_MIN = 0.f ;
            insolation_diffuse:RANGE_MAX = 1500.f ;
            insolation_diffuse:SCALED_MISSING = -32768 ;
            insolation_diffuse:SCALED_MIN = -32767 ;
            insolation_diffuse:SCALED_MAX = 32767 ;
            insolation_diffuse:add_offset = 750.f ;
            insolation_diffuse:scale_factor = 0.022888882f ;
      byte surface_temperature_retrieved(scan_lines_along_track_direction,
pixel_elements_along_scan_direction) ;
            surface_temperature_retrieved:SCALED = '\1' ;
            surface_temperature_retrieved:units = "K" ;
            surface_temperature_retrieved:standard_name =
"surface_temperature_retrieved" ;
            surface_temperature_retrieved:long_name = "surface temperature
retrieved using atmospherically corrected 11 micron radiance" ;
            surface_temperature_retrieved:coordinates = "longitude
latitude" ;
```

```
            surface_temperature_retrieved:RANGE_MISSING = -999.f ;
            surface_temperature_retrieved:valid_range = '\201', '\177' ;
            surface_temperature_retrieved:_FillValue = '\200' ;
            surface_temperature_retrieved:RANGE_MIN = 220.f ;
            surface_temperature_retrieved:RANGE_MAX = 340.f ;
            surface_temperature_retrieved:SCALED_MISSING = -128 ;
            surface_temperature_retrieved:SCALED_MIN = -127 ;
            surface_temperature_retrieved:SCALED_MAX = 127 ;
            surface_temperature_retrieved:add_offset = 280.f ;
            surface_temperature_retrieved:scale_factor = 0.47244096f ;
      byte surface_air_temperature_nwp(scan_lines_along_track_direction,
pixel_elements_along_scan_direction) ;
            surface_air_temperature_nwp:SCALED = '\1' ;
            surface_air_temperature_nwp:units = "K" ;
            surface_air_temperature_nwp:standard_name =
"surface_air_temperature" ;
            surface_air_temperature_nwp:long_name = "surface air
temperature from NWP ancillary data" ;
            surface_air_temperature_nwp:coordinates = "longitude latitude"
;
            surface_air_temperature_nwp:RANGE_MISSING = -999.f ;
            surface_air_temperature_nwp:valid_range = '\201', '\177' ;
            surface_air_temperature_nwp:_FillValue = '\200' ;
            surface_air_temperature_nwp:RANGE_MIN = 220.f ;
            surface_air_temperature_nwp:RANGE_MAX = 340.f ;
            surface_air_temperature_nwp:SCALED_MISSING = -128 ;
            surface_air_temperature_nwp:SCALED_MIN = -127 ;
            surface_air_temperature_nwp:SCALED_MAX = 127 ;
            surface_air_temperature_nwp:add_offset = 280.f ;
            surface_air_temperature_nwp:scale_factor = 0.47244096f ;
      short
surface_temperature_background(scan_lines_along_track_direction,
pixel_elements_along_scan_direction) ;
            surface_temperature_background:SCALED = '\1' ;
            surface_temperature_background:units = "K" ;
            surface_temperature_background:standard_name =
"surface_temperature_background" ;
            surface_temperature_background:long_name = "surface
temperature assumed using ancillary data sources" ;
            surface_temperature_background:coordinates = "longitude
latitude" ;
            surface_temperature_background:RANGE_MISSING = -999.f ;
            surface_temperature_background:valid_range = -32767s, 32767s ;
            surface_temperature_background:_FillValue = -32768s ;
            surface_temperature_background:RANGE_MIN = 220.f ;
            surface_temperature_background:RANGE_MAX = 340.f ;
            surface_temperature_background:SCALED_MISSING = -32768 ;
            surface_temperature_background:SCALED_MIN = -32767 ;
            surface_temperature_background:SCALED_MAX = 32767 ;
            surface_temperature_background:add_offset = 280.f ;
            surface_temperature_background:scale_factor = 0.0018311106f ;
      byte surface_relative_humidity_nwp(scan_lines_along_track_direction,
pixel_elements_along_scan_direction) ;
            surface_relative_humidity_nwp:SCALED = '\1' ;
```

```
            surface_relative_humidity_nwp:units = "%" ;
            surface_relative_humidity_nwp:standard_name =
"surface_relative_humidity" ;
            surface_relative_humidity_nwp:long_name = "near-surface
relative humidity from NWP ancillary data" ;
            surface_relative_humidity_nwp:coordinates = "longitude
latitude" ;
            surface_relative_humidity_nwp:RANGE_MISSING = -999.f ;
            surface_relative_humidity_nwp:valid_range = '\201', '\177' ;
            surface_relative_humidity_nwp:_FillValue = '\200' ;
            surface_relative_humidity_nwp:RANGE_MIN = 0.f ;
            surface_relative_humidity_nwp:RANGE_MAX = 110.f ;
            surface_relative_humidity_nwp:SCALED_MISSING = -128 ;
            surface_relative_humidity_nwp:SCALED_MIN = -127 ;
            surface_relative_humidity_nwp:SCALED_MAX = 127 ;
            surface_relative_humidity_nwp:add_offset = 55.f ;
            surface_relative_humidity_nwp:scale_factor = 0.43307087f ;
      byte surface_pressure_background(scan_lines_along_track_direction,
pixel_elements_along_scan_direction) ;
            surface_pressure_background:SCALED = '\1' ;
            surface_pressure_background:units = "hPa" ;
            surface_pressure_background:standard_name =
"surface_pressure_background" ;
            surface_pressure_background:long_name = "surface pressure
assumed using ancillary data sources" ;
            surface_pressure_background:coordinates = "longitude latitude"
;
            surface_pressure_background:RANGE_MISSING = -999.f ;
            surface_pressure_background:valid_range = '\201', '\177' ;
            surface_pressure_background:_FillValue = '\200' ;
            surface_pressure_background:RANGE_MIN = 700.f ;
            surface_pressure_background:RANGE_MAX = 1100.f ;
            surface_pressure_background:SCALED_MISSING = -128 ;
            surface_pressure_background:SCALED_MIN = -127 ;
            surface_pressure_background:SCALED_MAX = 127 ;
            surface_pressure_background:add_offset = 900.f ;
            surface_pressure_background:scale_factor = 1.5748031f ;
      byte k_index_nwp(scan_lines_along_track_direction,
pixel_elements_along_scan_direction) ;
            k_index_nwp:SCALED = '\1' ;
            k_index_nwp:units = "K" ;
            k_index_nwp:standard_name = "k_index" ;
            k_index_nwp:long_name = "k index computed from NWP ancillary
data sources" ;
            k_index_nwp:coordinates = "longitude latitude" ;
            k_index_nwp:RANGE_MISSING = -999.f ;
            k_index_nwp:valid_range = '\201', '\177' ;
            k_index_nwp:_FillValue = '\200' ;
            k_index_nwp:RANGE_MIN = -40.f ;
            k_index_nwp:RANGE_MAX = 80.f ;
            k_index_nwp:SCALED_MISSING = -128 ;
            k_index_nwp:SCALED_MIN = -127 ;
            k_index_nwp:SCALED_MAX = 127 ;
            k_index_nwp:add_offset = 20.f ;
```

```
            k_index_nwp:scale_factor = 0.47244096f ;
      byte total_precipitable_water_nwp(scan_lines_along_track_direction,
pixel_elements_along_scan_direction) ;
            total_precipitable_water_nwp:SCALED = '\1' ;
            total_precipitable_water_nwp:units = "cm" ;
            total_precipitable_water_nwp:standard_name =
"total_precipitable_water" ;
            total_precipitable_water_nwp:long_name = "total precipitable
water from NWP ancillary data" ;
            total_precipitable_water_nwp:coordinates = "longitude
latitude" ;
            total_precipitable_water_nwp:RANGE_MISSING = -999.f ;
            total_precipitable_water_nwp:valid_range = '\201', '\177' ;
            total_precipitable_water_nwp:_FillValue = '\200' ;
            total_precipitable_water_nwp:RANGE_MIN = 0.f ;
            total_precipitable_water_nwp:RANGE_MAX = 10.f ;
            total_precipitable_water_nwp:SCALED_MISSING = -128 ;
            total_precipitable_water_nwp:SCALED_MIN = -127 ;
            total_precipitable_water_nwp:SCALED_MAX = 127 ;
            total_precipitable_water_nwp:add_offset = 5.f ;
            total_precipitable_water_nwp:scale_factor = 0.039370079f ;
      short refl_0_65um_nom_unnormalized(scan_lines_along_track_direction,
pixel_elements_along_scan_direction) ;
            refl_0_65um_nom_unnormalized:SCALED = '\1' ;
            refl_0_65um_nom_unnormalized:units = "%" ;
            refl_0_65um_nom_unnormalized:standard_name =
"toa_bidirectional_reflectance_0_65_micron_nominal_unormalized_to_solar_ze
nith" ;
            refl_0_65um_nom_unnormalized:long_name = "top of atmosphere
reflectance at the nominal wavelength of 0.65 microns unnormalized to the
cosine of the solar zenith angle" ;
            refl_0_65um_nom_unnormalized:coordinates = "longitude
latitude" ;
            refl_0_65um_nom_unnormalized:RANGE_MISSING = -999.f ;
            refl_0_65um_nom_unnormalized:valid_range = -32767s, 32767s ;
            refl_0_65um_nom_unnormalized:_FillValue = -32768s ;
            refl_0_65um_nom_unnormalized:RANGE_MIN = -2.f ;
            refl_0_65um_nom_unnormalized:RANGE_MAX = 120.f ;
            refl_0_65um_nom_unnormalized:SCALED_MISSING = -32768 ;
            refl_0_65um_nom_unnormalized:SCALED_MIN = -32767 ;
            refl_0_65um_nom_unnormalized:SCALED_MAX = 32767 ;
            refl_0_65um_nom_unnormalized:add_offset = 59.f ;
            refl_0_65um_nom_unnormalized:scale_factor = 0.0018616291f ;
      short pixel_sst_unmasked(scan_lines_along_track_direction,
pixel_elements_along_scan_direction) ;
            pixel_sst_unmasked:SCALED = '\1' ;
            pixel_sst_unmasked:units = "K" ;
            pixel_sst_unmasked:standard_name =
"sea_surface_skin_temperature_unmasked" ;
            pixel_sst_unmasked:long_name = "sea surface skin temperature
at the pixel with land mask applied and cloud mask not applied" ;
            pixel_sst_unmasked:coordinates = "longitude latitude" ;
            pixel_sst_unmasked:RANGE_MISSING = -999.f ;
            pixel_sst_unmasked:valid_range = -32767s, 32767s ;
```

```
            pixel_sst_unmasked:_FillValue = -32768s ;
            pixel_sst_unmasked:RANGE_MIN = 265.f ;
            pixel_sst_unmasked:RANGE_MAX = 315.f ;
            pixel_sst_unmasked:SCALED_MISSING = -32768 ;
            pixel_sst_unmasked:SCALED_MIN = -32767 ;
            pixel_sst_unmasked:SCALED_MAX = 32767 ;
            pixel_sst_unmasked:add_offset = 290.f ;
            pixel_sst_unmasked:scale_factor = 0.00076296274f ;
      byte wind_speed_10m_nwp(scan_lines_along_track_direction,
pixel_elements_along_scan_direction) ;
            wind_speed_10m_nwp:SCALED = '\1' ;
            wind_speed_10m_nwp:units = "m/s" ;
            wind_speed_10m_nwp:standard_name =
"wind_speed_10m_above_ground" ;
            wind_speed_10m_nwp:long_name = "wind speed from the NWP
ancillary data at 10m above ground level" ;
            wind_speed_10m_nwp:coordinates = "longitude latitude" ;
            wind_speed_10m_nwp:RANGE_MISSING = -999.f ;
            wind_speed_10m_nwp:valid_range = '\201', '\177' ;
            wind_speed_10m_nwp:_FillValue = '\200' ;
            wind_speed_10m_nwp:RANGE_MIN = 0.f ;
            wind_speed_10m_nwp:RANGE_MAX = 50.f ;
            wind_speed_10m_nwp:SCALED_MISSING = -128 ;
            wind_speed_10m_nwp:SCALED_MIN = -127 ;
            wind_speed_10m_nwp:SCALED_MAX = 127 ;
            wind_speed_10m_nwp:add_offset = 25.f ;
            wind_speed_10m_nwp:scale_factor = 0.19685039f ;
      byte wind_direction_10m_nwp(scan_lines_along_track_direction,
pixel_elements_along_scan_direction) ;
            wind_direction_10m_nwp:SCALED = '\1' ;
            wind_direction_10m_nwp:units = "degrees" ;
            wind_direction_10m_nwp:standard_name =
"wind_direction_10m_above_ground" ;
            wind_direction_10m_nwp:long_name = "wind direction from the
NWP ancillary data at 10m above ground level" ;
            wind_direction_10m_nwp:coordinates = "longitude latitude" ;
            wind_direction_10m_nwp:RANGE_MISSING = -999.f ;
            wind_direction_10m_nwp:valid_range = '\201', '\177' ;
            wind_direction_10m_nwp:_FillValue = '\200' ;
            wind_direction_10m_nwp:RANGE_MIN = 0.f ;
            wind_direction_10m_nwp:RANGE_MAX = 360.f ;
            wind_direction_10m_nwp:SCALED_MISSING = -128 ;
            wind_direction_10m_nwp:SCALED_MIN = -127 ;
            wind_direction_10m_nwp:SCALED_MAX = 127 ;
            wind_direction_10m_nwp:add_offset = 180.f ;
            wind_direction_10m_nwp:scale_factor = 1.4173229f ;
      short refl_0_65um_nom_dark(scan_lines_along_track_direction,
pixel_elements_along_scan_direction) ;
            refl_0_65um_nom_dark:SCALED = '\1' ;
            refl_0_65um_nom_dark:units = "%" ;
            refl_0_65um_nom_dark:standard_name =
"toa_bidirectional_reflectance_0_65_micron_nominal_dark_sky_composite" ;
```

```
            refl_0_65um_nom_dark:long_name = "top of atmosphere
reflectance at the nominal wavelength of 0.65 microns generated from a
dark-sky compositing method" ;
            refl_0_65um_nom_dark:coordinates = "longitude latitude" ;
            refl_0_65um_nom_dark:RANGE_MISSING = -999.f ;
            refl_0_65um_nom_dark:valid_range = -32767s, 32767s ;
            refl_0_65um_nom_dark:_FillValue = -32768s ;
            refl_0_65um_nom_dark:RANGE_MIN = -2.f ;
            refl_0_65um_nom_dark:RANGE_MAX = 120.f ;
            refl_0_65um_nom_dark:SCALED_MISSING = -32768 ;
            refl_0_65um_nom_dark:SCALED_MIN = -32767 ;
            refl_0_65um_nom_dark:SCALED_MAX = 32767 ;
            refl_0_65um_nom_dark:add_offset = 59.f ;
            refl_0_65um_nom_dark:scale_factor = 0.0018616291f ;
      byte cloud_water_path(scan_lines_along_track_direction,
pixel_elements_along_scan_direction) ;
            cloud_water_path:SCALED = '\1' ;
            cloud_water_path:units = "g m-2" ;
            cloud_water_path:standard_name = "cloud_water_path" ;
            cloud_water_path:long_name = "integrated total cloud water
over whole column" ;
            cloud_water_path:coordinates = "longitude latitude" ;
            cloud_water_path:RANGE_MISSING = -999.f ;
            cloud_water_path:valid_range = '\201', '\177' ;
            cloud_water_path:_FillValue = '\200' ;
            cloud_water_path:RANGE_MIN = 0.f ;
            cloud_water_path:RANGE_MAX = 1200.f ;
            cloud_water_path:SCALED_MISSING = -128 ;
            cloud_water_path:SCALED_MIN = -127 ;
            cloud_water_path:SCALED_MAX = 127 ;
            cloud_water_path:add_offset = 600.f ;
            cloud_water_path:scale_factor = 4.7244096f ;
      byte rain_rate(scan_lines_along_track_direction,
pixel_elements_along_scan_direction) ;
            rain_rate:SCALED = '\1' ;
            rain_rate:units = "mm h-1" ;
            rain_rate:standard_name = "rain_rate" ;
            rain_rate:long_name = "derived rain rate" ;
            rain_rate:coordinates = "longitude latitude" ;
            rain_rate:RANGE_MISSING = -999.f ;
            rain_rate:valid_range = '\201', '\177' ;
            rain_rate:_FillValue = '\200' ;
            rain_rate:RANGE_MIN = 0.f ;
            rain_rate:RANGE_MAX = 32.f ;
            rain_rate:SCALED_MISSING = -128 ;
            rain_rate:SCALED_MIN = -127 ;
            rain_rate:SCALED_MAX = 127 ;
            rain_rate:add_offset = 16.f ;
            rain_rate:scale_factor = 0.12598425f ;
      byte wind_speed_cloud_top_nwp(scan_lines_along_track_direction,
pixel_elements_along_scan_direction) ;
            wind_speed_cloud_top_nwp:SCALED = '\1' ;
            wind_speed_cloud_top_nwp:units = "m/s" ;
```

```
            wind_speed_cloud_top_nwp:standard_name =
"wind_speed_cloud_top" ;
            wind_speed_cloud_top_nwp:long_name = "wind speed from the NWP
ancillary data at cloud-top level" ;
            wind_speed_cloud_top_nwp:coordinates = "longitude latitude" ;
            wind_speed_cloud_top_nwp:RANGE_MISSING = -999.f ;
            wind_speed_cloud_top_nwp:valid_range = '\201', '\177' ;
            wind_speed_cloud_top_nwp:_FillValue = '\200' ;
            wind_speed_cloud_top_nwp:RANGE_MIN = 0.f ;
            wind_speed_cloud_top_nwp:RANGE_MAX = 50.f ;
            wind_speed_cloud_top_nwp:SCALED_MISSING = -128 ;
            wind_speed_cloud_top_nwp:SCALED_MIN = -127 ;
            wind_speed_cloud_top_nwp:SCALED_MAX = 127 ;
            wind_speed_cloud_top_nwp:add_offset = 25.f ;
            wind_speed_cloud_top_nwp:scale_factor = 0.19685039f ;
      byte wind_direction_cloud_top_nwp(scan_lines_along_track_direction,
pixel_elements_along_scan_direction) ;
            wind_direction_cloud_top_nwp:SCALED = '\1' ;
            wind_direction_cloud_top_nwp:units = "degrees" ;
            wind_direction_cloud_top_nwp:standard_name =
"wind_direction_cloud_top" ;
            wind_direction_cloud_top_nwp:long_name = "wind direction from
the NWP ancillary data at cloud-top level" ;
            wind_direction_cloud_top_nwp:coordinates = "longitude
latitude" ;
            wind_direction_cloud_top_nwp:RANGE_MISSING = -999.f ;
            wind_direction_cloud_top_nwp:valid_range = '\201', '\177' ;
            wind_direction_cloud_top_nwp:_FillValue = '\200' ;
            wind_direction_cloud_top_nwp:RANGE_MIN = 0.f ;
            wind_direction_cloud_top_nwp:RANGE_MAX = 360.f ;
            wind_direction_cloud_top_nwp:SCALED_MISSING = -128 ;
            wind_direction_cloud_top_nwp:SCALED_MIN = -127 ;
            wind_direction_cloud_top_nwp:SCALED_MAX = 127 ;
            wind_direction_cloud_top_nwp:add_offset = 180.f ;
            wind_direction_cloud_top_nwp:scale_factor = 1.4173229f ;

// global attributes:
            :SOURCE = "CLAVR-x + PATMOS-x 6.5.1" ;
            :CREATED = "2013-03-28T19:31:41-05:00" ;
            :PROCESSING_NOTE = "Experimental PATMOS-x/CLAVR-x Production
at UW/CIMSS" ;
            :HDF_LIB_VERSION = "HDF Version 4.2 Release 5, February 17,
2010" ;
            :MACHINE = "saga.ssec.wisc.edu" ;
            :PROGLANG = "F90" ;
            :CLOUD_MASK_VERSION = "$Id:
naive_bayesian_cloud_mask_module.f90,v 1.55.2.45 2013/03/20 20:40:50
dbotambekov Exp $" ;
            :CLOUD_MASK_THRESHOLDS_VERSION = "" ;
            :CLOUD_TYPE_VERSION = "$Id: universal_cloud_type.f90,v 1.4
2013/03/18 17:06:11 heidinger Exp $" ;
            :ACHA_VERSION = "$Id: awg_cloud_height.f90,v 1.14 2013/02/09
12:56:09 heidinger Exp $" ;
```

```
           :DCOMP_VERSION = "$id: dcomp_clavrx_bridge_mod.f90,v 1.1.2.20
2013/03/07 17:25:34 heidinger exp $" ;
           :FILENAME = "goes15_2011_365_2330.level2.hdf" ;
           :L1B = "goes15_2011_365_2330" ;
           :RESOLUTION_KM = 4.f ;
           :START_YEAR = 2011s ;
           :START_DAY = 365s ;
           :START_TIME = 23.5f ;
           :END_YEAR = 2011s ;
           :END_DAY = 365s ;
           :END_TIME = 23.5f ;
           :ACHA_MODE = 6 ;
           :DCOMP_MODE = 3 ;
           :WMO_SATELLITE_CODE = 259 ;
           :SENSOR_NAME = "GOES-15 : Imager" ;
           :REFL_0_65UM_NOM_DARK_COMPOSITE_NAME =
"goes15_2011_365_2330_drk_ch1_pix.dat" ;
           :NAIVE_BAYESIAN_CLOUD_MASK_NAME =
"goes_no12um_no13um_cfsr05_bayes_mask.txt" ;
           :DATA_TYPE = "PIXEL" ;
           :USE_1B_THERMAL_CALIBRATION_FLAG = 0 ;
           :USE_1B_REFLECTANCE_CALIBRATION_FLAG = 0 ;
           :RENAVIGATION_FLAG = 2 ;
           :USE_SST_ANALYSIS_FLAG = 1 ;
           :SST_ANALYSIS_SOURCE_FLAG = 0 ;
           :NWP_FLAG = 3 ;
           :MODIS_CLEAR_SKY_REFLECTANCE_FLAG = 1 ;
           :CH1_GAIN_LOW = 0.f ;
           :CH1_GAIN_HIGH = 0.f ;
           :CH1_SWITCH_COUNT = 0.f ;
           :CH1_DARK_COUNT = 0.f ;
           :CH2_GAIN_LOW = 0.f ;
           :CH2_GAIN_HIGH = 0.f ;
           :CH2_SWITCH_COUNT = 0.f ;
           :CH2_DARK_COUNT = 0.f ;
           :CH3A_GAIN_LOW = 0.f ;
           :CH3A_GAIN_HIGH = 0.f ;
           :CH3A_SWITCH_COUNT = 0.f ;
           :CH3A_DARK_COUNT = 0.f ;
           :SUN_EARTH_DISTANCE = 0.98331589f ;
           :C1 = 1.191062e-05f ;
           :C2 = 1.4387863f ;
           :A_20 = -1.6616217f ;
           :B_20 = 1.0023206f ;
           :NU_20 = 2562.1382f ;
           :A_31 = -0.54594672f ;
           :B_31 = 1.0014476f ;
           :NU_31 = 936.39941f ;
           :A_32 = -0.3507058f ;
           :B_32 = 1.001025f ;
           :NU_32 = 833.46735f ;
           :SOLAR_20_NU = 14.56773f ;
           :TIME_ERROR_SECONDS = 0.f ;
           :NUMBER_OF_ELEMENTS = 1656 ;
```

```
            :NUMBER_OF_SCANS_LEVEL1B = 1355 ;
            :NUMBER_OF_SCANS_LEVEL2 = 1355 ;
            :PROCESSING_TIME_MINUTES = 1.7540359f ;
            :NONCONFIDENT_CLOUD_MASK_FRACTION = 0.087089144f ;
            :ACHA_SUCCESS_FRACTION = 1.f ;
            :DCOMP_SUCCESS_FRACTION = 0.60472631f ;
}
```